Response of monopiles subjected to combined vertical and lateral loads, lateral cyclic load, and scour erosion in sand

Li, Q.

Important note
To cite this publication, please use the final published version (if applicable).
Please check the document version above.

Response of monopiles subjected to combined vertical and lateral loads, lateral cyclic load, and scour erosion in sand

Response of monopiles subjected to combined vertical and lateral loads, lateral cyclic load, and scour erosion in sand

Dissertation

for the purpose of obtaining the degree of doctor
at Delft University of Technology
by the authority of the Rector Magnificus, Prof.dr.ir. T.H.J.J. van der Hagen
chair of the Board for Doctorates
to be defended publicly on
Monday 5 October 2020 at 10.00 hours

by

Qiang Li

Master of Engineering Mechanics,
Hohai University, China
born in Shandong, China

This dissertation has been approved by the promotors.

Composition of the doctoral committee:

Rector Magnificus	chairperson
Prof.dr. K. Gavin	Delft University of Technology, promotor
Dr. A. Askarinejad	Delft University of Technology, copromotor

Independent members:

Prof.dr. M.A. Hicks	Delft University of Technology
Prof.dr. G.R. Eiksund	Norwegian University of Science and Technology, Norway
Dr. V. Zania	Technical University of Denmark, Denmark
Dr. F. Pisanò	Delft University of Technology
Dr. F.S. Tehrani	Deltares

An electronic version of this dissertation is available at https://repository.tudelft.nl/

Contents

Summary

Although wind energy capacity has increased significantly in the last few decades, the installed capacity of offshore wind turbine still lags far behind that of onshore wind turbines due to the installation and foundation cost. The aim of this research project has been to clarify the influence of combined vertical and lateral loads, lateral cyclic load, and scour erosion on monopile foundations, in order to achieve more realistic and cost beneficial solutions for offshore wind turbine foundations and thereby increase its competitiveness when compared with other energy sources.

Monopiles are the most popular foundation system today for offshore wind turbines installed in shallow to medium water depths. These relatively light structures (low vertical load), need to resist substantial lateral and moment loads. There have been a dearth of studies conducted to investigate the influence of vertical load on the lateral response of these rigid monopiles and the few available have drawn contradictory conclusions. In addition the lateral and moment loading exerted on monopiles due to wind, wave, and water currents is cyclic in nature. This type of loading can lead to the accumulation of lateral displacement/rotation and possible degradation of soil resistance over time. This evolution of pile head displacement and the change in soil stiffness with increasing cycles of load is poorly understood. Cylindrical structures, like monopiles, founded in offshore regions are commonly subjected to scour erosion caused by flowing water and currents, which induces loss of soil support around the pile, reducing the lateral load capacity and causing increased pile displacement. As a result, the system dynamics of the structure might be adversely affected. The results of numerical models suggest that the shape of the scour hole affects the loss of pile lateral capacity, however, there is a shortage of experimental test data that measure this effect.

More than 60 centrifuge tests which are categorized into three groups are presented in this thesis, which consider the interaction of combined vertical and lateral loads, lateral cyclic load and scour erosion on the behaviour of rigid monopiles. The tests have been performed in homogeneous dry Geba sand in order to mimic simplified drained offshore soil conditions.

In chapter 3, the results of 20 of centrifuge tests are reported and analysed. These tests have been carried out to investigate and compare the effect of combined vertical and lateral loads on

pile lateral response in terms of initial stiffness of load-displacement curves and lateral capacity. The effect of various levels of vertical load, pile installation stress level and pile slenderness, or L/D ratio, on the observed lateral response of the piles were systematically studied. The results show that for piles with $L/D = 5$, higher vertical load improves the pile initial stiffness and lateral capacity. The vertical load was shown to enhance the soil reaction near to the pile and therefore the pile load-displacement behaviour. However, as the slenderness ratio of the piles decreased to 3, it was shown that for small applied vertical loads, V, less than 44% of the ultimate vertical load capacity, V_u, the pile's lateral resistance increased dramatically with an increase of vertical load. Whereas, for higher vertical loads considered, the beneficial effects of vertical load reduced in a manner similar to the behaviour observed for shallow footings.

In chapter 4, 23 tests were performed in both dense sand and medium dense sand. Influence of cyclic load directional characteristic and amplitude on pile lateral behaviour, and the behaviour of the monopile subjected to storm loading has been investigated. The experimental set up, the loading scheme and the data processing techniques were described and cyclic p-y (p signifies lateral soil reaction, y signifies lateral displacement) curves were generated. It was found that, compared with one-way loading, two-way asymmetric loading is a more damaging cyclic load directional characteristic. Within the imposed cycle number, the pile secant stiffness always increases with loading cycles. The pile displacement accumulation rate was found to be not sensitive to the cyclic load magnitude and sand relative density. Application of lower amplitude of cyclic loading after storm loading cycles led to reduction in the rate of accumulation of pile head displacements. At different soil depths, the p-y curves showed different evolution trends with the increase of cycle number. Equations for prediction of evolution of pile head displacement and secant stiffness were formulated based on centrifuge test results. Performance of the model was demonstrated and predicted results were compared with a field test data.

Chapters 5 and 6 of this thesis present 20 centrifuge model tests that evaluate the effect of scour erosion on the response of a laterally loaded pile with various scour profiles, by varying the scour type and scour depth. p-y curves were derived based on the measured pile moment distributions and the load-displacement data at the pile head. Design equations were obtained to evaluate the beneficial effect of local scour types compared with global scour, and to assess the detrimental effect scour on pile moment capacity.

Altogether, the research outcomes in this thesis provide useful suggestions in the design of offshore wind turbine monopile foundations.

1 Introduction

1.1 Current status of wind energy

For thousands of years, humans have used wind as an energy source for their daily life. Windmills were invented to grind grain and pump water. The onshore deployment of wind energy for generating electrical power has a long history which can date back to the 1880s, while the first offshore wind turbine (OWT) was installed only a few decades ago-in 1991 [1]. Generally, onshore wind turbines are easier to build than offshore wind turbines. In 2019, the International Renewable Energy Agency (IRENA) highlighted that: Onshore wind power is now, frequently, less expensive than any fossil-fuel option, without financial assistance and are today competitive with fossil energy production [2]. From the aspect of investment per megawatt (MW), offshore wind is still about 50% more expensive than onshore wind [3]. This might lay obstacles for the development of offshore wind turbine compared with onshore wind turbine.

However, onshore wind turbine developments can encounter local resistance due to environmental concerns, including adverse visual impact, noise-related trauma to humans, image flicker and electromagnetic interference [4]. In comparison to onshore, offshore sites offer favourable wind conditions, less land requirements as well as limited regulations. The bar chart in Figure 1.1 illustrates the ongoing and forecast of offshore and onshore wind energy installations all over the world from 2011 to 2026 (modified after Perveen et al. [5]). Although offshore wind still lags behind onshore wind, it can be seen that offshore wind energy production has started to boom. As offshore wind energy technology is getting mature one day by another, offshore wind farms are gradually beginning to prosper.
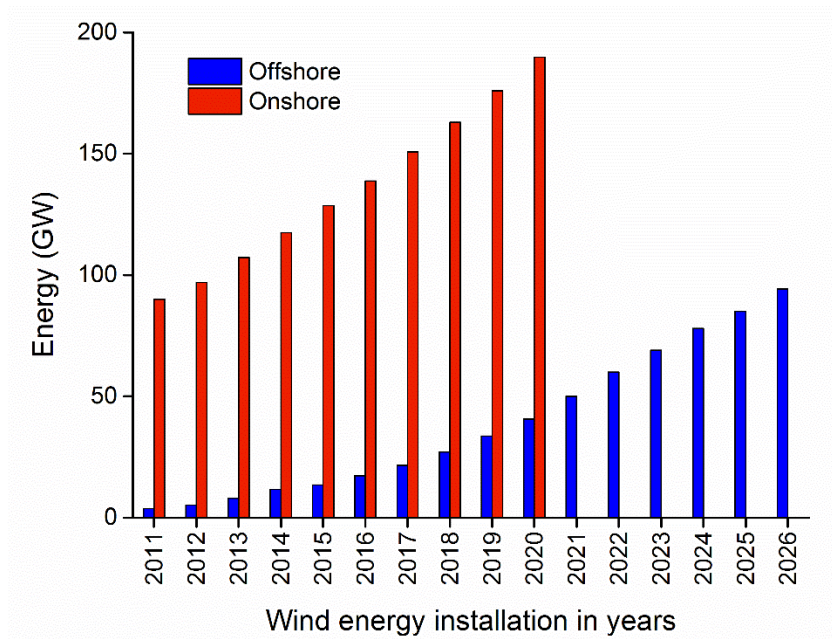
Figure 1.1 Offshore and onshore wind energy installations from 2011 to 2026 (modified after Perveen et al. [5])

1.2 Wind turbine foundations

Wind turbines can be constructed using several foundation types. Onshore wind turbine towers are usually bolted to concrete slab near the soil surface. In soft soil region, slender piles are commonly adopted under the slab [6]. OWT structures maybe founded on gravity base, suction caisson, monopile, tripod or braced frame (jacket) foundations or, more recently, floating platforms tethered to the seabed (Figure 1.2). The foundation choice is largely determined by the water depth, seabed characteristics, loading characteristics, and available construction technologies [7, 8].

Jacket or tripod foundations can be built with specific wall thickness at different parts of the structure, therefore optimal design can be achieved considering stress, strain and material usage compared with monopile. Monopile requires large pile diameter and wall thickness to resist the bending moment which means a larger amount of material usage, but is relatively easy in fabrication, transportation and construction.

Generally, monopile foundation is designed for water depths up to 30 m. Water depth of 30 – 40 m is considered as transition depth. For water depth larger than 40 m, jacket foundation shows more economical advantage [6].
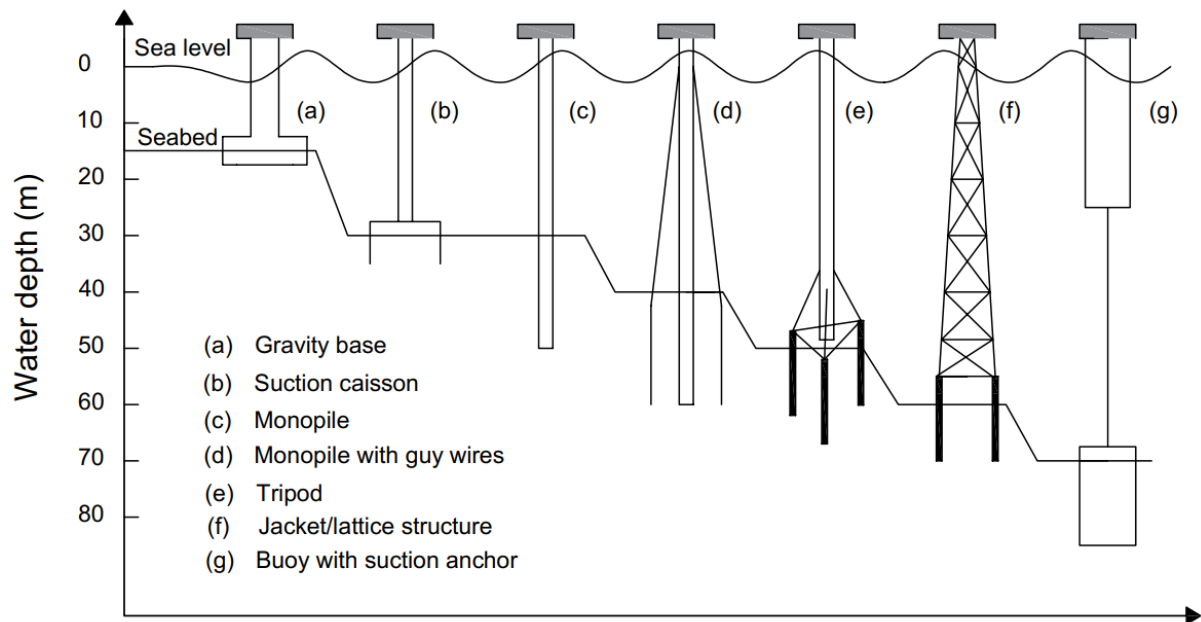
Figure 1.2 Support structure options for offshore wind turbines with range of applicable water depth (modified after Arshad and O'Kelly [8])

1.3 Monopile foundations

Monopile foundations are the most widely-used support structure for OWTs, due to relative simplicity in fabrication and installation [9]. Recent available figures state that monopiles have increased their market share from approximately 75% of offshore wind turbine foundations in 2012 [10] to more than 87% in 2019 [11]. The monopile foundation concept consists of an open-ended steel cylinder driven into the seabed. As the size of wind turbines is increasing, the size of the monopiles increases as well. Although diameters of monopiles used by OWTs are in a wide range from 4 to 10 m depending on the power capacity of the turbine, the embedded pile length-diameter (*L-D*) ratio keeps in a narrow range typically from 3 to 6 [12]. These structures are particularly adept at resisting large vertical load due to self-weight of the top structure, lateral load and moment from wind and wave actions, and are economically efficient. When unprotected, cylindrical structures (like offshore monopiles) can be prone to scour erosion due to current, tides and waves, which results in a loss of soil support around the piles [13]. The typical loads on an OWT and the marine hydraulic forces induced scour erosion around a monopile foundation are depicted in Figure 1.3.

For an OWT, the foundation costs account for around 25% to 34% of the total cost [14]. It means that reducing the cost of OWT support structure could significantly drive down the cost of energy and make offshore wind energy as a more competitive renewable energy source. Establishing a more accurate load and structural response prediction would increase the reliability in the design process, thereby over-conservative design can be avoided while an adequate factor of safety can still be maintained [6].
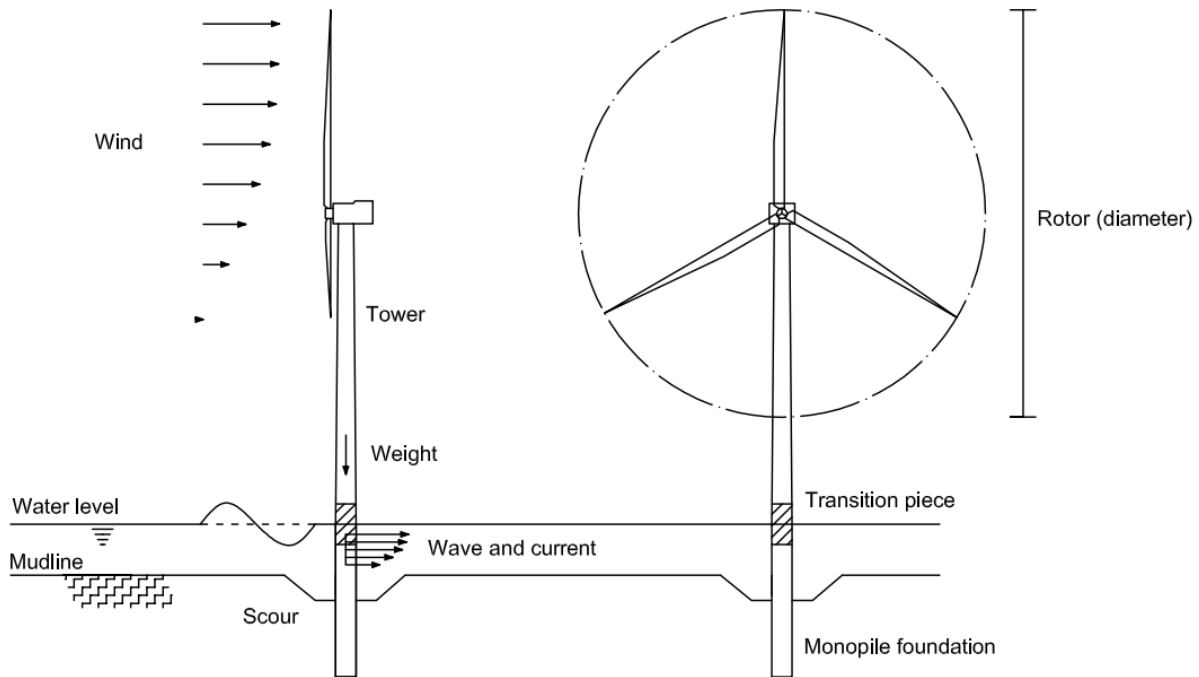
Figure 1.3 Loads on an offshore wind turbine and scour erosion around the monopile

1.3.1 Pile under combined vertical and lateral loads

Lesny and Wiemann [15] stated that the typical loads at seabed level for a 5 MW wind turbine supported by monopile foundation is approximately 35 MN of vertical load, 16 MN of lateral load, and 562 MNm of overturning moment. The vertical load is considered as static load originating from the self-weight of the wind turbine and the foundation, while the lateral load in contrast is cyclic. Interaction between the vertical load and the lateral load was recognized [16, 17]. However, according to current practices (i.e., API [18], DNV [19]), monopiles are designed separately for the vertical load and the lateral load based on the assumption that the effect of vertical load and lateral load is independent of each other [20].

Extensive research has been performed over the past century on piles subjected to a combination of vertical and lateral loads, the conclusions on the influence of vertical load on the lateral behaviour of piles are not consistent. Karasev et al. [21], Mu et al. [20] and Lu and Zhang [22] suggest that the presence of vertical loading improves the pile performance (defined as the lateral displacement measured at a given lateral load). In contrast Jain et al. [23] and Lee [24] report the opposite effect. Detailed information on the introduction and comparison of the above mentioned researches can be found in Chapter 3. If the presence of vertical load improves the pile lateral performance, it means the current design methodology which ignores this effect leads to over-conservative design. Additional cost savings can be achieved from pile fabrication and installation if a realistic pile design considering effect of vertical load on pile lateral response can be taken. Therefore, studying the interaction effects between vertical and lateral loads is essential for identifying key factors influencing pile response and for developing optimal pile foundation design.

1.3.2 Pile under lateral cyclic load

The lateral loading condition for offshore wind turbine monopiles is dominated by environmental loads from wave and wind. These loads act on the monopile in a cyclic manner with a variation in directional characteristic as well as amplitude. Long-term lateral cyclic load on the foundation changes the stiffness of the surrounding soil and therefore the interaction of the foundation and the soil and pose problems for the top structure through serviceability limit state (SLS) failure, owing to the accumulation of irreversible deformations. Any significant change in stiffness may further result in change of the system frequency, which would be highly problematic. For the design of a monopile foundation for offshore wind turbines, accumulation of rotation and the change in secant stiffness are two important issues. However, upon the most damaging load cyclic directional characteristic and evolution of pile head displacement and secant stiffness with cycle number, there are still some divergences in opinion.

Through literature study [25-50], several discrepancies are seen: (i) from the $1g$ experiment LeBlanc et al. [41] the most damaging load situation was for two-way loading, more specifically $\zeta_c = -0.6$ ($\zeta_c = H_{min}/H_{max}$, where H_{min} is the minimum load in a load cyclic, and H_{max} is the maximum load in a load cyclic), while centrifuge test series [43] did not show this trend, instead it indicated that one-way and two-way loading, $\zeta_c = 0$ and -0.4, both could be the most damaging

ones; (ii) from the tests by LeBlanc et al. [41] accumulation of rotation was seen regardless of the directional characteristic of the loading. This is in contrast to the observation from centrifuge tests [43], where it was observed that the pile starts to move back against its initial position in some kind of two-way loading ($\zeta_c \leq$ -0.63); (iii) from the test by LeBlanc et al. [41] pile stiffness was found to always increase regardless of cyclic directional characteristic, while it was shown that secant stiffness would decrease in one-way cyclic loading ($\zeta_c = 0$) in Klinkvort [43].

p-y curves commonly used now in the designing of laterally loaded monopiles are presented in API [18]. However, because these were formulated based on results from experiments on relatively long piles with diameters smaller than 1 m, i.e. slender piles, their ability to predict the response of rigid (large diameter) monopiles is questionable. Few consistent results regarding *p-y* curves of rigid monopiles exposed to lateral cyclic loading could be seen, and the most relevant researches [37, 43, 49, 59, 87] are summarized and compared in Chapter 4.

1.3.3 Pile under scour erosion

Monopiles have strict serviceability requirements, e.g. pile rotation at sea bed level typically must remain less than 0.25° [12]. Scour erosion reduces the pile lateral load capacity and increases pile head displacement and rotation. This can pose problems for the top structure through serviceability limit state (SLS) failure, or the generation of excessive fatigue stresses potentially leading to negative operational issues with a turbine. It is therefore of critical importance to consider the effect of scour on the bearing behaviour of unprotected monopiles subjected to lateral load.

Considerable research [50-61] has been undertaken on the effect of scour on the lateral response characteristics of piles using numerical modelling or scaled laboratory testing; however, limited experimental studies have evaluated the effect of scour-hole shape on the responses of piles. Interested readers are referred to the introduction section of Chapter 5 for the state-of-the-art research on scour-hole shape effect on monopiles. In current practice, when pile foundations under scour conditions are analysed, soils around the pile foundations are totally removed to the scour depth [19]. The effect of scour-hole shape is not fully addressed in the current

monopile design methodology, which is considered to lead to over-conservative design and extra foundation cost.

1.3.4 Summary

In summary, monopile foundation for offshore wind turbines resists complicated vertical and lateral loading conditions and often faces scour erosion problems when the seabed is without protection. Physical modelling of large diameter monopile is still few. Conflicting results concerning the effect of combined vertical and lateral loads and lateral cyclic load on the lateral response of piles are produced. Insufficient research upon scour erosion on pile lateral response considering the scour-hole shape effect can be seen. Therefore, limited guidance on how to achieve optimal pile design in these cases in order to reduce the foundation cost can be found.

1.4 Research objectives

The main goal of this study is to identify the influence of combined vertical and lateral loads, lateral cyclic load and scour erosion on the lateral response of monopiles in sands through physical modelling. Model pile tests were performed in a geotechnical centrifuge at an enhanced gravitational acceleration level of 100g. Open-ended piles with prototype diameter of 1.8 m were examined. The selected pile embedment ratios mimic the ratio of typical rigid monopiles used as offshore wind turbine foundations. The scope of the research work includes:

1. Studying the lateral response of rigid monopiles in sand subjected to combined vertical and lateral loads through a series of model pile load tests. Evaluating the influence of vertical load on the lateral response of model piles in sand by considering the influence of pile installation stress level and pile embedment ratio (L/D).

2. Identifying the most damaging lateral cyclic load directional characteristic, making clear the influence of cyclic type and cyclic magnitude on the pile lateral loading behaviour, generating experimental cyclic p-y reaction curves, and investigating how the storm loading can affect the pile long-term loading behaviour.

3. Assessing the effect of scour depth and type on laterally loaded piles considering combined lateral and moment loads at the seabed level. Generating equations to help to reflect the scour-hole shape in the evaluation of scour effect on the pile moment capacity, with the aim to improve the traditional pile design method which does not properly reflect the effect of the scour-hole shape.

1.5 Structure of this thesis

This thesis consists of seven chapters and is mainly a collection of papers published by the author. Therefore, some repetition can be seen on the introduction and specification of the details of physical modelling in each group of tests. The outline of each chapter is as follows:

Chapter 2, as an initial chapter, discusses general remarks about physical modelling: i.e. (i) geotechnical centrifuge; (ii) scaling laws; (iii) test set-up; (iv) pile instrumentation; (v) Geba sand properties and (vi) *p-y* reaction curve construction.

Chapter 3 presents test equipment, research methodology and test results on the study of effect of vertical load on the lateral response of monopiles. A total number of 20 centrifuge monotonic load tests were carried out. The influence of pile *L/D* ratio and pile installation stress level on the lateral load-displacement response, initial stiffness and lateral capacity were evaluated.

Chapter 4 describes the experimental set up, the loading scheme, the data acquisition and the processing techniques in the investigation of monopile under cyclic lateral loads. A total number of 23 centrifuge tests were carried out. The methodology to identify the most critical (damaging) load directional characteristic, and the influence of load directional characteristic and load magnitude on the accumulation of the pile head displacement and secant stiffness was summarized. The influence of storm loading on the pile long-term lateral loading behaviour was presented. Evolution of bending moment and cyclic *p-y* curves considering cyclic loading effect were studied.

In chapters 5 and 6, impact of scour erosion on the monotonic lateral response of a monopile in sand is presented. A total number of 20 centrifuge tests were carried out. Chapter 5 provides details of the equipment designed and fabricated to perform the model pile load tests considering scour effects. Three scour types (local narrow scour, local wide scour and global

scour) and three scour depths ($1D$, $1.5D$ and $2D$) were considered in this investigation, which represents the typical scour shapes and depths as suggested in real engineering projects. Test results were briefly shown from the aspects of lateral load-displacement relationship and bending moment distribution.

Chapter 6 compares the pile moment capacity, bending moment distribution and *p-y* curves from monotonic lateral load tests, considering the influence of scour type and scour depth. Simple empirical relations were proposed to evaluate the beneficial effect of local scour types compared with global scour, and to quantify the detrimental influence of scour on the pile moment capacity.

Chapter 7 contains the summary of the research work performed and the conclusions from this thesis. Some remaining knowledge gaps to quantify the influence of interactive effect of combined vertical and lateral loads, lateral cyclic load and scour erosion on the monopile response and suggestions how to investigate them are indicated.

2 Physical modelling

2.1 Geotechnical centrifuge

The TU Delft centrifuge, see Figure 2.1, is a beam-type apparatus [62]. Centrifuge tests are performed at enhanced acceleration field (Ag) on models that are geometrically A-times smaller than the prototype. The geo-centrifuge provides a unique environment of acceleration field, where the expected behaviour of a full-scale geotechnical structure can be observed, with high precision, using small scale models. The centrifuge at TU Delft enables models with dimensions up to 500 mm × 240 mm × 380 mm be tested up to a maximum of 300 times the gravitational acceleration ($300g$), see Table 2.1.

(a)
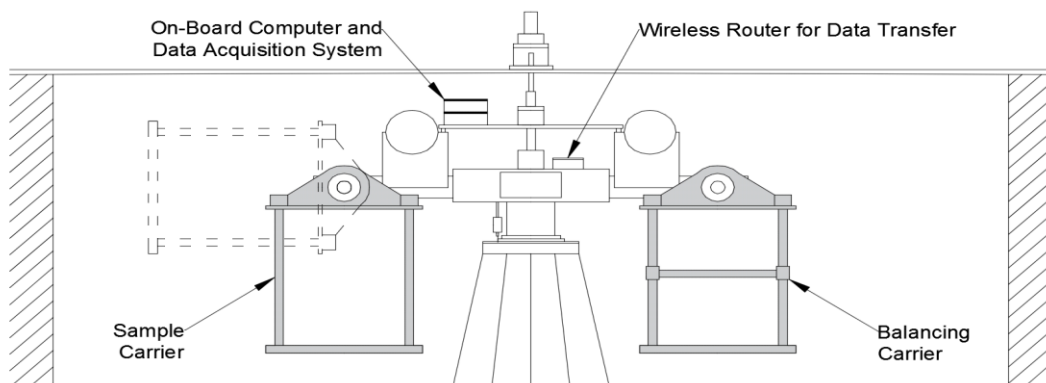
(b)

Figure 2.1 TU Delft beam centrifuge: (a) Photo; (b) Schematic layout (modified after Alderlieste [6])

Table 2.1 TU Delft centrifuge characteristics

Property		Value	Dimension
Radius of the centrifuge arm		1195	mm
Maximum design acceleration		300×9.81	m/s^2
Maximum design pay load (at 300g)		40	kg
Carrier dimensions	Height	500	mm
	Width	240	mm
	Length	380	mm

2.2 Scaling laws

For simulating geotechnical structures using a centrifuge, scaling laws must be considered. Table 2.2 provides a summary of typical scaling laws for modelling of pile structures in the centrifuge. In this table, A refers to the gravitational acceleration field adopted in a given test.

Table 2.2 Basic scaling laws for centrifuge modelling of monopiles

Term	Prototype	Model
Length	1	$1/A$
Area	1	$1/A^2$
Second moment of area	1	$1/A^4$
Flexural stiffness	1	$1/A^4$
Mass	1	$1/A^3$
Force	1	$1/A^2$
Stress	1	1
Strain	1	1
Density	1	1

2.3 Test set-up

A two-dimensional servo actuator applies loading to the pile, as schematically shown in Figure 2.2. The loading system is capable of applying vertical and lateral loads under either load or displacement controlled conditions. The lateral load (H) is applied at the pile head by lateral movement of the actuator, and is monitored by strain gauges located on the loading arm or parallel beam load cells depending on the characteristics of tests. The lateral displacements of the pile at the loading position (pile head) can be monitored by the lateral motor encoders, the accuracy of which are of the order of approximately 3×10^{-5} mm.

(a)   (b)
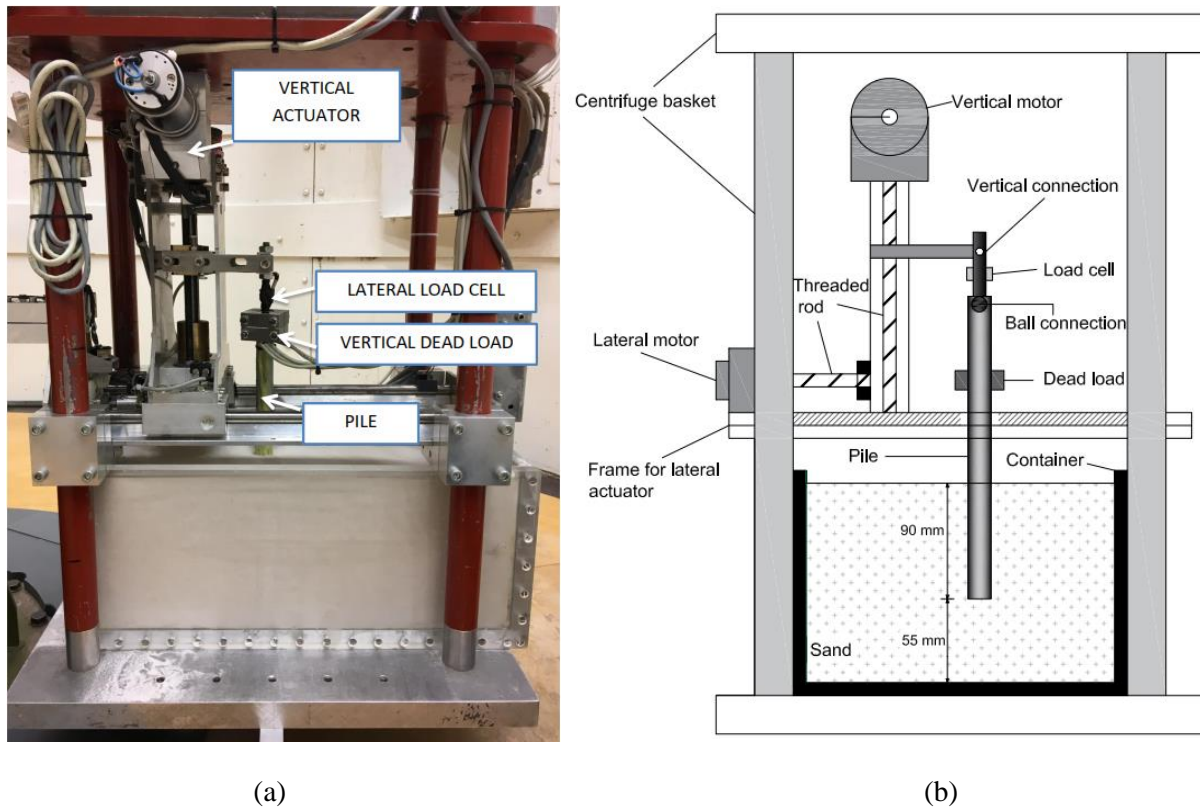
Figure 2.2 The two-dimensional loading actuator and typical monopile arrangement in centrifuge tests: (a) Photo; (b) Schematic layout

2.4 Pile instrumentation

The model piles used in this research are open-ended cylindrical tubes with an outer diameter (*D*) of 18 mm. Model piles are constructed using aluminium with an elasticity modulus of 70 GPa which is about a third of that of steel (210 GPa), which means the pile wall thickness when using aluminium can be increased to 3 times of the pile wall thickness when using steel. Pile diameter is selected so as to minimise boundary effects associated with the strong box, which houses the pile, and also to satisfy constraints associated with the mean grain particle size. The wall thickness of the model pile is derived based on the calculation for minimum wall thickness for monopiles [12, 18]. Using the similitude between the flexural rigidity (*EI*) of the prototype and the model (Table 2.3), the wall thickness is calculated to be 1 mm. Byrne et al. [25] has produced a database of piles, and present the results of the pile diameters normalised by pile wall thickness. For monopiles, the value of *D/t* varied from 39 to 80. In the present analysis, the *D/t* value for the steel prototype pile is 60.

All tests were performed at $100g$; therefore, the model pile properties correspond to a 1.8 m diameter rigid structure, with a wall thickness of 100 mm at the prototype scale. Certainly, this is a small pile with respect to those typically used in the offshore environment [12]. However, the pile slenderness ratio (L/D) was selected within the range of popular values in application. The primary dimensions and material properties of the pile are provided in Table 2.3.

Strain gauges were installed and calibrated for measuring bending moment (see Figure 2.3). Because of constraints regarding the loading mechanism, such pile was jacked into the sand sample prior to spinning up the sample (i.e. installation at $1g$) with the result that installation effects were not fully modelled. However, the same preparation method and testing procedure was followed for all of the tests.

Table 2.3 Model and corresponding prototype pile dimensions and properties

Property	Model pile	Prototype pile*
Length (embedded + loading eccentricity)	90 + 144 mm	9 + 14.4 m
Diameter, outer	18 mm	1.8 m
Wall thickness	1 mm	30 mm
Elasticity modulus (E)	70 GPa	210 GPa
Moment of inertia (I)	1936 mm^4	0.065 m^4
Flexural stiffness (EI)	0.136 kPa.m^4	13.7 GPa.m^4

*Assuming prototype pile is fabricated from steel; tests were performed at $100g$

(a)   (b)

Figure 2.3 Model pile with strain gauge layout: (a) Photo; (b) Schematic diagram

2.5 Geba sand properties

Fine, uniform Geba sand [63] was used in this study. It is mainly comprised of silica (99% SiO_2) and 84.2% of the grains have a diameter between 0.1 mm and 0.2 mm. The mechanical parameter for Geba sand has been determined by Charles University (CU) in Prague as a request from Royal IHC [64], through experimental tests in laboratory (triaxial, simple shear, and oedometer tests). The main properties are summarised in Table 2.4.

The ratio of pile diameter to average grain size of the sands (D/D_{50}) for the tests is approximately 164, which is larger than the value of 20 and 60 suggested by Gui et al. [65] and Remaud [66], where grain size effects become negligible for laterally loaded piles [67]. Dry sand specimens were prepared with air pluviation method to relative density (D_r) of 50% to 80%. The influence of water is excluded in this series of tests.

The inner plan dimensions of the sand container are 410 mm by 150 mm, with a specimen depth of 155 mm. The ratio of the smallest size of the sand box to the outer pile diameter is 8.3, which is larger than the limitation of 4 as suggested by Prakasha et al. [68]. For the largest pile embedment ratio ($L/D = 5$), the distance from the pile tip to the bottom of the strong box is 3.6D which is larger than the minimum value of 3 required to avoid boundary effects [68].

Table 2.4 Basic soil properties of Geba sand [69, 70]

Property	Sand
Median Particle Size, D_{50} (mm)	0.11
Curvature Coefficient, C_C	1.24
Uniformity Coefficient, C_U	1.55
Specific Gravity, G_S	2.67
Maximum Void Ratio, e_{max}	1.07
Minimum Void Ratio, e_{min}	0.64
Critical friction angle, φ_{cr} (º)	35

2.6 *p-y* reaction curve construction

The bending moment on pile can be calculated from discrete strain gauge data using Equation (2.1).

$$M(z) = EI\rho(z) \tag{2.1}$$

Where: *EI* is the flexural rigidity of the pile (Nm^2) and $\rho(z)$ is the curvature corresponding to a given applied load. Curvature is obtained as the ratio of the difference in measured compressive and tensile strains to the gauge lever arm (pile diameter) at each depth *z*, see Li et al. [71].

Lateral soil reaction-displacement (*p-y*) curves can be derived from bending moment profiles, with the soil reaction *p* being derived by double differentiation of the bending moment profile and the pile lateral displacement *y* at discrete locations obtained by double integration of the bending moment profile, see Equations (2.2) and (2.3).

$$p(z) = \frac{d^2 M(z)}{dz^2} \tag{2.2}$$

$$y(z) = \iint \frac{M(z)}{EI} dz dz \tag{2.3}$$

where *M(z)* is the bending moment at soil depth *z*.

Given the double differentiation propagates measurement errors it is common to apply curve fitting techniques to minimise these errors, see Xue et al. [72]. Polynomial curve-fitting method [73] is adopted herein for curve-fitting the moment data. The choice of the order of the fitted curve is important to minimise errors between the discrete moment points and the values from the continuous curve at these locations. A 5th order polynomial is used for the moment data to generate soil reaction (by differentiation). Boundary conditions of: 1) soil pressure at sand surface is assumed to be zero and 2) soil pressure at the pile pivot point (0.7*L* beneath the sand surface) is assumed to be zero were used to adjust the fitted bending moment function.

A 7th order polynomial is used to obtain soil displacements (by integration). When determining displacement at any depth, *y(z)*, two integration constants C_1 and C_2 were determined from: 1) the measured displacement at the loading position and 2) an assumed zero deflection condition at the point with zero lateral soil resistance [74].

3 Effect of vertical loading on the lateral behaviour of monopiles in sand

Influence of combined vertical and lateral loading on the response of monopiles used to support offshore wind turbines (OWTs) is investigated. In current practice, resistance of monopiles to vertical (self-weight) and lateral (wind and wave) loading are considered separately. As the size of OWTs has increased, the slenderness ratio (pile embedment length L normalised by diameter D) has decreased. Although referred to as monopiles, the foundations used for current OWTs are in fact intermediate footings with geometries between those of pile and shallow foundation systems. Whilst load interaction effects are usually not significant for slender piles, they are critical for shallow footings. Previous research on load interaction effects for piles has resulted in conflicting findings. This potentially arises from variations in the nature of boundary conditions and pile slenderness considered. In this study, monotonic lateral load tests were carried out in a geotechnical centrifuge on vertically loaded monopiles in dense sand. The influence of vertical loading is quantified in terms of how it impacts on the overall lateral load-displacement behaviour and soil reaction-displacement (p-y) curves along the embedded monopile. The influence of installation-related stresses are studied by installing the monopiles at both 1g and in-flight. Pile slenderness effect is considered by varying the pile slenderness (L/D) ratio over the range typically used in practice. Results indicate that for piles with L/D = 5, increasing vertical loading improved both the pile initial stiffness and lateral capacity. A similar trend was observed for piles with L/D = 3, when the vertical loading was below 44% of the pile's ultimate vertical capacity. For higher vertical loading considered, the beneficial effects reduced in a manner similar to the behaviour observed for shallow footings.

3.1 Introduction

The development of offshore wind resources has experienced rapid growth in recent years due to its position as the most mature technology to facilitate the energy transition. Monopiles are by far the most commonly used foundation for supporting offshore wind turbines (OWTs) maintaining a 87% market share for structures installed in 2019 [11, 75]. Monopiles comprise a single open-ended steel tube that is usually driven into the seabed. The typical pile sizes used to support early OWTs had diameter, D, in the range 4 to 6 m and embedded length, L, in the range 20 to 30 m, with L/D between 5 and 6 [76]. As turbine sizes grew to 10 MW the pile diameter required to limit turbine rotations increased to between 8 m and 10 m [25]. The combination of the relatively low turbine weight and large pile diameter means the embedded length of these monopiles has not increased significantly and the L/D ratios are reducing towards values in the range 2 to 3. Although known as monopiles, these foundations are more correctly termed intermediate foundation classified in ISO 1990-1-4 as having L/D in the range 1 to 10.

A number of researchers have studied the combined loading problem for shallow and skirted foundations. It has been identified that interaction effects such that the lateral load, H, and moment, M, capacity of footings depend on the current vertical load level, V [77-79]. Whilst a number of studies have considered load-interaction effects on piles, in much of this work the focus was not on monopile behaviour. Karasev et al. [21] conducted full-scale combined load tests on cast-in place concrete piles ($D = 600$ mm, $L = 3$ m and $L/D = 5$) in sandy loam. The test results indicate that the vertical load has a favourable effect on the lateral response of the piles (i.e. the lateral displacement of piles decreases considerably with increasing vertical load). Jain et al. [23] performed laboratory combined load tests on fully and partially embedded long flexible open-ended piles ($D = 32$ mm, $L = 1000$ mm and $L/D = 31.25$) in sand with a relative density D_r of 78%. In this case they reported that application of a vertical load increases the lateral displacement of the pile. Lee [24] performed laboratory model pile load tests to assess the influence of vertical loading on the lateral response of piles in sand. The effect of installation was considered by testing driven and non-displacement piles. The tests were performed in sand samples prepared in a pile testing chamber with investigated D_r in the range from 38% to 91%. The model closed-ended steel piles had $D = 30$ mm, $L = 1100$ mm and L/D of 37. In keeping with the results of Jain et al. [23], the authors found that lateral displacement of the model pile head increases with increasing vertical load. Mu et al. [20] performed combined load tests in a

centrifuge. The monopile had $D = 6$ m, $L = 50$ m and $L/D = 8.3$. Strain gauges were installed on the pile to study the influence of vertical loading on the bending moment and lateral soil resistance-displacement (p-y) curves. It was found that the presence of vertical loading decreases the lateral displacement of the monopile. Lu and Zhang [22] reported centrifuge tests where combined loading was applied to a pile with $D = 1$ m, $L = 16.5$ m and $L/D = 16.5$. They also found that lateral displacement measured at a given applied lateral load decreases as the vertical load increases.

In summary, Karasev et al. [21], Mu et al. [20] and Lu and Zhang [22] suggest that the presence of vertical loading improves the pile performance (defined as the lateral displacement measured at a given lateral load). In contrast Jain et al. [23] and Lee [24] report the opposite effect. At least part of the reason for this discrepancy might be related to variations in the pile top fixity applied in the experiments and the range of L/D ratios considered. Notwithstanding this contradiction there is a dearth of data which considers the pile performance under a range of vertical loads, L/D ratios and installation methods under controlled loading conditions and soil conditions.

In this paper, the effect of vertical loading on the lateral loading response of monopiles used for offshore wind turbines is examined using centrifuge testing. The contributions of the present study relate to investigate the effect of slenderness ratios typically adopted for OWTs on the lateral load capacity and p-y curves for monopiles in dense sand. Given the challenge of pile installation in the centrifuge a number of studies report tests on pre-installed piles. In order to check the impact of installation technique on the pile response, a series of tests are compared where the piles were installed in-flight and pre-installed. The centrifuge testing program is summarised in the next section. Section 2.3 presents an investigation of the influence of vertical loading on the lateral load-displacement behaviour. A comparison of the p-y curves derived experimentally in this research and those prescribed in literature is also presented. Finally, in section 2.4, conclusions of this work are provided.

This research aims at investigating monopile behaviour in dense sand condition, therefore the influence of sand relative density was excluded from this test program. Lateral load was applied under displacement controlled mode, the loading rate was low and the loading process can be deemed as quasi-static. Fully drainage condition can be expected even when carrying out tests in saturated sand specimen. Therefore, dry sand was used to form the foundation in order to decrease the difficulties in specimen preparation and save time.

3.2 Experimental procedure

The experiments presented in this paper were undertaken using the beam centrifuge at Delft University of Technology described by Allersma [62] and Zhang and Askarinejad [80]. A brief summary of the main test elements relevant for this paper are provided herein. Three aluminium tubular model piles used in the tests have an outer diameter $D = 18$ mm and wall thickness $t = 1$ mm. The properties of these piles are provided in Table 3.1, at both model and prototype scales. One pile ($P1$) was instrumented with ten strain gauges and the remaining two were uninstrumented. A photograph of the instrumented pile ($P1$) and one uninstrumented pile ($P2$) is shown in Figure 3.1.

Table 3.1. Model and corresponding prototype pile dimensions and properties of test piles

Pile ID	Strain gauge	Model					Prototype[*]		
		L_T (mm)	E (GPa)	D (mm)	t (mm)	L/D (-)	E (GPa)	D (m)	L/D (-)
$P1$	10 pairs	240	70	18	1	5	210	1.8	5
$P2$	None	240	70	18	1	5	210	1.8	5
$P3$	None	204	70	18	1	3	210	1.8	3

*Assuming prototype pile is fabricated from steel and g-level = 100.
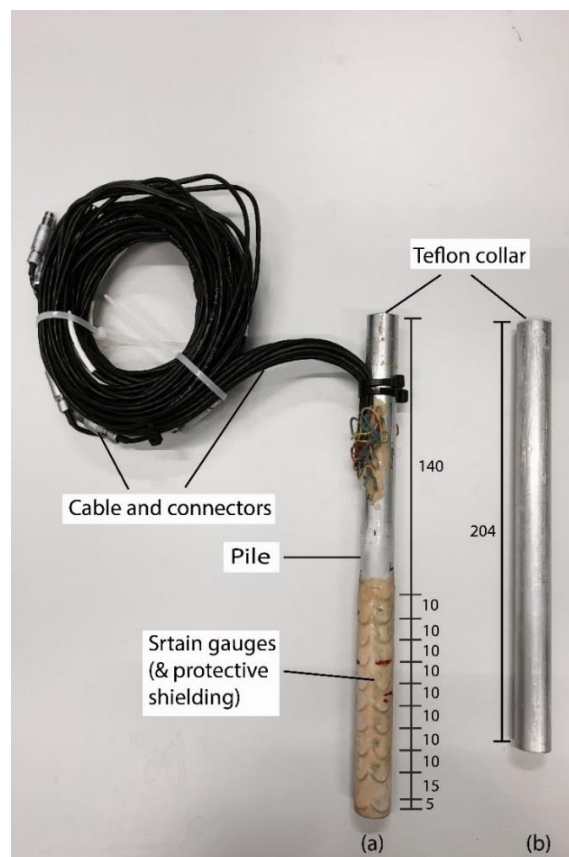
Figure 3.1 Photograph of model monopiles: (a) $P1$ and (b) $P3$ (unit: mm)

The tested piles simulate a 1.8 m diameter steel pipe pile with wall thickness of 30 mm at prototype scale. The piles were installed by jacking to L/D ratios of 3 or 5. The terminology adopted to describe the pile response is summarized in Figure 3.2. Here L is pile embedded length, e is the loading eccentricity, D is the pile outer diameter. R_0 is the distance from the pile pivot point to the pile toe. H is the applied lateral load, y is the pile lateral displacement, and θ is the pile rotation angle. The loading eccentricity, e, was constant in all tests at 8D.
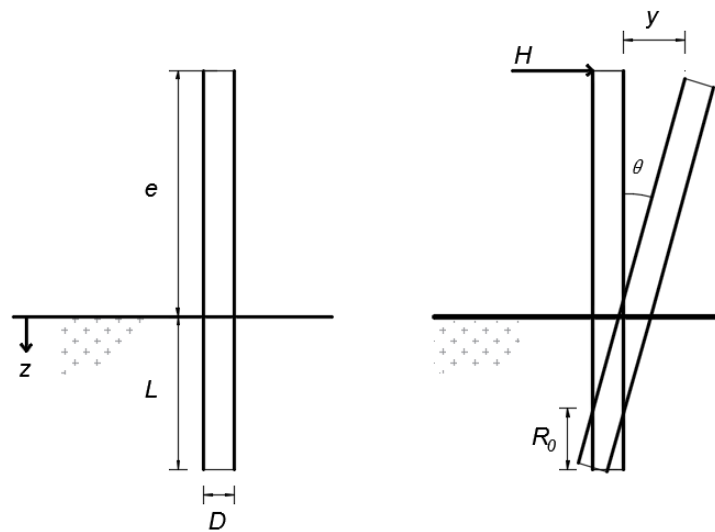
Figure 3.2 Sketch of pile

The piles were installed in dense Geba sand with D_r = 80% formed using the air pluviation technique. The geotechnical parameters of Geba sand are shown in Table 3.2, for detailed information see Maghsoudloo et al. [69]. The ratio of the outer pile diameter to average grain size of the sand (D/D_{50}) for the tests conducted is approximately 164, which is sufficient to avoid particle size effects [81-83]. The plan dimensions of the sand sample are 410 mm by 150 mm, with a sample depth of 155 mm. The ratio of the smallest size of the sand box to the outer pile diameter is 8.3, which is larger than the limitation of 4 as suggested by Prakasha et al. [68]. For the largest pile embedment ratio (L/D = 5), the distance from the pile tip to the bottom of the strong box is 3.6D which is larger than the minimum value of 3 required to avoid boundary effects [68].

Table 3.2. Geotechnical properties of Geba sand [69, 70]

e_{min}	e_{max}	G_S	D_{50} (mm)	C_C	C_U	φ_{cr}
0.64	1.07	2.67	0.11	1.24	1.55	35°
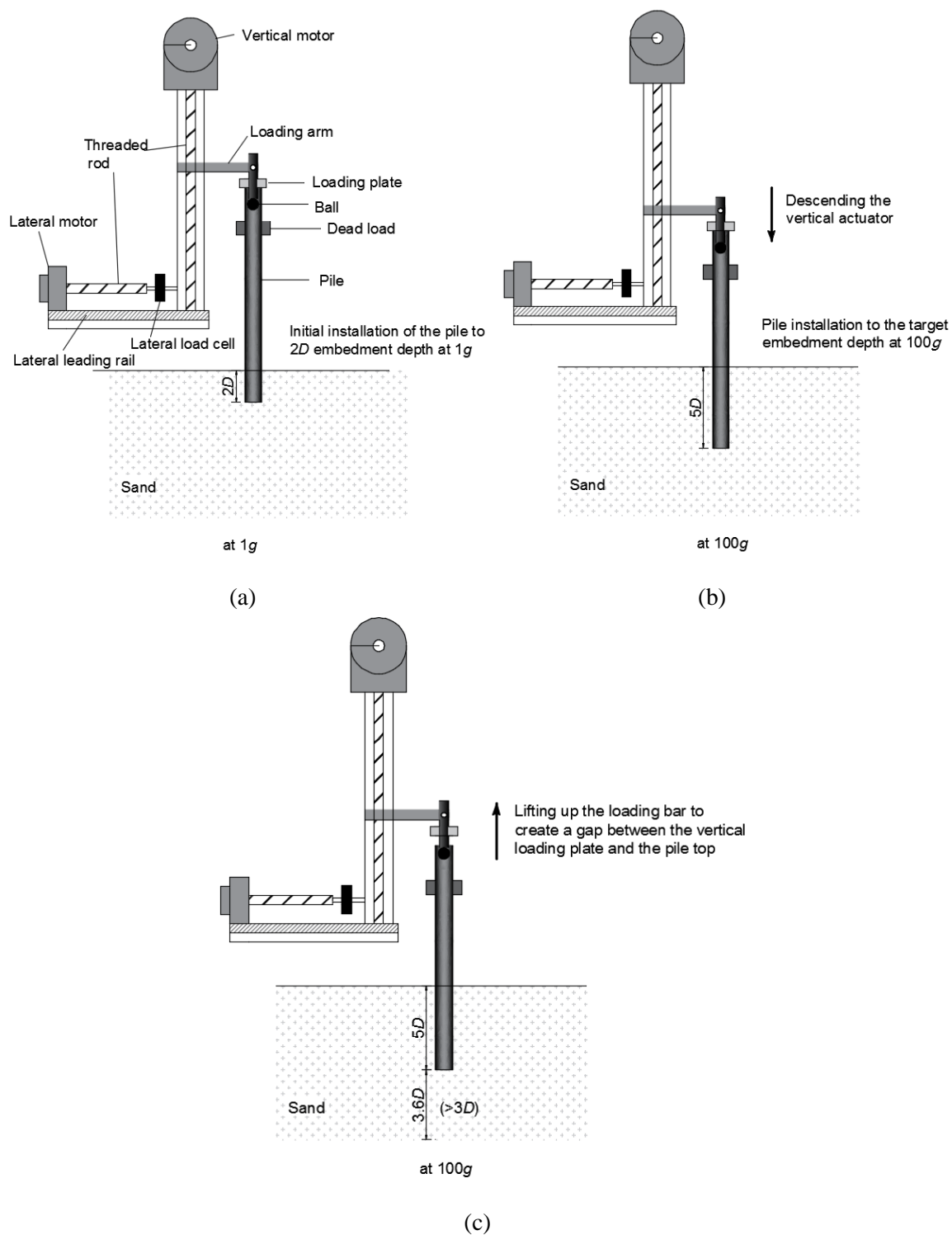
Figure 3.3 Schematic showing in-flight pile installation procedures: (a) Initial installation of the pile to 2*D* embedment depth at 1*g*; (b) Pile in-flight installation (5*D* embedment depth shown as an example); (c) Raising of actuator to accommodate subsequent lateral load test

Pile installation was achieved using a displacement controlled actuator at a rate of 0.05 mm/s. The instrumented pile, *P1* was jacked to its final penetration depth 5*D* at 1*g*. The un-

instrumented piles were jacked to an initial depth of $2D$ at $1g$ to maintain vertical stability at elevated g-levels, see Figure 3.3(a). Following this the centrifuge was spun-up to $100g$ and the piles were jacked to their final embedment depth $5D$ (*P2*) and $3D$ (*P3*), see Figure 3.3(b).

A friction-reducing ball connection [71] was used to transfer the lateral load produced by actuator to the pile head, see Figure 3.4. The ball was placed vertically into the open-end of the pile head, where it rested in contact with the internal wall of the pile. Between the pile inner surface and the ball, a Teflon collar was used to minimize interface friction.
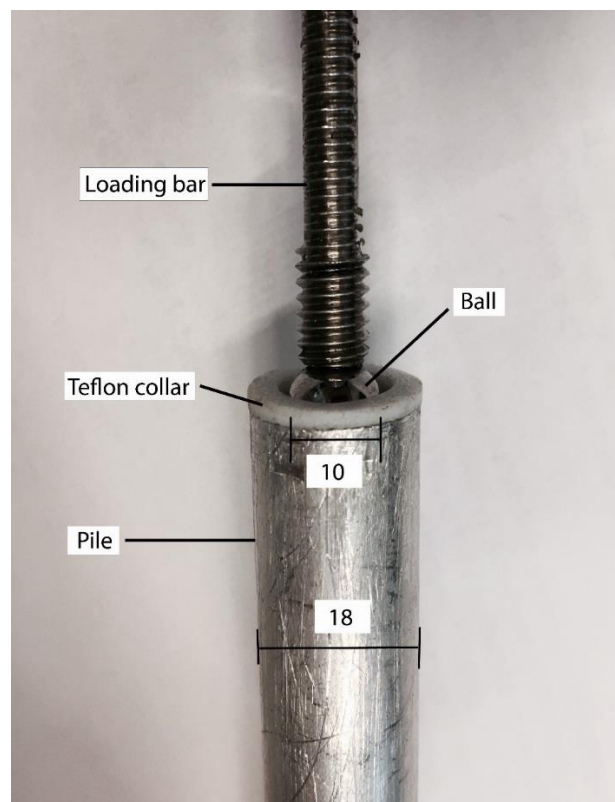
Figure 3.4 Ball connection for reducing pile-head constraint (all dimensions in mm)

During combined loading tests the vertical load (*V*) was applied using dead weights. The lateral load (*H*) for the pile installed at $1g$ was monitored at the pile head by parallel beam load cells (HTC-SENSORS; TAL220) with a measuring range of ±100 N and sensitivity 0.05%, see Figure 3.5.

In order to perform lateral tests following in-flight installation without stopping the centrifuge, a 200 N load cell (SIMBATOUCH; SBT620 with a sensitivity 0.2%) was placed in between the lateral motor and the vertical loading tower, see Figure 3.3. The parallel beam load cell

cannot be used in this test program, due to the potential high bending moment caused by the pile vertical installation.

The vertical and lateral displacements of the pile at the loading position (pile head) can be monitored by the vertical and lateral motor encoders, the accuracy of which are of the order of approximately 3×10^{-5} mm.

The experimental programme comprises a total of 14 centrifuge tests, summarised in Table 3.3. The tests are described using pile number, acceleration level during installation and test type. Therefore P1-1g-L1 refers to the 1st lateral load test performed on Pile *P1*, which was installed at 1g. Each test was conducted twice to ensure repeatability.
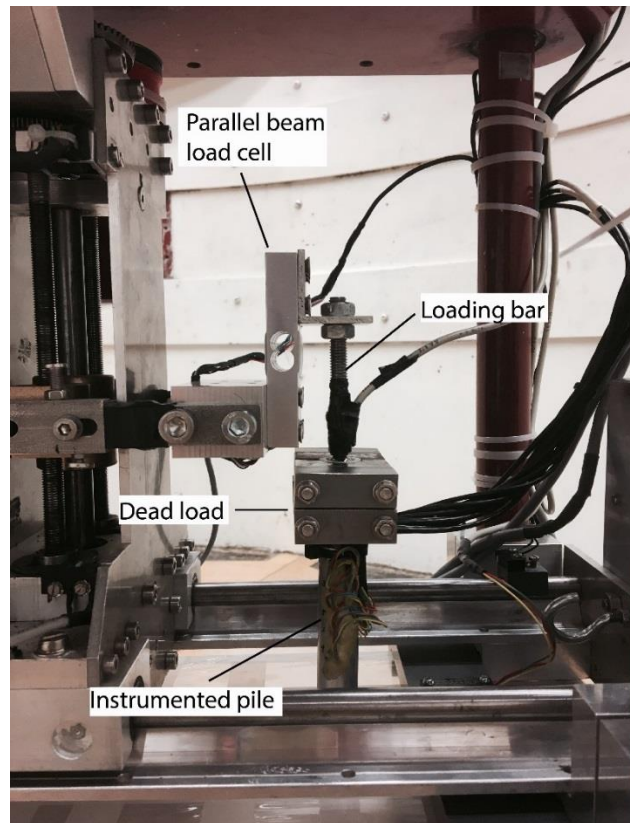
Figure 3.5 Picture of arrangement of testing components on the instrumented pile (pile *P1*)

Table 3.3. Summary of pile test programme

Test number	Pile *L/D*	Test nature	Vertical load	k_{ini} (MN/m)
		Obtain vertical		-
P2-100*g*-V	2*	capacity (V_u)	0 to V_u	-
				-
P1-1*g*-L1	5	Assess influence	0	9.2
P1-1*g*-L2	5	of vertical loading	$0.15V_u$	10.2
P1-1*g*-L3	5	on lateral capacity	$0.225V_u$	11.5
P1-1*g*-L4	5		$0.3V_u$	12.2
P2-100*g*-L1	5		0	11.5
P2-100*g*-L2	5		$0.225V_u$	13.1
P2-100*g*-L3	5	Assess influence	$0.45V_u$	15.3
P2-100*g*-L4	5	of vertical loading	$0.675V_u$	16.7
P2-100*g*-L5	5	on lateral capacity	$0.9V_u$	20.4
P3-100*g*-L6	3		0	1.8
P3-100*g*-L7	3		$0.27V_u$	3.6
P3-100*g*-L8	3		$0.55V_u$	4.9
P3-100*g*-L9	3		$0.82V_u$	7.6

*Pile has 2*D* initial embedment before the vertical load test begins

3.3 Experimental results

3.3.1 Vertical load-displacement response

As a first-step in the experimental procedure the vertical capacity, V_u, of each pile was determined. For the piles installed in flight, V_u was defined as the vertical load (jacking force) required to achieve the target penetration depth. Considering Figure 3.6, it can be seen that the results from repeat tests are extremely consistent, this was seen throughout the test programme. The vertical capacity for Pile *P3*, with *L/D* = 3, is 12 MN; whilst Pile *P2*, with *L/D* = 5, has a vertical capacity of 20 MN. The effect of installation method, i.e. installed at 1*g* rather than 100*g* is evident from the initial stiffness of Pile *P1*. For consistency, V_u of *P1* is assumed to be equal to *P2* in the following.
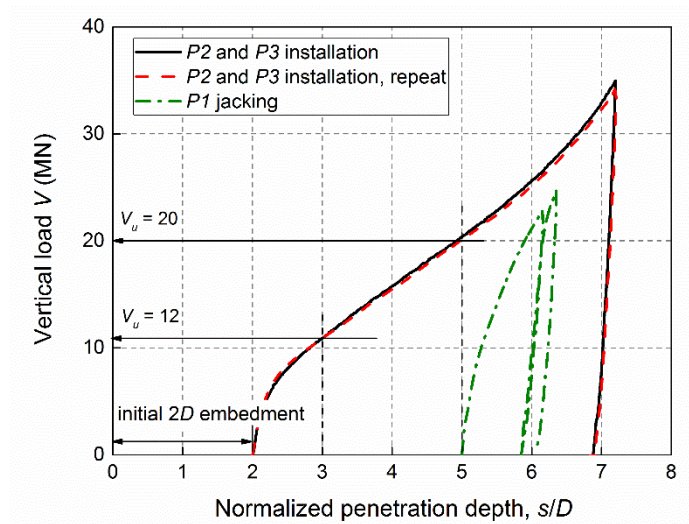
Figure 3.6 Determination of vertical capacity of the tested piles

3.3.2 Lateral load-displacement response

In this section, the lateral load-displacement behaviour of each pile for each of the cases detailed in Table 3.3 is reported.

Influence of the installation stress level on the pile lateral response

The lateral load-displacement response curves for the pile installed at $L/D = 5$ are shown in Figure 3.7. The pile installed in-flight (P2-100g-L1) exhibits both larger initial stiffness (k_{ini}) and lateral resistance than that of the pile pre-installed at 1g (P1-1g-L1). This suggests retention of high mean stresses caused by the installation process affect the lateral load-displacement response even at very large lateral displacements. When the pile was in-flight installed, the inner filling ratio (plug length of the sand divided by the pile embedment length) is 54.7%. While when pile was pre-installed, fully coring was observed. Definitely, when plugging appears, the volume of sand inside the pile is smaller than that without plugging (fully coring). Therefore, under the plugging condition, the density of the sand around the pile can be larger than without plugging, which helped to explain the increased pile lateral resistance. The same trend is evident in Figure 3.7 for combined loading tests where the vertical load was fixed at $0.225V_u$.

In this paper the lateral capacity, H_u is defined as the lateral resistance developed when the pile head displacement at the mudline level reaches 10% of the pile diameter (D) in keeping with recommendations by Lee [24]. Although both piles in Figure 3.7 are seen to develop lateral

resistance that increase with displacement, H_u is defined as 0.64 MN and 0.93 MN for piles *P1* and *P2,* respectively.
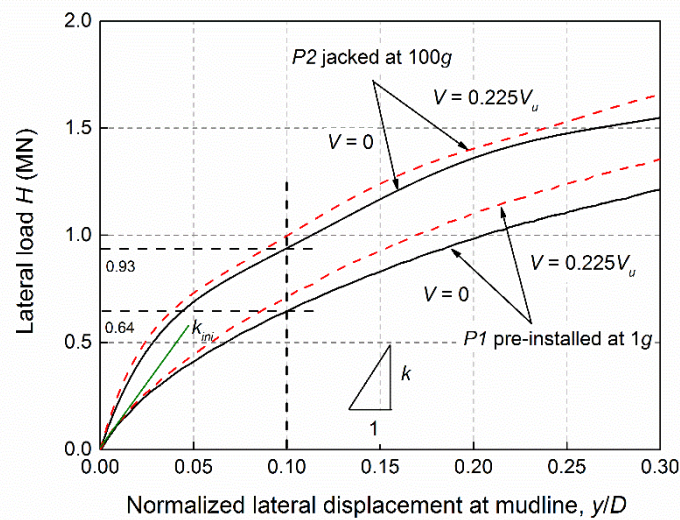
Figure 3.7 Influence of pile installation stress level on the lateral load-displacement curves ($L/D = 5$)

Effect of vertical loading on the pile lateral response

The influence of vertical loading on the lateral load-displacement response for the piles installed to $L/D = 5$ are compared in Figure 3.8. It is apparent that an increase in vertical load resulted in an increase in both the initial stiffness and lateral capacity of the piles. This trend is broadly similar for piles pre-installed at $1g$ and jacked at $100g$ within the mudline lateral pile displacement of $0.1D$.

The likely mechanism controlling the increase in initial stiffness and the lateral capacity in the presence of vertical loading is the increased mean stress level in the sand caused by the pre-application of the vertical load. This causes an increase in the sand stiffness and strength thereby increasing the lateral resistance [22, 84]. The experimental results presented in Figure 3.8 are consistent with the centrifuge study of Mu et al. [20] and Lu and Zhang [22].
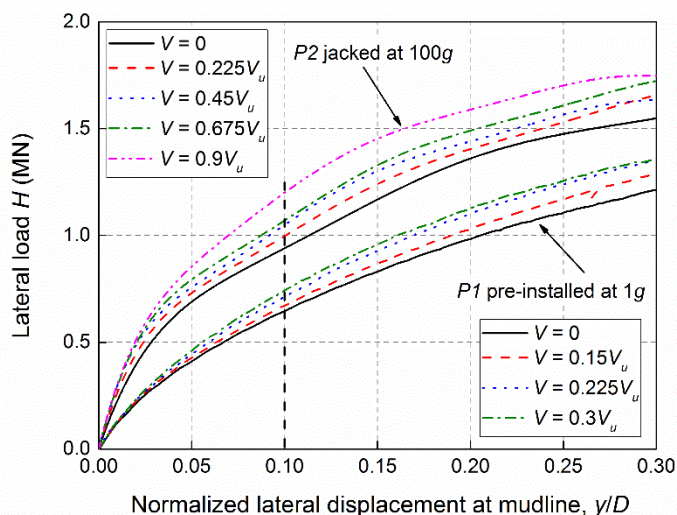
Figure 3.8 Influence of vertical loading on the lateral load-displacement curves: piles pre-installed at $1g$ and jacked at $100g$, $L/D = 5$
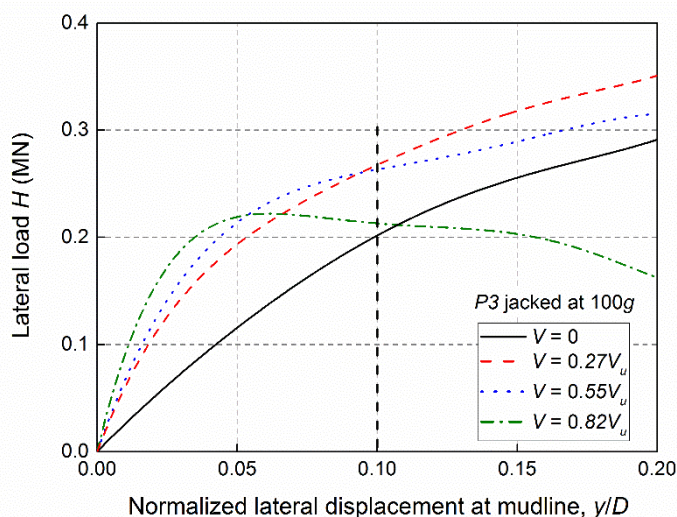
Figure 3.9 Influence of vertical loading on the lateral load-displacement curves for pile jacked at $100g$ with $L/D = 3$

The influence of vertical loading on the lateral load-displacement response for the piles installed to $L/D = 3$ are shown in Figure 3.9 (see Table 3.3). The data shows that the initial stiffness of the curves increased with the application of vertical load. The pile lateral resistance also increased up to a lateral mudline displacement of approximately $0.05D$. For tests with applied vertical loads of 0, $0.27V_u$ and $0.55V_u$ the lateral resistance continued to increase with increasing lateral displacement. However, the rate of increase for the pile with a vertical load of $0.27V_u$ is higher than the pile with $0.55V_u$, such that at $y/D = 0.1$, the lateral capacity measured in both tests was approximately equal. In the test where the applied vertical load is $0.82V_u$, the resistance reduces for displacements larger than $0.05D$ and the H_u value at $y/D = 0.1$ is only

slightly higher than the pile with no vertical load. From the data it is clear that the pile slenderness ratio (L/D) and the vertical load level (V/V_u) has an influence on the load-interaction response of monopiles, see Lu and Zhang [22].

Effect of vertical loading on the pile lateral capacity

The influence of vertical loading on the pile lateral capacity (H_u) can be expressed by the following equation [20, 84]:

$$\vartheta = H_{u,V>0}/H_{u,V=0} \tag{3.1}$$

where ϑ is defined as the normalized pile lateral capacity; $H_{u,V>0}$ is defined as the pile lateral capacity under combined vertical and lateral loads; and $H_{u,V=0}$ is defined as the pile lateral capacity under pure lateral load. It should be noted that the data in Figure 3.9 makes it clear that ϑ is very sensitive to the definition of the y/D value at which the pile lateral capacity is defined.

A summary of the ϑ values from all tests is shown in Figure 3.10, which reveals the following:

1. The data shows that for the range of parameters considered in the test programme ϑ is always greater than unity, meaning the application of vertical loading is always beneficial to the lateral capacity of piles.

2. For piles with $L/D = 3$ the lateral capacity increases initially as the vertical load increases. The normalized pile lateral capacity reaches a peak value when the vertical load is between $0.4V_u$ and $0.5V_u$. When vertical load surpasses a certain value early failure in the sand might happen, therefore the beneficial effect of vertical loading on the pile lateral capacity reduces. A parabolic failure locus similar in shape to those reported for shallow foundations by Nova and Montrasio [77] appears to match this pile response well.

3. For piles with L/D of 5, the pile lateral capacity increases non-linearly with increasing vertical load, the benefit increases as vertical load level increases. At a given V/V_u value the beneficial effect is smaller than that seen on the pile with $L/D = 3$ for V/V_u below 0.8.

4. Comparing the data for pile with $L/D = 5$, i.e. *P1* and *P2* we note that the results are very sensitive to the V_u value chosen for the normalisation. Whilst V_u was measured

directly for the *P2* and *P3* as the jacking force required for installation, see Figure 3.6, pile *P1* was jacked at 1*g* and thus the V_u value that should be adopted in the normalisation is not straight-forward. A vertical load test performed in-flight from an initial embedment depth of 5*D* on this pile is shown in Figure 3.11. It is clear that a very large pile displacement of 0.9*D* was required to mobilise the V_u value of 20 MN adopted for consistency with *P2* (thus the pile embedment is 5.9*D*). An alternative definition of V_u that might be more in keeping with the stress state effective at the time of the lateral load test is to define V_u at the point at which the pile stiffness decreases significantly in the vertical load test. From Figure 3.11 an alternative definition of V_{u_pre} for *P1* is 6.5 MN. Replotting the data in Figure 3.10 with this lower V_u value for pile *P1* shows comparable behaviour with pile *P2*.
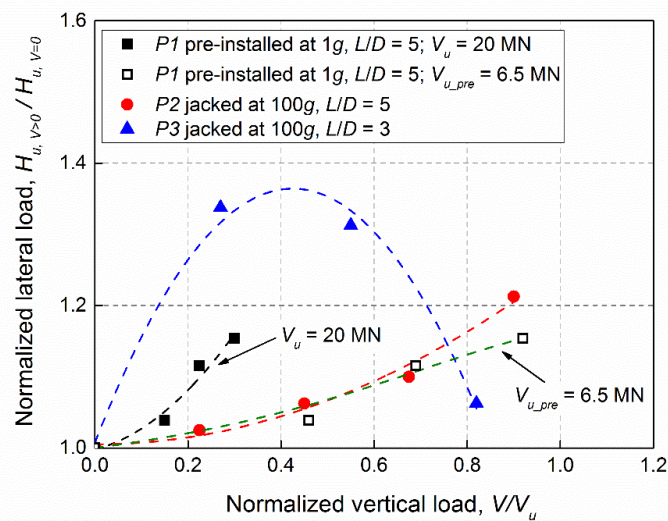
Figure 3.10 Influence of vertical loading on the lateral capacity of the model piles
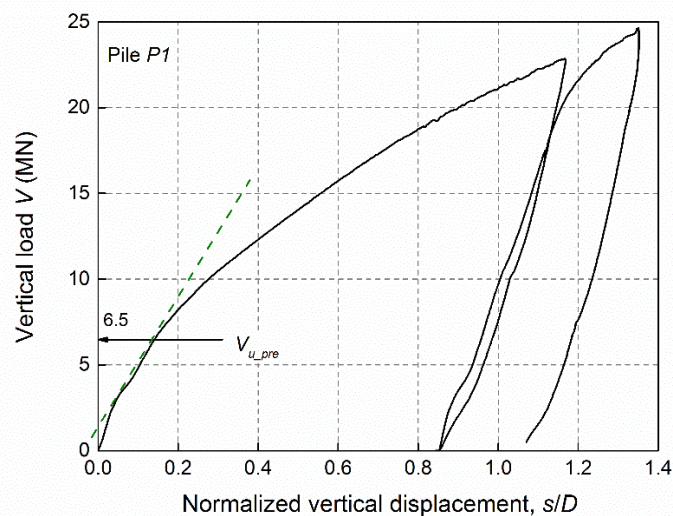
Figure 3.11 Vertical load-displacement curve on the pre-installed pile with *L/D* = 5

3.3.3 Influence of vertical loading on *p-y* curves for monopiles

In the previous section, it was observed that the application of vertical loading is beneficial for the lateral load-displacement behaviour of a pile. In this section, the impact of vertical loading on the *p-y* curves mobilised along the depth of pile *P1* is discussed.

Bending moment distribution

The bending moment on pile *P1* can be calculated from discrete strain gauge data using Equation (3.2).

$$M(z) = EI\rho(z) \tag{3.2}$$

Where: *EI* is the flexural rigidity of the pile (Nm^2) and $\rho(z)$ is the curvature corresponding to a given applied load. Curvature is obtained as the ratio of the difference in measured compressive and tensile strains to the gauge lever arm (pile diameter) at each depth *z*, see Li et al. [71].

The evolution of bending moment for a pile with $V = 0$ (Test P1-1*g*-L1) is shown in Figure 3.12. As the lateral load increases to 0.393 MN, the bending moment increases uniformly with the maximum bending moment occurring at a depth, *z*, of between 2 and 3 m at each loading stage. Note, the strain gauge at the depth $z = 6$ m was damaged, therefore the data was missing.
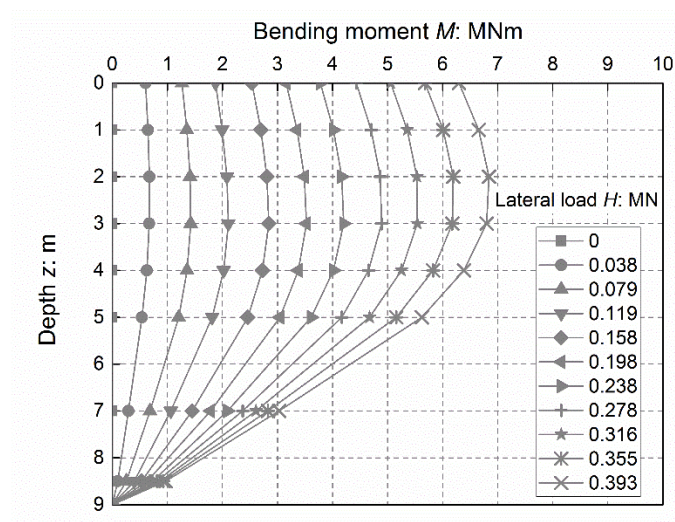
Figure 3.12 Pile bending moment distribution ($V = 0$)

Derivation of *p-y* curves from strain gauges

Lateral soil reaction-displacement (*p-y*) curves can be derived from bending moment profiles, with the soil reaction *p* being derived by double differentiation of the bending moment profile and the pile lateral displacement *y* at discrete locations obtained by double integration of the bending moment profile, see Equations (3.3) and (3.4).

$$p(z) = \frac{d^2 M(z)}{dz^2} \tag{3.3}$$

$$y(z) = \iint \frac{M(z)}{EI} dz dz \tag{3.4}$$

Where: *M(z)* is the bending moment at depth *z*, and *EI* denotes the pile flexural rigidity. Given the double differentiation propagates measurement errors it is common to apply curve fitting techniques to minimise these errors, see Xue et al. [72]. Polynomial curve-fitting method [73] is adopted herein for curve-fitting the moment data. The choice of the order of the fitted curve is important to minimise errors between the discrete moment points and the values from the continuous curve at these locations. A 5th order polynomial is used for the moment data to generate soil reaction (by differentiation) and a 7th order polynomial is used to obtain soil displacements (by integration).

Using this approach, *p-y* curves derived from the bending moment profile for test pile P1-1*g*-L1 (*V* = 0) are shown in Figure 3.13. The normalised lateral displacement profiles seen in Figure 3.13(a) show that the pile lateral displacement (*y*) is almost linearly distributed demonstrating rigid pile behaviour, with 'toe-kick' [85, 86] evident at pile penetrations below 6.3 m. The corresponding normalised soil reaction profiles along the pile are shown in Figure 3.13(b) with large soil resistance mobilised at the pile toe. The data can be combined in the form of *p-y* curves in Figure 3.13(c), which shows the lateral soil resistance and stiffness increase with depth as expected.

(a)   (b)

(c)
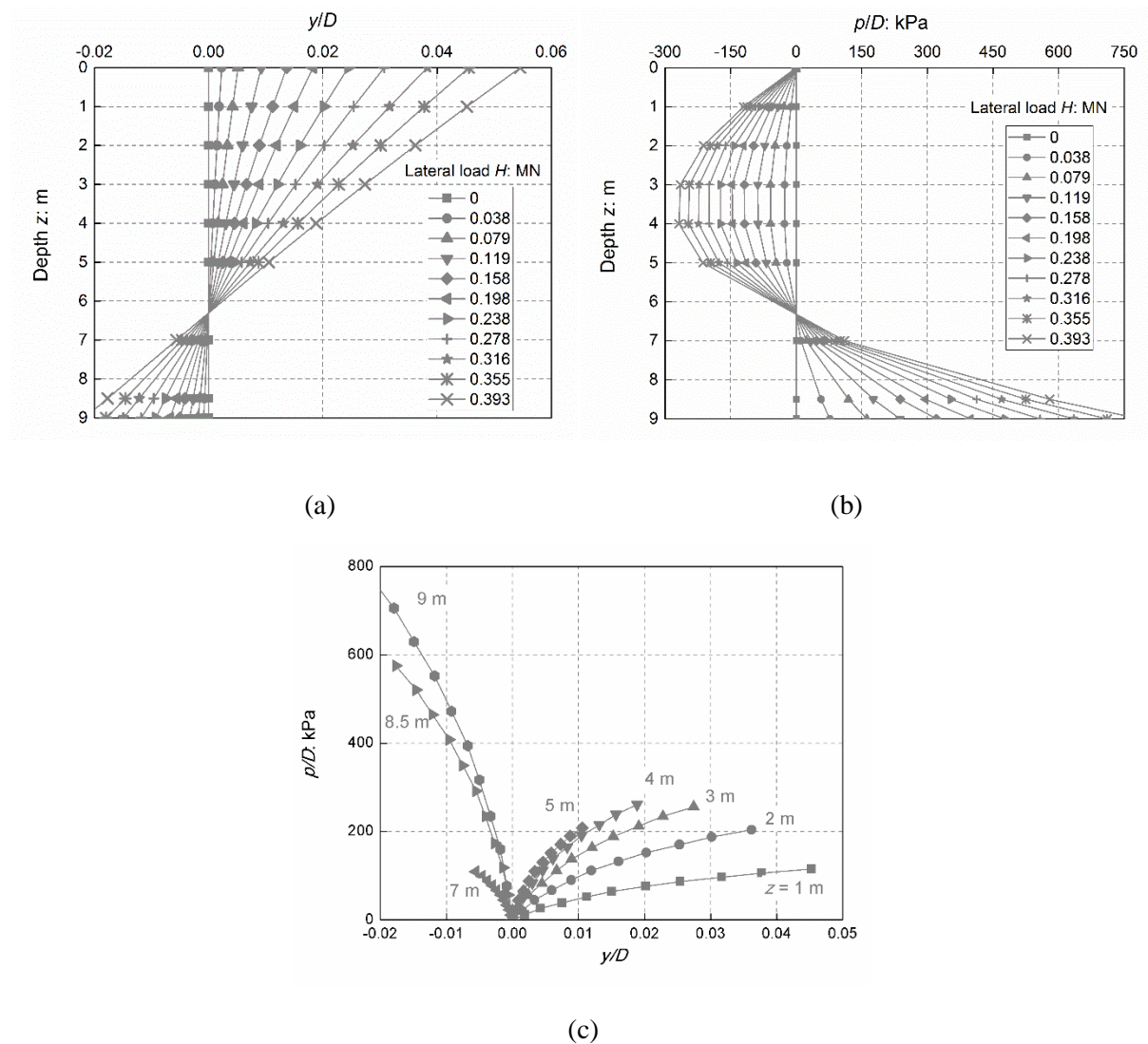
Figure 3.13 Derivation of *p-y* curves for test P1-1*g*-L1 (*V* = 0): (a) Displacement profiles; (b) Soil reaction profiles; (c) *p-y* curves

Effect of vertical loading on *p-y* curves

In this section, the influence of applied vertical loading on the derived *p-y* curves is studied. The curves are derived using the procedure detailed in the previous section. Figure 3.14(a-d) show the influence of vertical load level on the *p-y* curves derived at increasing depths, from z = 2 m to 5 m respectively on the active side of the pile. It is evident that the stiffness and normalised resistance (p/D) generally increase as the vertical load level increases from 0 to $0.3V_u$.
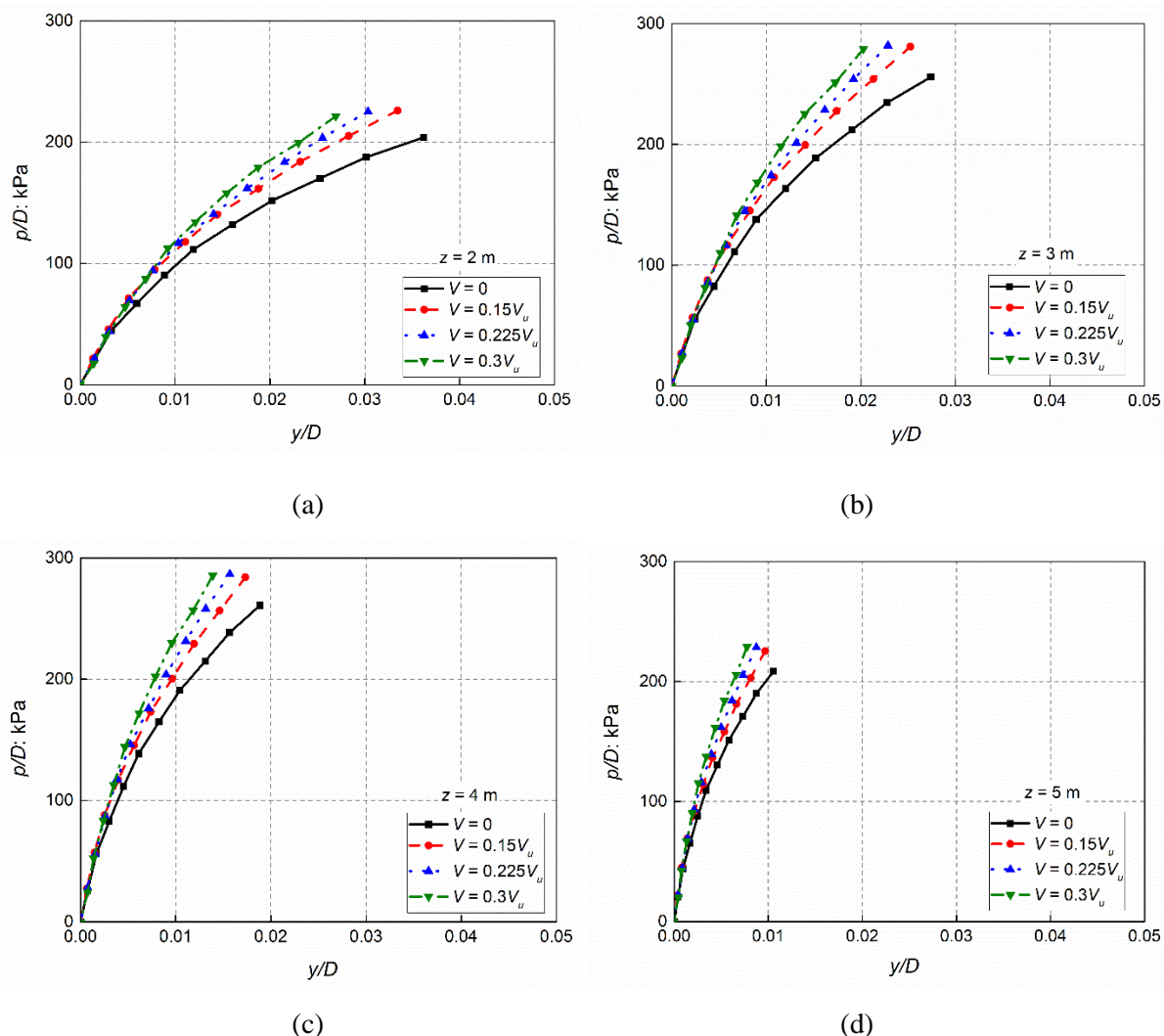
Figure 3.14 Influence of vertical loading on *p-y* curves at various depths (a, b, c, d: *z* = 2-5 m)

Mu et al. [20] suggests the influence of applied vertical loading on the soil resistance can be quantified using the following equation:

$$\chi = \frac{p_V - p_0}{p_0} \qquad (3.5)$$

where χ is defined as the improvement in lateral soil resistance at some reference displacement level due to the application of vertical loading. p_0 is the lateral soil resistance for zero vertical load and p_v is the lateral soil resistance when the applied vertical load is non-zero.

Considering Figure 3.14(a) and taking y/D = 0.01 as the reference displacement level, the normalised soil reaction p_v/D increases by 10%, 23% and 46% over the p_0/D value as the vertical load increases to $0.15V_u$, $0.225V_u$ and $0.3V_u$ respectively. Similar data from all soil

depths is summarised in Figure 3.15, which shows an approximate linear increase of χ as the vertical load level increases.
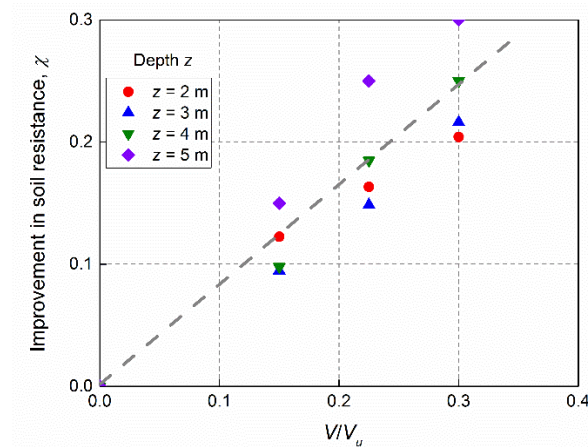
Figure 3.15 Improvement in soil resistance under applied vertical load (at $y = 0.01D$)

Comparison with experimental and API *p-y* curves

The *p-y* curves implemented in the offshore design codes, such as the American Petroleum Institute [API, 18] edition, were adapted from load tests on relatively slender piles. Recognising the limitations of the approach for rigid monopiles, several authors have derived *p-y* curves for piles of varying geometries. Choo and Kim [87] proposed experimental *p-y* curves based on centrifuge tests of 6 m diameter (at prototype scale) monopiles installed in dense sand. Qi et al. [88] conducted a series of centrifuge tests at a scale of 1:250 to investigate the influence of scour erosion on the lateral behaviour of piles. The model pile used has an equivalent prototype diameter of 2.75 m and an embedded length of 31.25 m.

The *p-y* curves derived experimentally in this paper were compared with those from API [18], Choo and Kim [87] and Qi et al. [88]. To facilitate comparison across scales, *p-y* curves were normalized (presented in dimensionless form). These curves at a normalized soil depth of $z = 2D$ are shown in Figure 3.16. The *p-y* curves from this paper correspond well to the *p-y* curve from the pile with $L/D = 7.1$ from Choo and Kim [87], which was installed in a single layer of dense sand with $D_r = 82\text{-}86\%$. The *p-y* curve derived by Qi et al. [88] on the other hand exhibits very soft behaviour, though the pile tested has a larger *L/D* (11.4).

For the *p-y* curve derived using the API method, "failure" is reached at a relatively small lateral displacement (e.g. 0.008*D*). The initial stiffness in the API *p-y* relationship is much greater than

those determined from the centrifuge experiments. The API method is otherwise considered to be conservative, however, in this case the initial stiffness and strength are over-predicted significantly.
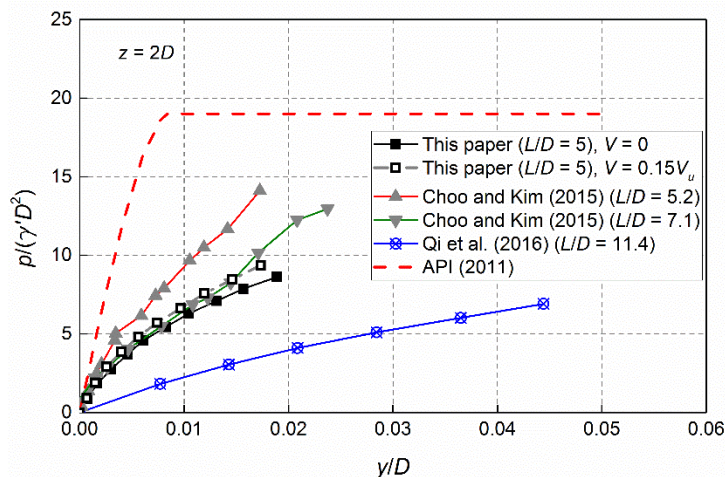
Figure 3.16 Comparison of normalized *p-y* relationships obtained in this study with those from previous literature at a normalized depth $z = 2D$

The experimental data in Figure 3.16 suggests that the *p-y* response is very sensitive to pile *L/D* ratio. This is in keeping with the results of major experimental and numerical test programmes such as the recently completed PISA project [89, 90]. Considering the significant difference between the *p-y* curves determined from the centrifuge experiments and the API recommendations, further large-diameter rigid pile tests should to be carried out to formulate the database for establishing design criteria. This is especially urgent given the lateral bearing behaviour of large diameter monopiles are still designed based on *p-y* relationships.

3.4 Conclusions

In this study, an experimental investigation into the influence of vertical loading on the lateral response features of monopiles is conducted using physical (centrifuge) modelling. A series of vertical, lateral and combined loading tests were performed on both piles installed at 1*g* and 100*g* (in-flight) in dry dense sand ($D_r = 80\%$). Two different *L/D* ratios were considered to investigate the effect of pile slenderness ratio. The conclusions drawn from this study can be summarized as follows:

1. The application of vertical loading is beneficial to the lateral capacity and stiffness of piles with L/D in the range 3 to 5.

2. For piles with an L/D ratio of 5, the beneficial effect of vertical loading increases as the ratio of V/V_u increases.

3. For piles with $L/D = 3$ the lateral capacity increases initially as the vertical load increases. The normalized pile lateral capacity reaches a peak value when the vertical load is between $0.4V_u$ and $0.5V_u$. For higher vertical loads early failure in the sand might happen, therefore the beneficial effect of vertical loading reduces.

4. Notwithstanding this the net benefit to the lateral capacity on piles with $L/D = 3$ is higher than for a pile with $L/D = 5$ when the ratio V/V_u is below 0.8.

5. For a pile with $L/D = 5$, the normalised lateral soil resistance p/D measured at a normalised lateral displacement of $0.01D$ increases approximately linearly as the V/V_u increases.

6. The data shows that the method of pile installation has a clear influence on the stiffness and lateral bearing resistance of the piles tested in this study. The plugging behaviour for the in-flight installed pile may have caused a denser sand condition around the pile. Installing the piles in-flight leads to a higher retention of lateral stress, which manifest as a larger initial stiffness and higher lateral resistance at corresponding displacements than for piles pre-installed at $1g$.

The test results show that the influence of vertical loading on the pile lateral capacity are dependent on the pile L/D ratio. A comparison of the experimental p-y curves reveals that application of vertical loading increases both the stiffness of the p-y curves and the soil resistance. Future work will focus on quantifying the benefits obtained under combined loading conditions in a design framework. The results in this paper will be on interest for the offshore geotechnical design of large-diameter monopiles.

4 Lateral response of rigid monopiles subjected to cyclic loading: centrifuge modelling

In this study, a total number of 21 centrifuge tests were carried out to investigate monopile behaviour under lateral cyclic loading. The instrumented model pile simulates an offshore wind turbine foundation with an embedment ratio of 5 installed in sand layers with two relative densities of 80% and 50%. Influence of cyclic load directional characteristic and amplitude on pile lateral behaviour was studied. Moreover, the behaviour of the monopile subjected to storm loading has been investigated. Reaction curves were generated based on the measured bending moment distribution along the depth and the load-displacement data near the pile head. The data analysis focused on the influence of cyclic load on the accumulation of lateral displacement, evolution of secant stiffness, the changing of bending moment and the alternation of the p-y reaction curves. The most damaging cyclic loading type (the cyclic type which can cause the most accumulated pile displacement) is identified as two-way loading, and cyclic loading always increases the pile secant stiffness. Cyclic p-y curves show different evolution trends according to soil depths. A new model for the prediction of evolution of pile head accumulated displacement and change in secant stiffness has been formulated. An example of the developed procedure is presented for a typical field monopile subjected to a cyclic loading. Lastly, the performance of the new model is demonstrated and predicted results are compared with a field test data.

4.1 Introduction

The current design codes of monopiles for offshore wind turbine (OWT) foundations are largely based on the application from oil and gas industry. The fundamental difference between monopiles used as OWT foundations and those in the oil and gas industry is the lower embedment ratio (L/D) generally used for OWT foundations, ranging between 3 and 6 [3]. These foundations are subjected to a large number of loading cycles, and strict permanent rotational limits are imposed. Moreover, OWT are dynamically sensitive structures and slight changes in stiffness of the foundation might result in an undesirable shift in the natural frequency of the whole structure. Therefore, understanding the influence of cyclic load on the accumulation of lateral displacements, change in secant stiffness, bending moment, and soil reaction is of great importance for a safe design of these structures.

Two non-dimensional parameters are widely used to describe the applied cyclic load:

$$\zeta_b = \frac{H_{max}}{H_u} \tag{4.1}$$

$$\zeta_c = \frac{H_{min}}{H_{max}} \tag{4.2}$$

where, H_u is defined as pile lateral capacity determined from a monotonic test, H_{min} is the minimum load in the loading cycle, and H_{max} is the maximum load in the same cycle. The value of ζ_b can be used to define the load amplitude for the cyclic loading, while ζ_c can be used to describe the directional characteristic of the cyclic loading. A visual interpretation of these two parameters is given in Figure 4.1.
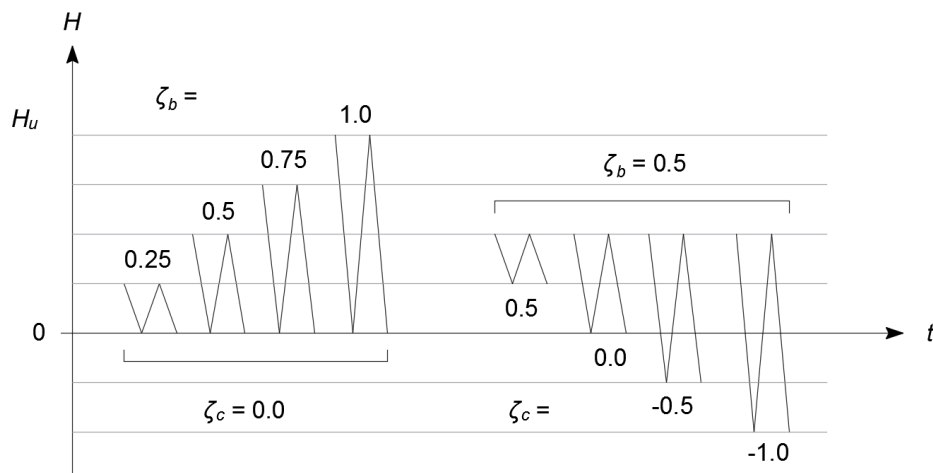
Figure 4.1 Characteristics of cyclic loading defined in terms of ζ_b and ζ_c

A number of experimental studies have been conducted to investigate the response of monopiles under lateral cyclic load [25-49]. LeBlanc et al. [41] carried out $1g$ experiment on a pile with L/D ratio of 4.5 embedded in a dry loose sand (D_r = 4-38%) layer. It was found that the most damaging loading type (the cyclic type which can cause the most accumulated pile displacement) is two-way loading with ζ_c = -0.6. Moreover, they reported that the secant stiffness increased with the number of cycles. Klinkvort et al. [91] carried out a centrifuge test series simulating cyclic load on a monopile with L/D of 6 in dense sand (D_r = 79-96%). It was indicated that two-way loading (ζ_c = -0.4) is the most damaging load situation. However, they observed that secant stiffness for each cycle tended to decrease when ζ_c > 0.1. Based on the results of a second series of centrifuge tests using similar pile (L/D = 6) and sand (D_r = 90%) Klinkvort and Hededal [92] showed that one-way loading (ζ_c = 0) is the most damaging loading type. Although LeBlanc et al. [41] reported accumulation of rotation was observed regardless of the characteristics of the loading from the $1g$ experiments, it was in contrast to the observation done in centrifuge test by Klinkvort and Hededal [92], where it was seen that the pile starts to move back towards its initial position in two-way loading where $\zeta_c \leq$ -0.63.

Monopiles for offshore wind turbines are typically designed to withstand the lateral loads and overturning moments due to wind and wave effects, based on the Winkler model and is commonly referred to as the *p-y* approach [18, 19]. In this method, *p* is the soil reaction imposed on the pile and *y* is the corresponding lateral pile displacement. However, this approach is formulated using results obtained from experiments on piles with small diameters (usually smaller than 1 m) and with large embedment ratios (for example, L/D = 34 in Mustang Island tests by Cox et al. [34]). Recent experimental data indicates some uncertainty on the reliability of the existing *p-y* approach to predict the lateral behaviour of offshore monopiles [10]. Choo and Kim [87] carried out centrifuge tests on prototype piles with 6 m diameter and L/D ratios of 5.2 and 7.1 in dense sand layers. It was found that the experimental *p-y* relationships for large-diameter monopiles exhibit a softer behaviour than those proposed by the API [18].

The research on the evaluation of cyclic *p-y* curves of large diameter monopiles is rather limited and the slenderness of the monopiles (L/D) has a large variety, therefore, few consistent results regarding *p-y* curves of rigid monopiles exposed to lateral cyclic loading can be seen. Verdure et al. [37] presented a centrifuge programme carried out on a slender pile ($L/D \approx 17$) under one-way lateral cyclic loading for as much as 50 load cycles. Two different zones were observed when looking at the effect of cyclic load on soil reaction mobilization. At small soil depths, the

soil reaction at maximum load decreases with the number of cycle while the pile displacement increases; at larger depths, on the contrary, both the soil reaction and the pile displacement increases with the number of cycles. Klinkvort [43] performed multiple centrifuge tests on rigid monopiles ($L/D = 6$) to simulate a 1-m-diameter monopile at the prototype scale with up to 500 load cycles. An elasto-plastic spring element using the p-y curve concept is applied allowing definition of unloading-reloading branches, hence enabling modelling of pile cyclic response. Lee et al. [49] performed centrifuge model tests on a pile with diameter of 3.3 m and L/D of 12 to examine the lateral behaviour of a monopile embedded in dry sand under cyclic loading. The experimental cyclic p-y curve was obtained through the tests, and the maximum soil resistance points that were found for each load cycle were used to find the cyclic p-y backbone curve for each depth. The two variables which are needed to define the cyclic p-y backbone curve, i.e. the initial modulus of subgrade reaction and ultimate soil resistance, were suggested as functions of the physical properties of the soil and the pile. The cyclic p-y curve of the first cycle and the 100th cycle were formulated to present the upper limit and lower limit.

In the framework of this study, a series of centrifuge model tests has been conducted to simulate open-ended monopiles with an embedment ratio of 5 subjected to both significant lateral load and overturning moments. Given the contrasting findings from previous studies, this work focuses on two important issues for the design of monopile foundations for offshore wind turbines, namely: (i) the accumulation of the lateral displacement; (ii) the evolution of the secant stiffness per loading cycle. The bending moment profiles have been obtained from strain measurements along the pile and the experimental p-y curves are developed. Comparison has been made between the p-y curves obtained from this study and from API [18]. Influence of storm loading on the cyclic p-y reaction curves has also been investigated. The impact of number of cycles, load magnitude and the directional characteristic of loading on these properties were captured by a model framework featured with both non-dimensional and dimensional functions.
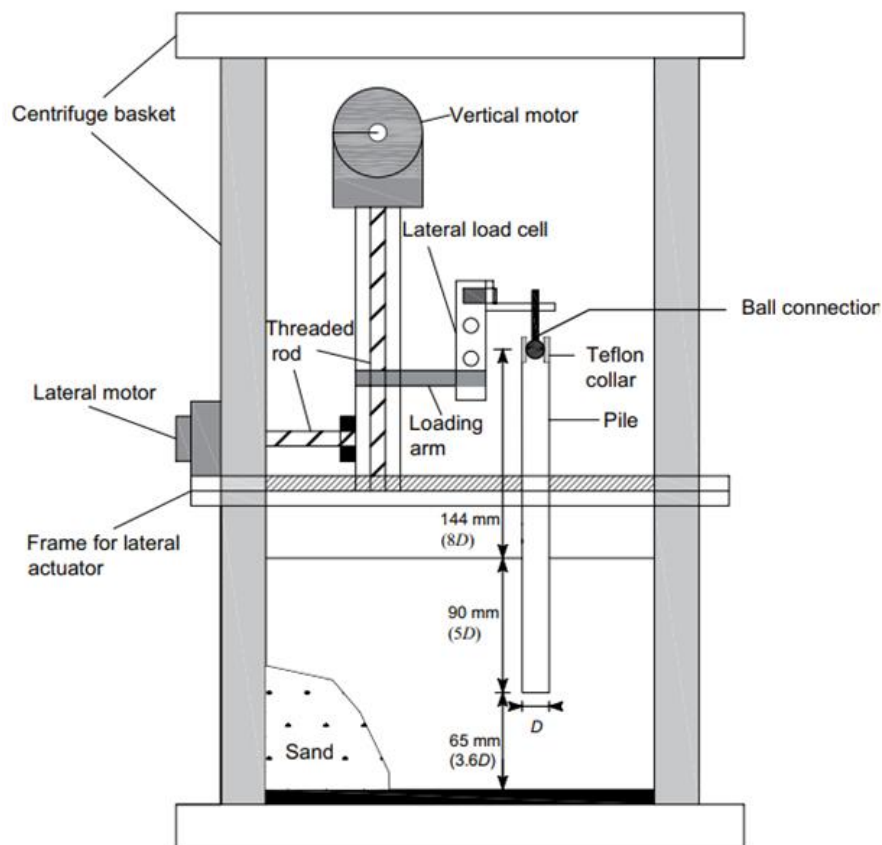
Figure 4.2 Schematic diagram of the two dimensional loading actuator

4.2 Centrifuge model test

4.2.1 Test facility

The tests were performed using the beam centrifuge of the Geo-Engineering Section at TU Delft [93]. These tests were conducted at 100 times the gravitational acceleration ($100g$). A two dimensional actuator (Figure 4.2) was used to impose lateral load (H) at the pile head. The applied lateral load was measured by parallel beam load cell (HTC-SENSORS; TAL220; measuring range 100 N; sensitivity 0.05%). Lateral displacements at pile head was measured by the signal encoder of the actuator, the accuracy of which is of the order of approximately 3 $\times$ 10^{-5} mm. A specially-designed friction-reducing ball connection was constructed to enable the application of lateral load without inducing any rotational fixity at the pile head. The detailed information on the actuator and the friction-reducing ball connection can be found in Li et al. [71].

4.2.2 Model pile characteristics and installation

An open-ended aluminium tubular pile was used, with an outer diameter (D) of 18 mm and a wall thickness (t) of 1 mm. The load eccentricity e and the embedment depth L of the pile were kept constant at $e = 8D$ and $L = 5D$, respectively. The primary dimensions and material properties of the pile are provided in Table 4.1.

The model pile was instrumented with ten pairs of strain gauges, calibrated for measuring bending moments. The strain gauges are type of FLA-3-11 fabricated by Tokyo Sokki Kenkyujo. The strain gauges were spaced evenly (10 mm) except for the lowest one (15 mm). The pile was coated with a thin layer of epoxy to protect the strain gauges.

The model piles were installed at $1g$ by jacking at a constant rate. The $1g$ installation was conducted due to a risk of damage to the strain gauges, if the installation was done at $100g$ due to the higher shear stresses. However, $1g$ installation does not represent the prototype installing technique and might results in some discrepancies in the lateral stiffness and capacity of the pile [37].

Table 4.1 Characteristics of the model and prototype piles (adapted from Li et al. [71])

Property	Model value	Prototype value*
Length (embedded + additional)	90 + 150 mm	9 + 15 m
External diameter	18 mm	1.8 m
Wall thickness	1 mm (aluminium)	30 mm (steel)
Young's modulus (E)	70 GPa (aluminium)	210 GPa (steel)
Stiffness (EI)	0.136 kPa.m^4	13.7 GPa.m^4
Load eccentricity above sand surface	144 mm	14.4 m

*Assume the prototype pile is made in steel.

4.2.3 Soil characteristics and sample preparation technique

The sand used in this series of centrifuge tests is called Geba sand which is commonly used for mortar and concrete mixes [63]. Its main component is silica (99% SiO_2). The geotechnical properties of the sand are summarised in Table 4.2. The ratio of pile diameter to average grain size of the sands (D/D_{50}) is 164, which is larger than the value of 20 and 60 suggested by Gui et al. [65] and Remaud [66], respectively, where grain size effect becomes negligible for both vertically and laterally loaded piles [81, 82].

Table 4.2 Basic properties of Geba sand [69, 70]

Property	Sand
Average grain size, D_{50} (mm)	0.11
Curvature coefficient, C_C	1.24
Uniformity coefficient, C_U	1.55
Specific gravity, G_S	2.67
Maximum void ratio, e_{max}	1.07
Minimum void ratio, e_{min}	0.64
Critical friction angle, φ_{cr} (º)	35

Dry sand was pluviated into a rectangular model container (centrifuge strongbox) with inner dimensions of 410 (length) $\times$ 150 (width) $\times$ 165 (height) mm^3. Two series of homogeneous sand specimens with relative densities (D_r) of 80% and 50% were prepared.

4.2.4 Loading test programme

Two monotonic and nineteen cyclic tests have been performed, see Table 4.3. The effect of load amplitude was investigated by changing ζ_b ($\zeta_b \in$ [0.2, 0.3, 0.4, 0.5]) while keeping ζ_c at 0, in both dense sand and medium dense sand. To check the effect of loading characteristic, several values of ζ_c with intervals of $\Delta\zeta_c = 0.25$ in dense sand ($D_r = 80\%$) and $\Delta\zeta_c = 0.33$ in medium dense sand ($D_r = 50\%$) were tested. In the simulation of storm loading, test was carried out in dense sand ($D_r = 80\%$), where ζ_c was kept at 0, while 40 cycles was firstly applied at $\zeta_b = 0.17$ to simulate the operational loading, followed by 20 cycles of storm loading with $\zeta_b = 0.5$, then 40 cycles applied at $\zeta_b = 0.17$ again.

Table 4.3 List of centrifuge tests

Test no.	Type	D_r (%)	ζ_c	ζ_b	No. of cycles	α	β
1	Monotonic	80	-	-	-	-	-
2	Monotonic	50	-	-	-	-	-
3	Cyclic	80	-0.75	0.2	153	0.0448	0.0217
4	Cyclic	80	-0.5	0.2	143	0.0668	0.0233
5	Cyclic	80	-0.25	0.2	142	0.0674	0.0264
6	Cyclic	80	0	0.2	42	0.0581	0.0122
7	Cyclic	80	0.25	0.2	150	0.0640	0.0032
8	Cyclic	80	0.5	0.2	141	0.0610	0.0051
9	Cyclic	80	0.75	0.2	151	0.0592	0.0079
10	Cyclic	80	0	0.3	152	0.0791	0.0143
11	Cyclic	80	0	0.4	62	0.0611	0.0178
12	Cyclic	80	0	0.5	102	0.0652	0.0317
13	Cyclic (storm loading)	80	0	0.17	40	0.0570	-
			0	0.51	20	0.2687	-
			0	0.17	40	-0.004	-
14	Cyclic	50	-0.67	0.2	61	0.0838	0.0280
15	Cyclic	50	-0.33	0.2	50	0.0888	0.0146
16	Cyclic	50	0	0.2	151	0.0878	0.0087
17	Cyclic	50	0.33	0.2	67	0.0557	0.0167
18	Cyclic	50	0.67	0.2	152	0.0549	0.0115
19	Cyclic	50	0	0.3	122	0.0816	0.0148
20	Cyclic	50	0	0.4	83	0.0840	0.0210
21	Cyclic	50	0	0.5	151	0.0708	0.0374

4.3 Centrifuge model test results

4.3.1 Monotonic tests

In order to find the pile lateral capacity in dense sand and medium dense sand respectively, two monotonic load tests were performed under displacement controlled mode, where the pile was loaded at a constant displacement rate of 0.02 mm/s. Each test was conducted two times to ensure repeatability. Test repeatability check was done and test results are shown in Figure 4.3. All the data presented is in prototype scale in this paper, unless otherwise noted.

As $e = 8D$, $L = 5D$, pile pivot point is usually assumed to be located at 0.7L (Haiderali et al., 2014; Chortis et al., 2020). Therefore, the lateral displacement at sand surface equals to 0.3 times the lateral displacement at pile head. From Figure 4.3, the load-displacement curves did not reach a peak, i.e. maximum pile lateral resistance, in any of the tests. Therefore, a lateral reference capacity, H_u, was defined at a lateral displacement of 0.135 m (0.075D) at sand

surface. Therefore, the pile lateral capacities were determined to be 600 kN and 440 kN in dense and medium dense sand layers, respectively.
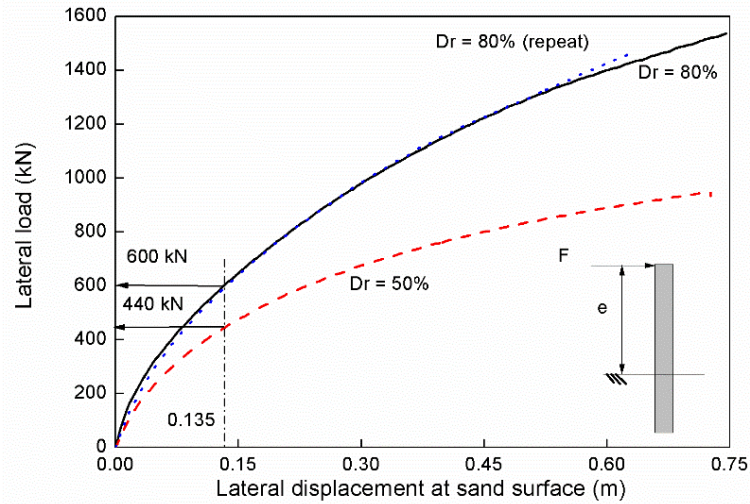
Figure 4.3 Monotonic test results

4.3.2 Cyclic tests

The range of amplitudes of cyclic loads has been selected based on the pile lateral capacity (H_u). The cyclic loading tests were carried out under load controlled mode. Examples of the performed cyclic test series are shown in Figure 4.4. The first loading phase of the cyclic loads fit the monotonic loading curves quite well, which is an indication of the repeatability of the tests.

A power law is used to relate the accumulation rate of pile head displacement to the number of loading cycles:

$$\frac{y_{max,N}}{y_{max,S}} = N^\alpha \tag{4.3}$$

where, $y_{max,N}$ is the lateral displacement corresponding to H_{max} at the Nth cycle and $y_{max,S}$ is the lateral displacement corresponding to H_{max} at the end of monotonic loading phase, respectively. A schematic illustration of these two parameters is shown in Figure 4.5. Figure 4.6 shows an example of the normalised maximum pile head displacement ($y_{max,N}$ /$y_{max,S}$) for a one-way loading test (test no. 10 in Table 4.3). The values of α for all tests are listed in Table 4.3.

(a)   (b)
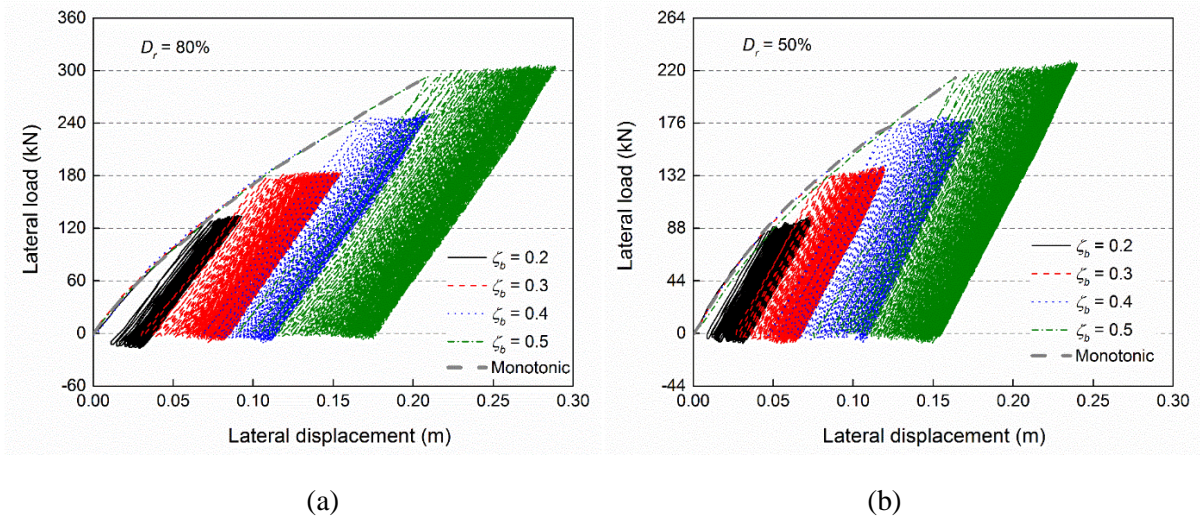
Figure 4.4 Pile lateral load-displacement response during cyclic load tests for the case of $\zeta_c = 0$: (a) $D_r = 80\%$; (b) $D_r = 50\%$
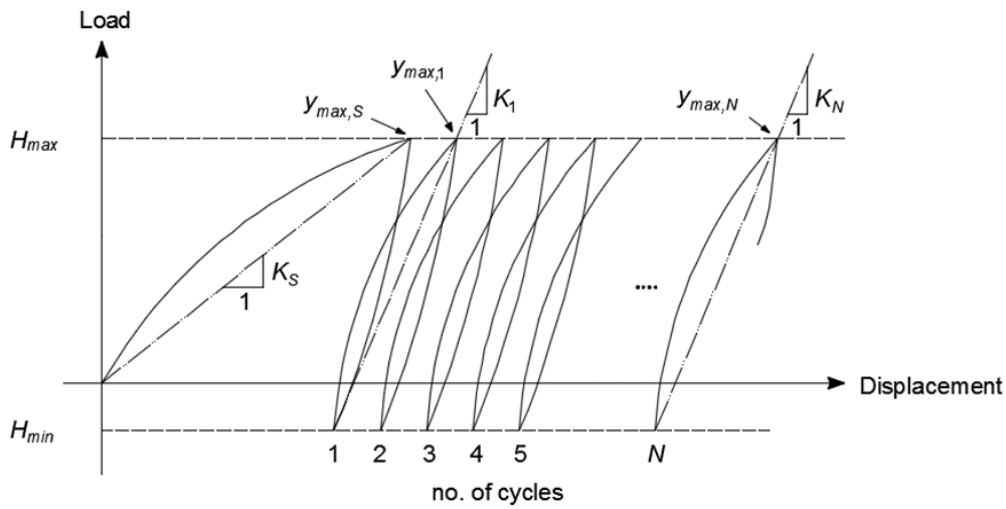
Figure 4.5 Schematic drawing of determination of maximum and minimum accumulated displacements
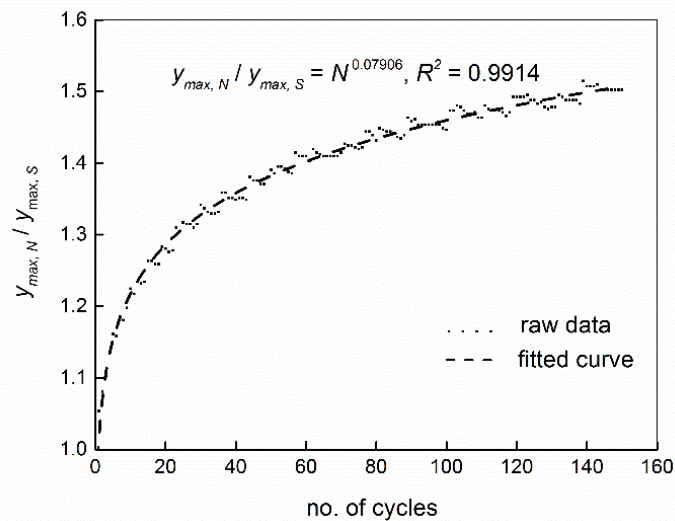
Figure 4.6 Maximum displacement from every cycle: $D_r = 80\%$, $\zeta_c = 0$, $\zeta_b = 0.3$ (test no. 10)

Influence of load directional characteristic ratio (ζ_c) on the accumulated pile head displacement

Twelve cyclic tests were performed in both dense and medium dense sand specimens to identify the most damaging load type in terms of accumulated pile head displacement. Parameter α from Equation (4.3) is used as an indication and is shown in Figure 4.7 as a function of ζ_c for both dense and medium dense sand specimens. In this series of tests, ζ_b is kept constant at 0.2 and the value of ζ_c is changing. According to LeBlanc et al. [41] when $\zeta_c = -1$, it is expected that α would be zero, since the load applied is equal in both directions. The two dashed lines in Figure 4.7 are the best fits of the two series of test data.

It can be observed that sand relative density has an influence on the value of α, i.e. in general α is higher for the pile installed in the sand layer with lower relative density. This observation is more pronounced in cases of two-way loading conditions ($\zeta_c \leq 0$) and for larger values of ζ_c the effect of relative density is minor. Moreover, it can be observed that the values of α do not vary much as a function of ζ_c for medium dense sand with $D_r = 50\%$ in the range of $\zeta_c \in (-0.67, 0)$.

From the data presented, the maximum value of α was found to lie in the range between $\zeta_c = -0.25$ and -0.5. The peak value of α is not that obvious, but perhaps could be located at $\zeta_c = -0.4$. The positive value of α for all of the tests indicates that under all of the loading types the pile always accumulates displacement in one direction (the direction of the first monotonic loading). The phenomenon that pile starts to move back towards its initial position in some two-way loading conditions ($\zeta_c \leq -0.63$) as reported by Klinkvort and Hededal [92] was not observed in this research.
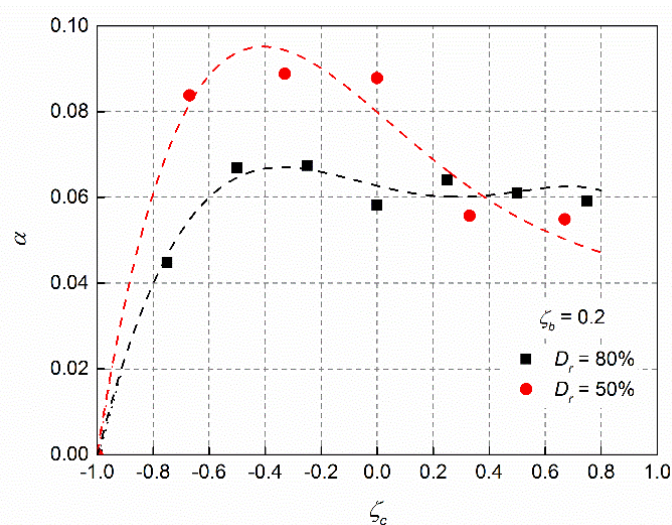
Figure 4.7 Load characteristic effects from cyclic tests

Influence of load amplitude ratio (ζ_b) on the accumulated pile head displacement

The effects of cyclic load amplitude on the accumulated pile lateral displacement regime were investigated by keeping $\zeta_c = 0$ (one-way loading) while changing ζ_b from 0.2 to 0.5. Eight cyclic tests were performed in dense and medium dense sand layers. The value of α derived from the results of these tests is plotted in Figure 4.8. It can be seen that, α is not sensitive to the sand relative density under this specific loading case. Moreover, α is barely influenced by the load amplitude ratio ζ_b. These observations fit well with the results reported by Truong et al. [46], in which the accumulation coefficient of pile head displacement was found to be not sensitive to the cyclic magnitude ratio (ζ_b) but varied with the cyclic directional characteristic ratio (ζ_c).
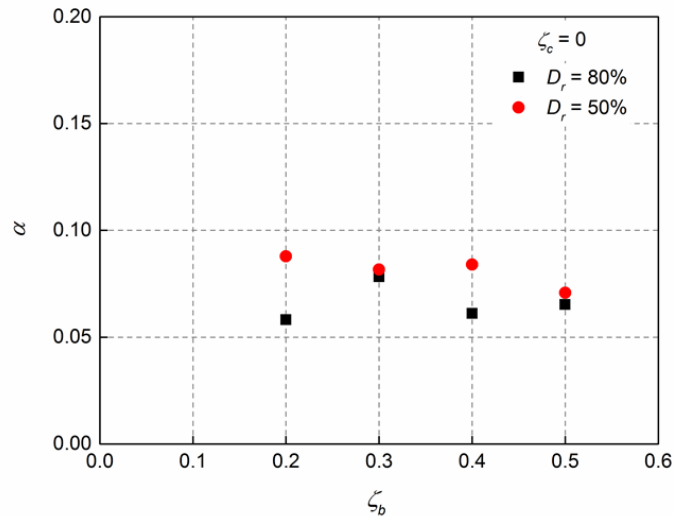
Figure 4.8 Load amplitude effects from cyclic tests

4.3.3 Effect of loading cycles on the pile secant stiffness

The secant stiffness (K) is defined here as the ratio between load increment and displacement increment during a loading phase (either monotonic or cyclic), as illustrated in Figure 4.5.

The secant stiffness in the monotonic loading phase, K_S is calculated based on the first monotonic loading according to Equation (4.4):

$$K_S = \frac{H_{max}}{y_{max,S}} \tag{4.4}$$

where H_{max} is the maximum load applied in the monotonic loading phase, $y_{max,S}$ is the lateral displacement corresponding to H_{max} at the end of the monotonic loading phase .

While secant stiffness under cyclic loading, K_N (for cycle N), is calculated based on the following equation:

$$K_N = \frac{H_{max} - H_{min}}{y_{max,N} - y_{min,N}}$$ (4.5)

where H_{max} and H_{min} are the maximum and minimum loads applied in the cyclic load test, $y_{max,N}$ and $y_{min,N}$ are the lateral displacements corresponding to H_{max} and H_{min} for cycle N, respectively.

In Figure 4.9, the relative secant stiffness K_N/K_1 is plotted against the number of cycles on a logarithmic scale. It is evident that secant stiffness increases with the number of cycles in all the investigated loading cases.

In a similar fashion to the evolution of relative maximum pile head displacement ($y_{max,N}/y_{max,S}$), the evolution of secant stiffness can also be approximated by a power function:

$$\frac{K_N}{K_1} = N^\beta$$ (4.6)

The results of the fitted power function are summarised for each test in Table 4.3.
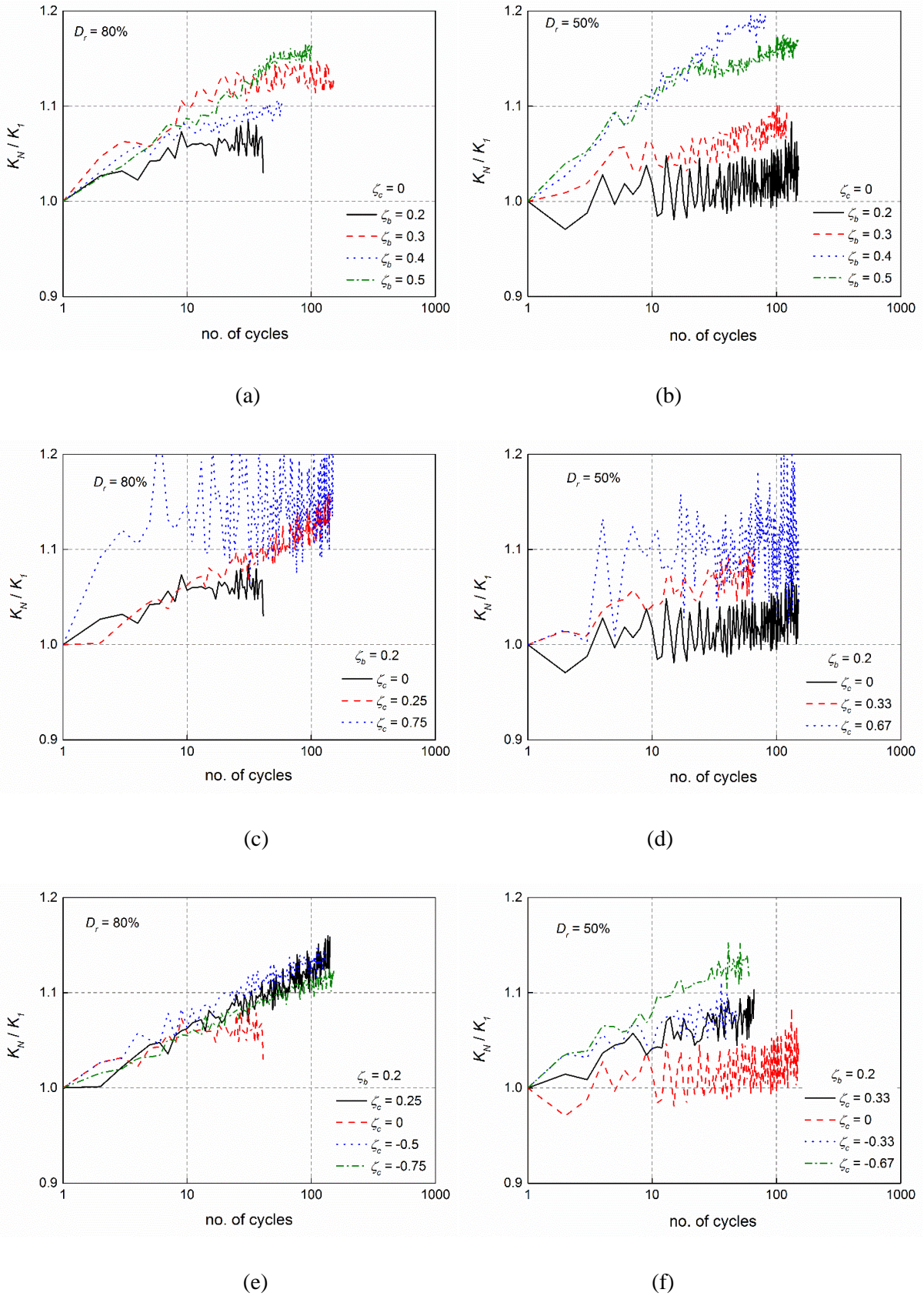
Figure 4.9 Change in secant stiffness from cyclic tests

The values of β from Table 4.3 are plotted in Figure 4.10(a) and Figure 4.10(b) as functions of ζ_c and ζ_b, respectively in both dense sand and medium dense sand.

<div align="center">(a)   (b)</div>
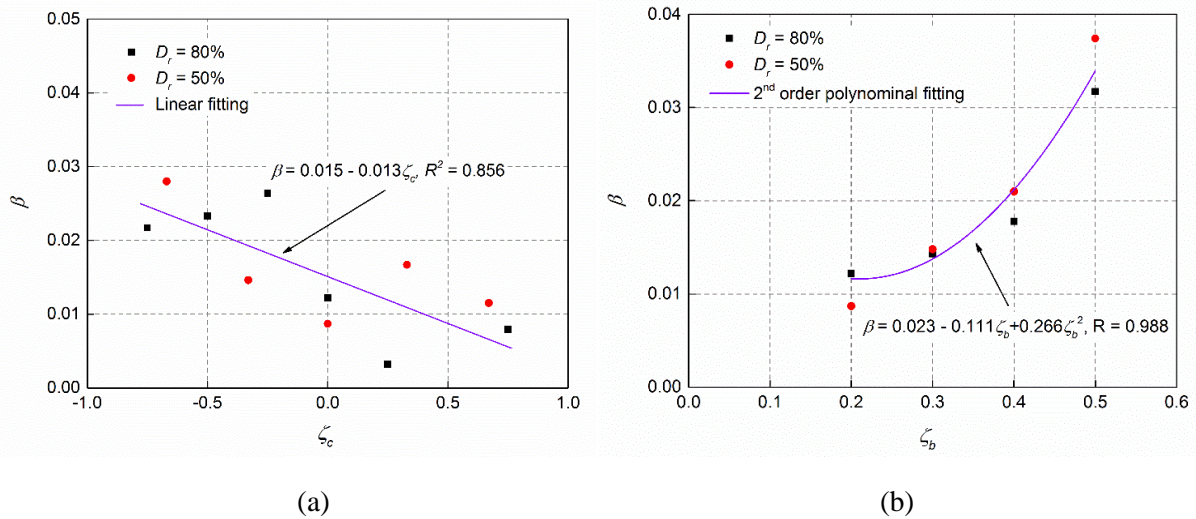
Figure 4.10 Cyclic dimensionless functions for changing in secant stiffness

From Figure 4.10(a), a linear dependency of β on cyclic characteristic ratio ζ_c can be found:

$$\beta = 0.015 - 0.013\zeta_c \tag{4.7}$$

All the β values are positive, which means the secant stiffness keeps increasing as a function of the number of cycles under all of the investigated cyclic directional characteristic ratio (ζ_c). It should also be noticed that a gradual transition from one-way to two-way loading (i.e. traveling from right to left along the x-axis of Figure 4.10(a) leads to an increase of β.

From Figure 4.10(b), an increasing cyclic load magnitude leads to an increase in the relative secant stiffness accumulation rate, β. A second order polynomial fit seems to capture the trend well, see Equation (4.8).

$$\beta = 0.023 - 0.111\zeta_b + 0.266\zeta_b{}^2 \tag{4.8}$$

From Figure 4.10, it is not possible to make a clear distinction between the results for $D_r = 80\%$ and $D_r = 50\%$. This indicates that β is somewhat independent of sand relative density.

4.3.4 Effect of loading cycles on the pile bending moment

The evolution of pile bending moment with the increase of cycle numbers needs to be evaluated for the design of laterally loaded monopiles. An example of the recorded bending moment (M) along the pile embedment depth (z) at the H_{max} of each cycle is shown in Figure 4.11(a) (test no. 12 in Table 4.3). Figure 4.11(b) shows the bending moment according to number of cycles at soil depths of $z/D = 0$ to 2.78. The results indicate that:

1) At depths from $z/D = 0$ to 2.78, bending moment at the H_{max} shows very limited increase (~4%) with the increase of number of cycles within the first 20 cycles. Afterwards the bending moment keeps constant.

2) The maximum bending moment in a certain cycle (the so called "peak maximum bending moment") appears at the soil depth of $z/D = 1.67$, which is upper one-third of the whole pile embedment length. With the increase of cycle number, the depth of "peak maximum bending moment" is observed to be not influenced. Similar observations have been reported on rigid pile ($L/D = 6.5$) [44], semi-rigid pile ($L/D \approx 9.3$) [48] and flexible pile ($L/D \approx 15.6$) [94].

(a)   (b)
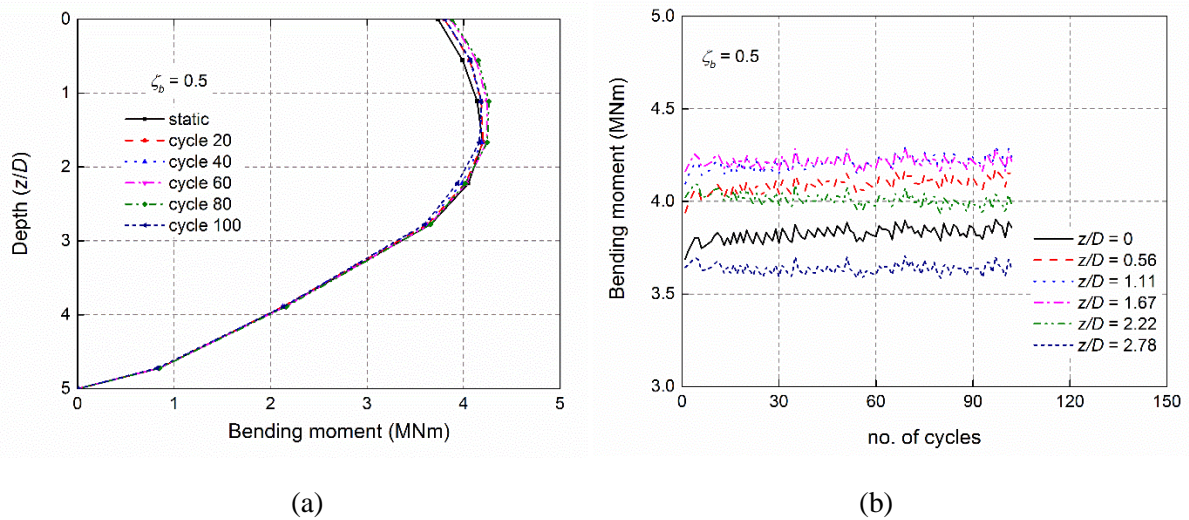
Figure 4.11 (a) Bending moment profiles at H_{max} versus depth; (b) Evolution of bending moment according to the number of cycles (test no. 12)

4.3.5 Effect of loading cycles on *p-y* curves

p-y curves construction

The bending moment at any depth was calculated from the average measured values of the strain from each pair of strain gauges attached on both side of the pile. By fitting a polynomial to the bending moment (M) at multiple soil depths (z), a distribution curve $M(z)$ can be obtained. The soil reaction p and the pile displacement y can be derived according to the beam theory equations:

$$p = \frac{\mathrm{d}^2 M(z)}{\mathrm{d}z^2}, \quad y = \iint \frac{M(z)}{EI}\,\mathrm{d}z\mathrm{d}z \tag{4.9}$$

where, p is the soil resistance; y is the pile displacement; EI is the pile flexural rigidity; and $M(z)$ is the moment distribution curve according to depth.

In the derivation of y, the bending moment data $M(z)$ was firstly fitted by a 7th order polynomial function that was then integrated twice. The two required constants C_1 and C_2 were the known displacement at the loading position and an assumed zero displacement condition at the point with zero lateral resistance ($0.7L$). A 5th order polynomial function was used to fit the bending moment data $M(z)$ for the calculation of soil reaction p.

Test results

The *p-y* curve derived from test no. 13 under operational loading at soil depth $z/D = 1.11$ is shown in Figure 4.12 for illustration purpose. As shown in Figure 4.12, the point with the coordinates of p and y values under the peak load value (H_{max}) for each cycle is named A_N, where N denotes the corresponding cycle number. In the following analysis, full hysteresis loops of the *p-y* curves in the cyclic loading periods will not be shown. For clarity of illustration, the evolution of the A_N points influenced by cycles will be focused on. This methodology is adopted by Verdure et al. [37] and Lee et al. [49].
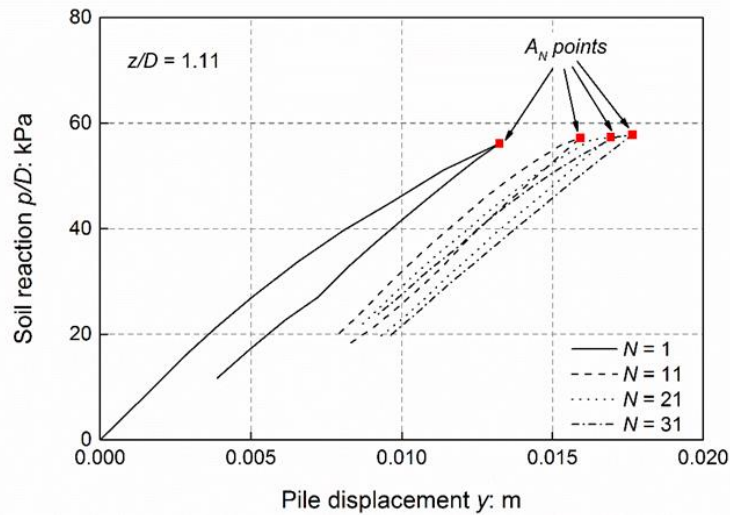
Figure 4.12 Hysteresis loops of cyclic *p-y* curve (test no. 13)

Figure 4.13 shows the *p-y* curves along the whole pile embedment length derived from test no. 12 (ζ_b = 0.5). The *p-y* curves from the monotonic loading periods were marked by symbol, while the A_N points were shown without symbol. The *p-y* curves in the monotonic loading periods show a rapid increase of the stiffness over the soil depths, due to the increase of soil stiffness. Similar observation can be found in Verdure et al. [37], Qi et al. [59], Choo and Kim [87] and Lee et al. [49].

From Figure 4.13, it can be observed that the pile displacement keeps increasing with cycle number at all the soil depths during the whole loading process. The evolution of A_N points shows different trends along the pile embedment depth. The *p-y* relationship in the cycle loading period reflects that:

1) Above the pile pivot point (z/D = 0.56 to 2.78), the soil reaction *p* shows a very tiny decrease trend when the cycle number increases.

2) Below the pile pivot point (z/D = 3.89 to 5), the soil reaction *p* is barely influenced by the cycle number.
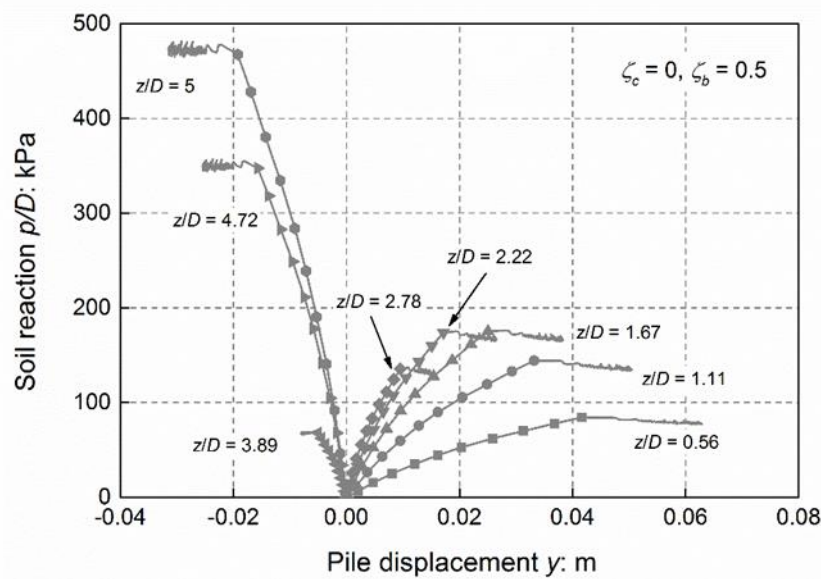
Figure 4.13 Monotonic *p-y* curve and the evolution of A_N points (test no. 12)

Comparison of cyclic *p-y* curves from this study with API

The *p-y* reaction curves at depths z/D = 0.56, 1.11, 1.67 and 2.22 were compared between test no. 12 and API [18], as shown in Figure 4.14. It can be seen that the initial stiffness (k_i) increases with increasing depth obtained both from this study and API [18]. In general, the API [18] method predicts both higher initial stiffness (k_i) and ultimate soil reaction (p_u) for each depth. At depth z/D = 0.56, with the increase of cycle number the soil reaction keeps increasing, and achieved higher soil reaction than the predicted p_u from API [18]. According to API [18] ultimate soil reaction (p_u) can be reached within a relatively small displacement (0.008-0.012 m), whereas from centrifuge test in this study the peak soil reaction appears at displacements much larger than API [18].

Choo and Kim [87] stated that the significantly higher k_i values obtained from API compared with those from centrifuge experiments may be explained as an effect of pile diameter, considering that the API [18] database is formulated based on field load tests with small diameter piles (D < 1 m). It implies that design rigid monopiles based on the traditional theory (i.e. API [18]) might place the pile into a dangerous situation considering the unrealistic high k_i values predicted, especially when carry out dynamic analysis of pile within small strain range.

Considering the significant difference between the *p-y* curves determined from the centrifuge experiments and the API [18] recommendation, further large-diameter rigid pile test is suggested to be carried out to formulate the database for the establishing of design criteria, especially when the lateral bearing behaviour of large diameter monopiles is designed based on *p-y* relationships.
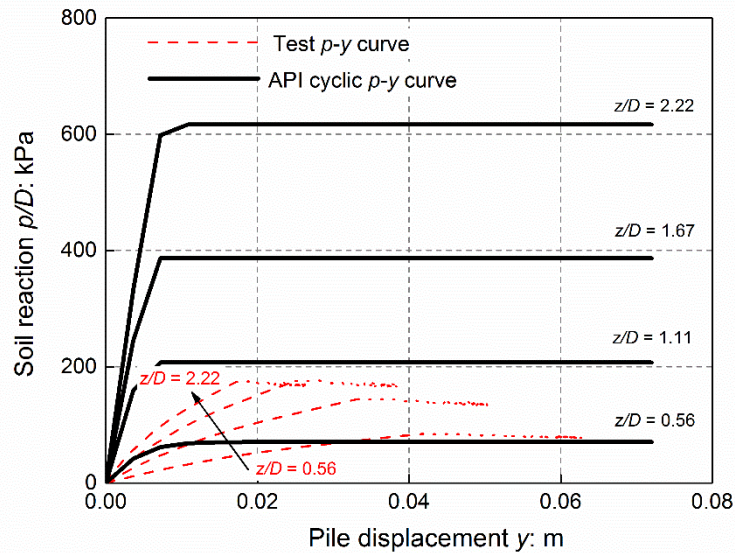
Figure 4.14 Comparison of cyclic *p-y* relationships obtained in this study with API [18] (API inputs: γ = 15.16 kN/m³ and φ = 35°)

4.3.6 Storm loading test

Lateral load-displacement response

The load-displacement response of pile subjected to storm loading scenario (test no. 13) is shown in Figure 4.15. During the first 40 cycles of "operational one-way loading" (ζ_b = 0.17) and during the following 20 cycles of storm loading (ζ_b = 0.5), similar trends in the accumulated pile displacement can be observed. The minimum and the maximum displacements increase as a function of the number of cycles. However, in the last 40 cycles (ζ_b = 0.17), opposite behaviour has been observed (i.e. both minimum and the maximum displacements of the pile decrease with the increasing number of loading cycle).
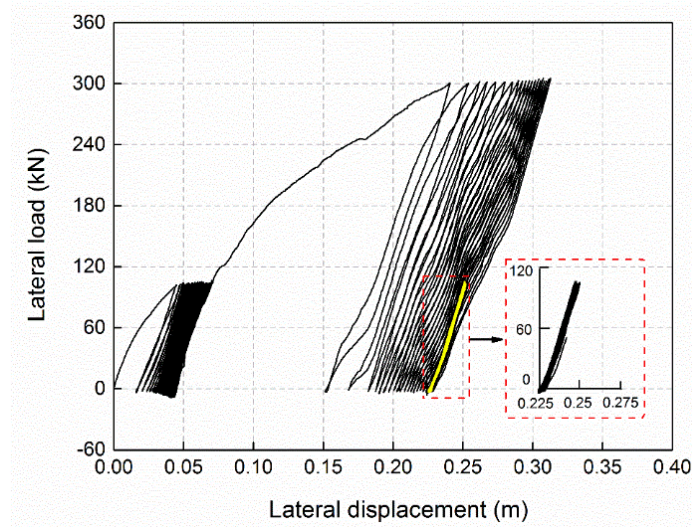
Figure 4.15 Pile lateral load-displacement response during storm loading test (test no. 13)

(a)

(b)

(c)

(d)
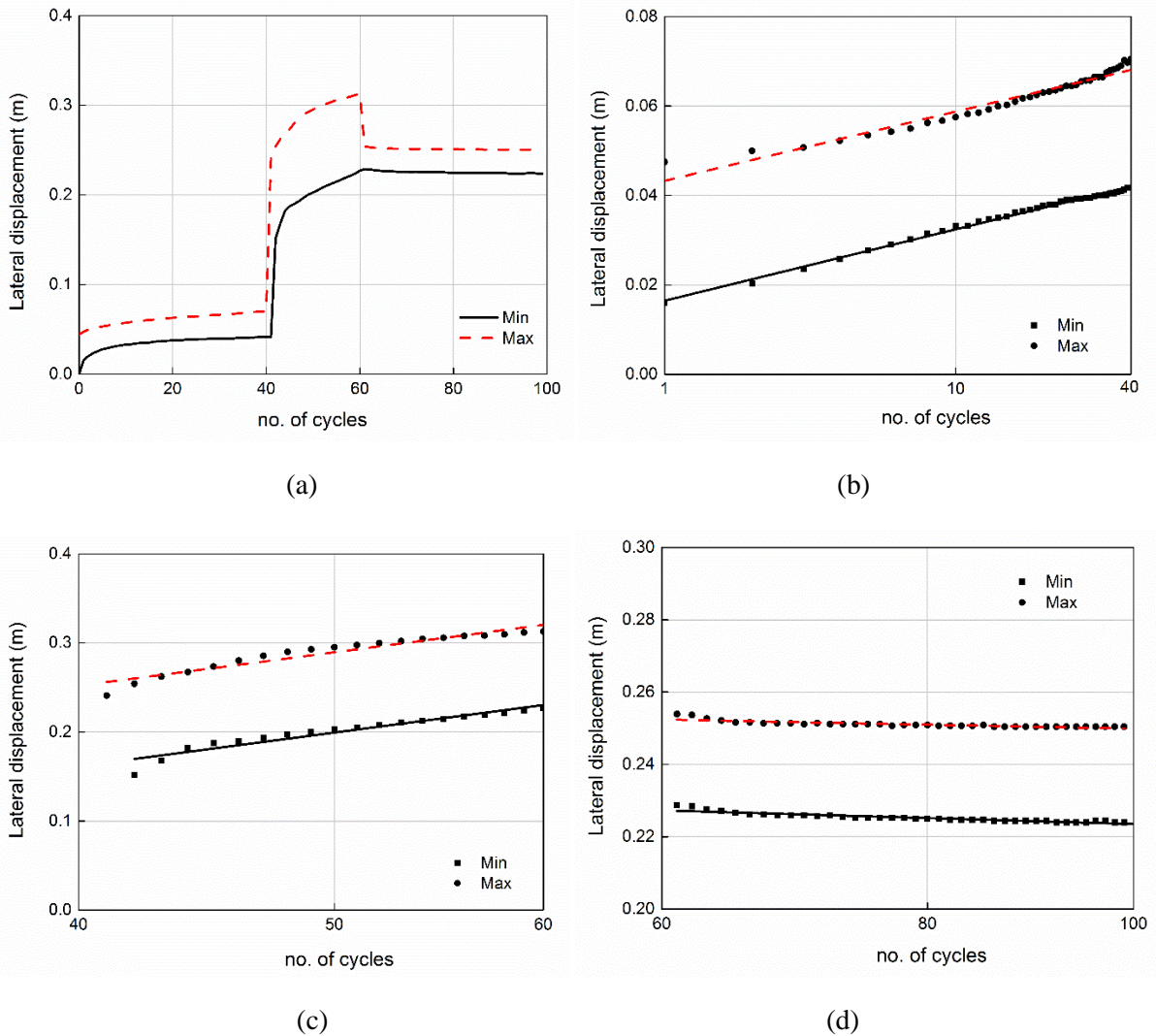
Figure 4.16 Accumulated permanent pile lateral displacements in storm loading test: (a) The whole process; (b) From the 1st to the 40th cycle; (c) From the 41st to the 60th cycle; (d) From the 61st to the 100th cycle

Figure 4.16(a) shows the maximum and minimum accumulated lateral displacements in storm loading test. Figure 4.16(b) shows the maximum and minimum accumulated lateral displacements under the first series of operational load cycles ($\zeta_b = 0.17$). Figure 4.16(c) shows the maximum and minimum accumulated lateral displacements under storm load cycles ($\zeta_b = 0.5$), where much larger accumulated displacements are seen compared with that under normal load cycles ($\zeta_b = 0.17$). Figure 4.16(d) shows the maximum and minimum accumulated displacements in the operational load cycles after storm ($\zeta_b = 0.17$). It can be seen that the minimum and maximum pile lateral displacements in each cycle decrease approximately linearly with the increasing number of loading cycles on a logarithmic scale. The corresponding α values are also listed in Table 4.3. The test result of storm loading case confirms the finding of Truong et al. [46] that application of lower levels cycling after higher level cycling leads to reduced pile head displacement (or rotation).

Influence of storm loading on *p-y* reaction curves

Figure 4.17 shows the experimental cyclic *p-y* curve loops at soil depths $z/D = 1.11$ during the storm loading. Figure 4.17(a) shows the cyclic load test result from cycle no. $N = 1$ to $N = 101$, while Figure 4.17(b) shows the cyclic load test result from cycle no. $N = 61$ to $N = 101$ with an enlarged scale compared with Figure 4.17 (a). The results show that:

1. Soil resistance was kept almost constant with the increase of cycle number, under both operational amplitude cyclic loading and storm loading.

2. The storm loading leads to significant increase in both the pile displacement and soil reaction. In the loading period, with the increase of pile displacement (or applied load), the stiffness of *p-y* curve of the 41st cycle decreases dramatically.

3. In the operational load cycles after the storm loading (from the 61st cycle to the 101st cycle), with the increase of cycle number, pile displacement shows tiny decrease while the soil reaction gets stabilized. Large residual pile lateral displacement is induced by the storm load cycles; however, the soil resistance is still at similar level compared with that in the operational load cycles before the storm loading.

(a)   (b)
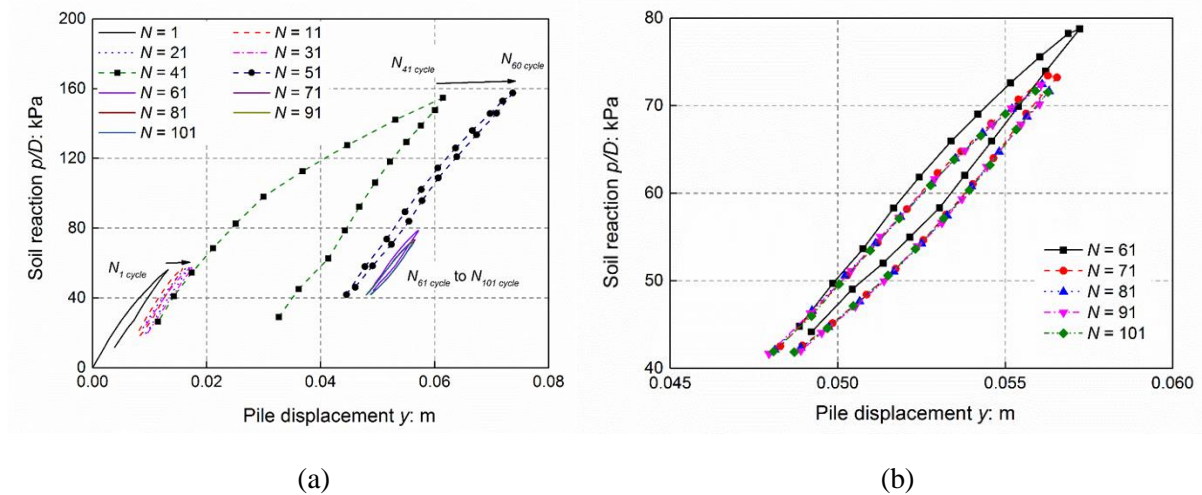
Figure 4.17 Cyclic *p-y* curve loops in the storm loading test (test no. 13): (test no. 7, z/D = 1.11): (a) from cycle no. *N* = 1 to *N* = 101 and (b) from cycle no. *N* = 61 to *N* = 101 with enlarged scale

4.4 New design approach

The centrifuge test results show that the accumulated pile lateral displacement and evolution of secant stiffness depends on: (i) the number of cycles; (ii) the magnitude and the characteristic of the load; (iii) the relative density of the sand. Therefore, these two design parameters (i.e. accumulated lateral pile displacement and change in the foundation stiffness) can be predicted from the results of a monotonic test combined with a series of functions determined from results presented in the previous sections. Accordingly, a new design approach is developed in this section, an example of the application is presented and the performance is compared with the data from a field test on a laterally loaded monopile.

4.4.1 Functions to describe the evolution of accumulated pile head displacement

The results indicate that the displacement accumulation rate α is a function of load amplitude (ζ_b) and load directional characteristic (ζ_c). Assuming independence between these two parameters, α can be written as a superposition of two non-dimensional functions each depending on only one of these two variables as described in Equation (4.10).

$$\alpha(\zeta_c, \zeta_b) = T_c(\zeta_c) \cdot T_b(\zeta_b) \tag{4.10}$$

For pure one-way loading, i.e. $\zeta_c = 0$, T_c can be normalised as 1. Therefore the non-dimensional function T_b can be found from a series of tests where ζ_b is changed while ζ_c is maintained at 0,

which is shown in Figure 4.18(a). It can be observed that the function $T_b(\zeta_b)$ is a constant function:

$$\alpha(\zeta_c = 0,\ \zeta_b) = 1 \cdot T_b(\zeta_b) = 0.07335 \qquad (4.11)$$

The function T_c therefore, can be found by performing a series of tests with a constant ζ_b and then dividing the results of α with previously determined function $T_b(\zeta_b)$:

$$T_c(\zeta_c) = \frac{\alpha}{T_b(\zeta_b)} \qquad (4.12)$$

The result from Figure 4.18(a) indicate that for $\zeta_c > 0.2$ the value of $\alpha \approx 0.058$ for piles installed in either dense or medium dense sand layers. However, for $\zeta_c \leq 0.2$, the value of α as a function of the relative density of the sand layer can be describe using two individual functions (as shown in Figure 4.18b):

$$T_c(\zeta_c) = -1.707(\zeta_c + 0.31)^2 + 0.949 \quad (D_r = 80\%) \qquad (4.13)$$

$$T_c(\zeta_c) = -1.14(\zeta_c + 0.323)^2 + 1.263 \quad (D_r = 50\%) \qquad (4.14)$$

Therefore, provided that the value of $y_{max,S}$ is determined from a monotonic test and relative density of the sand layer is known, the accumulated lateral displacement of the pile head could be predicted for various combinations of amplitude and directional characteristic of loading for a certain number of cycles.
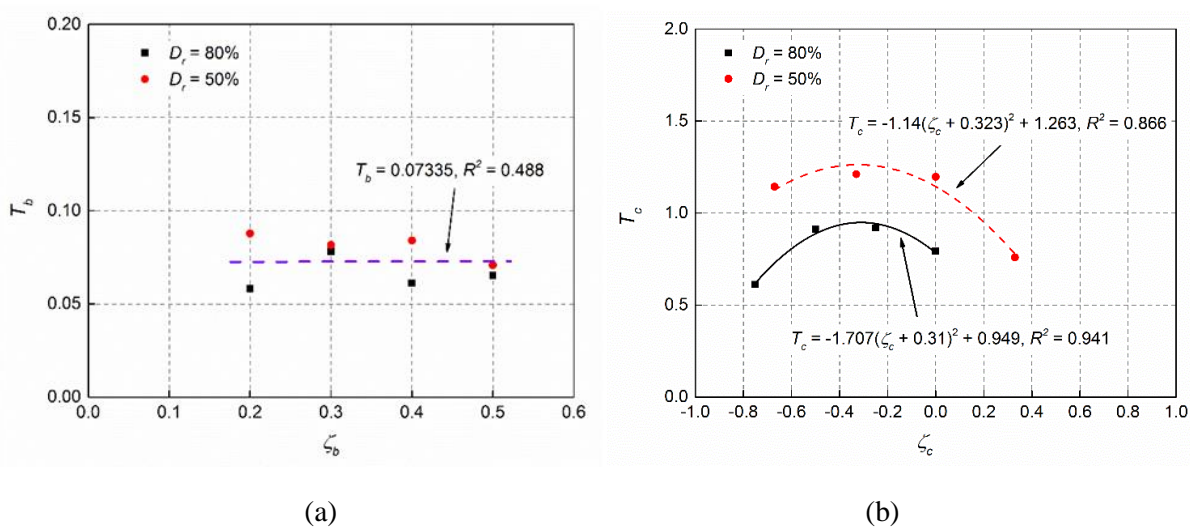
Figure 4.18 Cyclic dimensionless functions for accumulation of maximum pile head displacement: (a) T_b - ζ_b; (b) T_c - ζ_c

4.4.2 Functions to describe the evolution of secant stiffness

Similar to the approach described for the prediction of the accumulated lateral displacement, the secant stiffness increment rate β can be written as a superposition of two non-dimensional functions as shown in Equation (4.15).

$$\beta(\zeta_c, \zeta_b) = R_c(\zeta_c) \cdot R_b(\zeta_b) \tag{4.15}$$

For pure one-way loading, i.e. $\zeta_c = 0$, the value of R_c can be normalised as 1. Therefore the relationship of non-dimensional functions R_b and ζ_b (as shown in Figure 4.19a) can be expressed by the following equation:

$$R_b(\zeta_b) = 0.023 - 0.111\zeta_b + 0.266\zeta_b{}^2 \tag{4.16}$$

Figure 4.19(b) shows results for the cyclic load directional characteristic function R_c. The results seem to follow a linear relationship, see Equation (4.17):

$$R_c(\zeta_c) = 1.31 - 1.1\zeta_c \tag{4.17}$$

Therefore, provided that the value of K_1 is known, the secant stiffness of the pile could be predicted for various combinations of amplitude and directional characteristic of loading for a certain number of cycles. The next section describes an empirical procedure to determine the value of K_1.

(a)   (b)
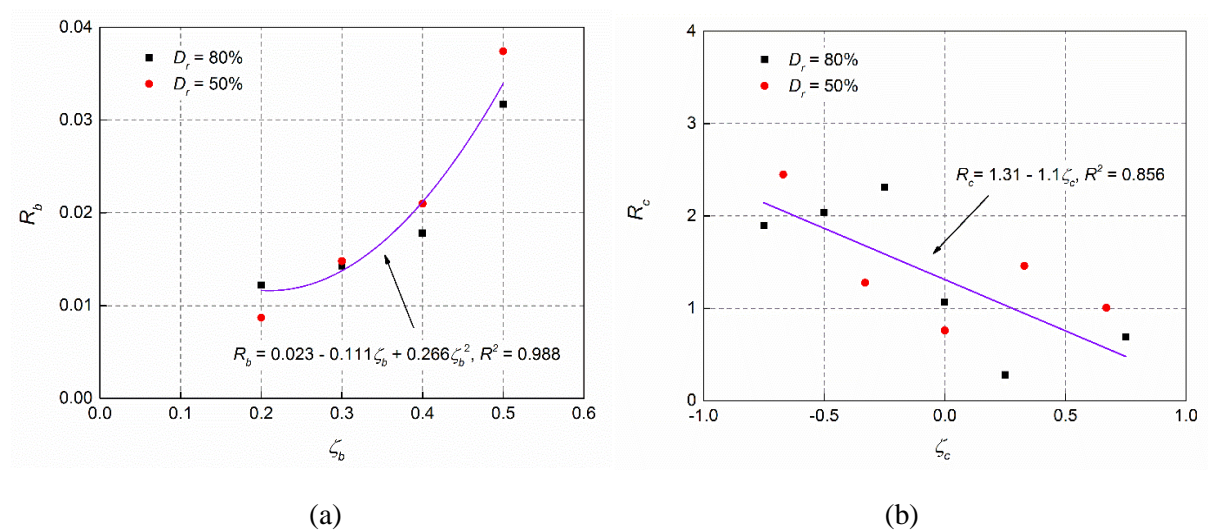
Figure 4.19 Cyclic dimensionless functions for evolution of secant stiffness: (a) R_b - ζ_b; (b) R_c - ζ_c

4.4.3 Functions to describe the initial cyclic secant stiffness (K_1)

The cyclic secant stiffness at the first loading cycle $K_1(\zeta_c, \zeta_b)$ can be written as a superposition of two functions as shown in Equation (4.18).

$$K_1(\zeta_c, \zeta_b) = K_c(\zeta_c) \cdot K_s(\zeta_b) \tag{4.18}$$

The value of K_1 can be found from the results of a set of monotonic test and cyclic tests with varying directional characteristics. The function $K_s(\zeta_b)$ can be established directly from one monotonic load-displacement curve, or from the monotonic loading phase of a cyclic load test. The results are shown in Figure 4.20(a), and it can be seen that a linear-fit captures well the variation of $K_s(\zeta_b)$:

$$K_s(\zeta_b) = 21.8 - 17\zeta_b \times 100 \text{ (kN/m)} \tag{4.19}$$

$K_c(\zeta_c)$ is then evaluated from the cyclic tests, and the test results from this study are shown in Figure 4.20(b). It can be seen that a linear fit also captures the trend of $K_c(\zeta_c)$:

$$K_c(\zeta_c) = 0.057\zeta_c + 1.25 \tag{4.20}$$

(a)   (b)
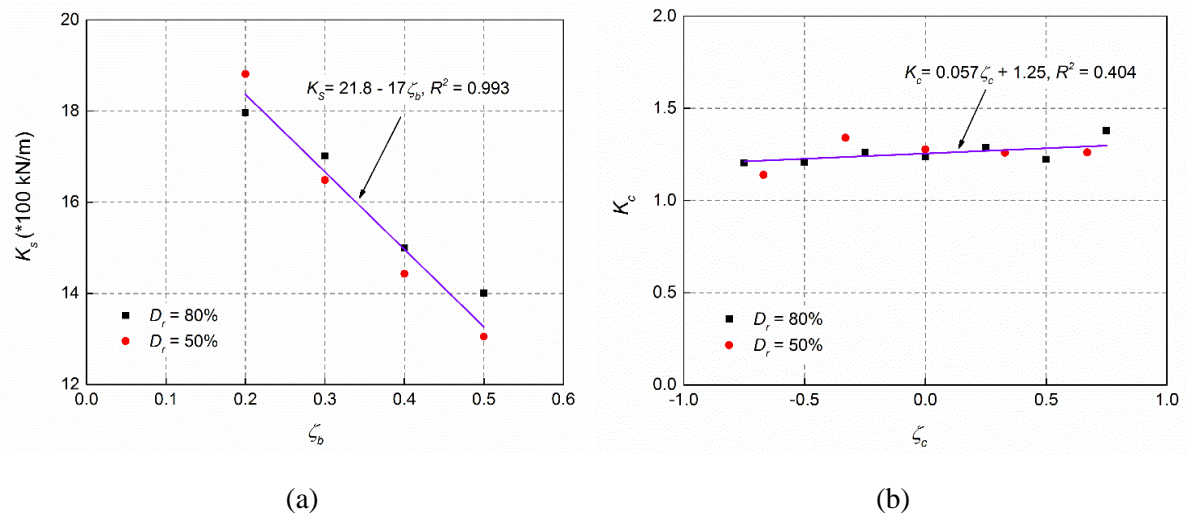
Figure 4.20 Cyclic dimensionless functions for initial cyclic secant stiffness: (a) K_s - ζ_b; (b) K_c - ζ_c

Results shown in Figure 4.20 indicate that the secant stiffness functions of K_c and K_s are not sensitive to sand relative density.

As all the non-dimensional functions ($T_c(\zeta_c)$, $T_b(\zeta_b)$, $R_c(\zeta_c)$, $R_b(\zeta_b)$, $K_c(\zeta_c)$) along with dimensional function $K_s(\zeta_b)$ are established, accumulation of maximum pile head displacements and change in secant stiffness depending on the number of cycles can be predicted by the proposed design procedure.

Although the design procedure was formulated based on tests with limited number of load cycles (maximum number of 153 cycles each test), it can be seen from the study of Verdure et al. [37], LeBlanc et al. [41], Li et al. [42] and Klinkvort and Hededal [43] that the overall pile displacement accumulation rate and change in secant stiffness at large load cycles (for example, cycle number N > 1000) follows the same trend captured within about 50 cycles. In agreement with the method proposed by Little and Briaud [95] and Long and Vanneste [35], the exponential behaviour of accumulated rotation vs. cycle number appears as straight lines in double logarithmic axes for up to 105 cycles. Therefore, in the following as an attempt pile behaviour under large number of load cycles is predicted by extrapolating data measured in tests with small number of load cycles.

4.4.4 Example

Demonstration of the proposed design procedure

To demonstrate the use of the proposed design procedure, an example is given here. A rigid pile with $D = 1.8$ m, embedded length of $L = 5D$ and load eccentricity of $e = 8D$ is considered in this example. The sand is assumed to be dry, with a friction angle of 35°. The goal is to predict the increase in secant stiffness and accumulated pile head displacement when the pile is subjected to 10^7 loading cycles with $\zeta_b = 0.3$ and $\zeta_c = -0.2$.

The dimensions of the pile in this example are selected to be similar to those of the prototype pile of this study as the monotonic loading data, as the only required input for this model, is available (Figure 4.3). The results depicted in Figure 4.3 show that $\zeta_b = 0.3$ is equivalent to a maximum lateral load of $H_{max} = 0.3 \times 600$ kN $= 180$ kN and $H_{max} = 0.3 \times 440$ kN $= 132$ kN in dense and medium dense sand layers, respectively. The corresponding displacement $y_{max,S}$ is determined from Figure 4.3 to be 0.067 m in dense sand and medium dense sand conditions. The secant stiffness for the first cycle of cyclic loading $K_1(\zeta_c, \zeta_b)$ can be determined from Equation (4.18) and Figure 4.20 to be 2068 kN/m.

Therefore, the accumulation rate of pile head displacement α can be calculated according to Equation (4.12) and Figure 4.18. The values of α are calculated to be 0.068 and 0.091 for the cases of dense and medium dense sand layers, respectively. Hence, using Equation (4.3) the accumulated pile head displacements after 10^7 cycles can be calculated as 2.99 and 4.34 times of $y_{max,S}$ (Equation 4.21 and 4.22), which are 0.2 m and 0.29 m in dense and medium dense sand, respectively.

$$\frac{y_{max,N}}{y_{max,S}} = N^\alpha{=}(10^7)^{0.068} \approx 2.99 \quad (D_r = 80\%) \tag{4.21}$$

$$\frac{y_{max,N}}{y_{max,S}} = N^\alpha{=}(10^7)^{0.091} \approx 4.34 \quad (D_r = 50\%) \tag{4.22}$$

By using $K_1(\zeta_c, \zeta_b)$, the accumulation rate of secant stiffness follows Equation (4.15). β is calculated to be 0.02 in both dense sand and medium dense sand without difference. Then according to Equation (4.6),

$$\frac{K_N}{K_1} = N^\beta = (10^7)^{0.02} = 1.38 \tag{4.23}$$

This result indicates that the secant stiffness is estimated to increase by approximately 38% during the lifespan of the wind turbine.

Comparison with field test data and other prediction models

Li et al. [44] conducted a field test on a rigid pile with a diameter of $D = 0.34$ m and an embedded length of $L = 6.5D$. The pile was installed in a dense sand layer and loaded with an eccentricity $e = 1.2D$. More than 1000 one-way lateral load cycles were applied to the pile head with $\zeta_b = 0.3$ and $\zeta_c = 0$. The monotonic load-displacement curve of this test indicates a $y_{max,S} = 0.0042$ m and according to the loading features and using Equation (4.12) and Figure 4.18, the accumulation rate of pile head displacement α can be calculated to be 0.07335. Therefore, the following equation can describe the pile accumulated displacement:

$$\frac{y_{max,N}}{y_{max,S}} = N^\alpha{=}(10^3)^{0.07335} \tag{4.24}$$

The pile rotation can be calculated by assuming the pile as a rigid body and the pile rotation point to be located at 0.7L beneath the sand surface. Based on these assumptions, the relationship between the pile rotation at sand surface and cycle number can be established.

The comparison between predicted results by Little and Briaud [95], LeBlanc et al. [41], Klinkvort and Hededal [43] and this study and the field test data reported by Li et al. [41] is shown in Figure 4.21. The model from this study provides a better prediction of the measured response. The prediction model developed by Little and Briaud [95] slightly under estimates the pile accumulated rotation (with an average error of -19%), while prediction model developed by LeBlanc et al. [41] slightly over estimates the pile accumulated rotation (with an average error of 8%). The model developed by Klinkvort and Hededal [43] over estimates the pile accumulated rotation for up to 91%. As mentioned by Li et al. [44], the variation in the prediction models partly results from soil variability and experimental measurement errors.
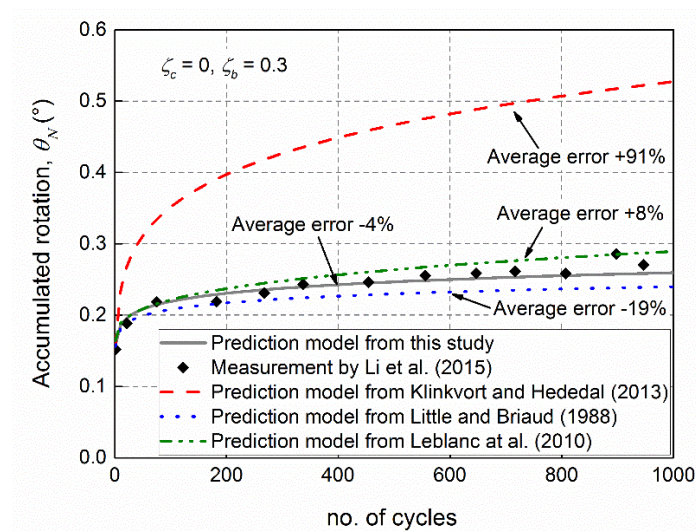
Figure 4.21 Comparison on the pile accumulated rotation between model predictions and field test data

4.5 Conclusions

Centrifuge tests were carried out on an open-ended monopile with L/D ratio of 5 in dry sand with two relative densities of 50% and 80%, to evaluate cyclic load induced accumulation of pile head displacement and evolution of secant stiffness. Two key parameters were focused on: cyclic directional characteristic ratio (ζ_c) and cyclic magnitude ratio (ζ_b). Using the measured bending moment at various depths along the pile shaft and the load-displacement data at pile head, cyclic p-y reaction curves were constructed. Equations were formulated based on the test

data for the prediction of accumulated pile head displacement and change in secant stiffness. The following conclusions can be drawn:

1. The most damaging cyclic load type is two-way loading, with $\zeta_c \approx$ -0.4, regardless of the sand relative densities. When $\zeta_c \leq 0.2$, pile has faster rate in generating accumulated maximum displacement in medium dense sand compared with that in dense sand. When $\zeta_c > 0.2$ (one way cyclic loading), pile maximum displacement accumulation rate was found to be not sensitive to the sand relative density. The pile displacement accumulation coefficient (α) was found to be not sensitive to the cyclic magnitude ratio (ζ_b).

2. Cyclic loading results in an increase in the secant stiffness per cycle irrespective of the sand relative density. When the applied load was changed from one-way to two-way, an increasing rate on accumulation of secant stiffness was observed. An increase in the cyclic load magnitude ratio ζ_b led to an increase in the relative secant stiffness accumulation rate (β).

3. The pile maximum bending moment was found to be not sensitive to the change of cyclic magnitude ratio (ζ_b) and cyclic characteristic ratio (ζ_c), and the increase of cycle numbers.

4. Above the pile pivot point, the soil reaction p shows a very tiny decrease trend when the cycle number increases, while below the pile pivot point the soil reaction p keeps constant with the increase of cycle number. Compared with the $p\text{-}y$ reaction curves on rigid monopile derived from centrifuge tests, the API [18] method overestimated the stiffness of the $p\text{-}y$ reaction curves, which is supposed to be less conservative.

5. Large amplitude loading cycles simulating a storm condition dramatically increased the accumulation rate of pile head displacement. However, application of lower amplitude of cyclic loading after storm loading cycles led to a reduction of the pile displacements. In the operational loading cycles both prior to and after the storm loading, the soil reaction keeps constant with the increase of cycle number.

6. The design procedure which can be applied for any load amplitude, load directional characteristic and cycle numbers to predict pile lateral loading behaviour (originally established by Klinkvort and Hededal [43]) was re-evaluated in this study. The related three sets of functions ($T_c(\zeta_c)$, $T_b(\zeta_b)$, $R_c(\zeta_c)$, $R_b(\zeta_b)$, $K_c(\zeta_c)$, $K_s(\zeta_b)$) were reformulated based on the centrifuge test results from this research. The accumulation of pile head displacement and the evolution of secant stiffness can therefore be predicted by a

monotonic response together with the aforementioned functions. A power law function along with the parameters determined from this study was found to predict the pile response tested in field by Li et al. [44] with less than 5% average error.

The proposed prediction model is formulated based on certain kinds of pile and sand, and pile installation method. If prediction is going to be made on other types of piles only the prediction procedure can be referred to. The non-dimensional and dimensional functions should be determined on the targeted pile and sand under designed pile installation method. Moreover, it should be noted that the number of cycles applied to the piles tested in the centrifuge is several orders of magnitude smaller than those that monopiles experience in their lifetime.

5 Centrifuge modelling of the impact of local and global scour erosion on the monotonic lateral response of a monopile in sand

The majority of offshore wind turbines are founded on large-diameter, open-ended steel monopile foundations. These structures must resist large lateral loads and overturning moments due to environmental (wind and wave) actions, while vertical loads tend to be small in comparison. Recent developments in the size of turbines and increases in hub heights have resulted in pile diameter sizes increasing rapidly, whilst the embedment length to diameter ratio (L/D) ratio is reducing. The erosion of soil from around piles, termed scour, changes the strength and stiffness properties of the soil and affects the system's load resistance responses. In practice, design scour depths of up to 1.3D are routinely assumed during the lifetime of a turbine, however the impact on monopiles with low L/D ratios is not yet fully understood. In this paper, centrifuge tests are performed to assess the effect of scour on the performance of piles with low L/D ratios. In particular, the effect of combined loads, scour type (shape) and scour depth are considered. A loading system is developed that allows for the application of realistic load eccentricity and consideration of combined vertical, horizontal and moment loading at the seabed level. An instrumented 1.8 m diameter pile with L/D = 5 is used. A friction-reducing ball-type connection is designed to transfer the lateral load to the pile without inducing any rotational pile-head constraint, associated with loading rigs in tests of this nature. Results suggest that interaction effects between vertical and lateral loads are minimal. Scour has a significant impact on the lateral load-capacity and stiffness of the pile, leads to increases in the magnitude of bending moments along the pile shaft, and lowers the location of peak bending moment along the pile. The response varies with scour type, with global scour resulting in larger moments than local scour. The shape of the local scour hole is found to have a significant impact on the pile response, suggesting that shape effects should be explicitly considered in design.

72

5 Centrifuge modelling of the impact of local and global scour erosion
on the monotonic lateral response of a monopile in sand

5.1 Introduction

The majority of offshore wind turbines (OWTs) constructed to date are founded on monopile foundations. Developments in construction methods and improved design procedures [25, 90] has resulted in a gain in market share for monopiles from approximately 75% of offshore wind turbine foundations in 2011 [10] to more than 87% in 2017 [75]. Monopiles are an efficient, cost effective, and proven technology to resist the large lateral loads and moments due to wind and wave actions, and thus provide a low-risk solution for offshore developers. Whilst all limit states are important, monopiles have strict serviceability requirements, e.g. total rotation at seabed level typically must remain less than 0.5° [12, 96].
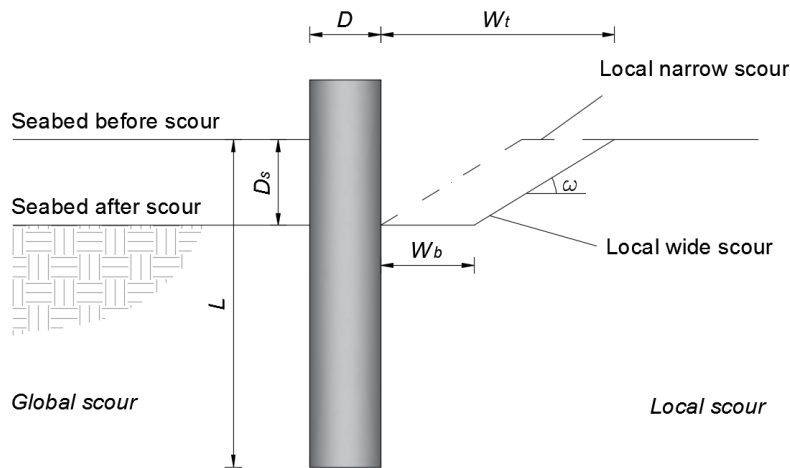
Figure 5.1 Schematic of local and global scour (W_b = bottom width of scour hole; W_t = top width of scour hole; ω = scour slope angle; L = pile embedment length; D = diameter; D_s = scour depth)

When structures are founded in water, there is potential for erosion of the supporting soils, a mechanism known as scour. Interested readers are referred to Wang et al. [97] for a comprehensive review on scour in the context of bridges. For the present application, scour erosion around unprotected offshore piles changes the support conditions and can pose a significant problem [55, 56]. Scour increases the free cantilevered length of monopiles, leads to a reduction in the soil's effective stress, reducing the strength and stiffness of the remaining soil, and can thus compromise the serviceability and safety of structures [98, 99]. There are two main types of scour relevant to offshore structures, see Figure 5.1: (i) 'global scour', where the elevation of the soil surface is reduced globally due to natural sea bed migration or the presence of a whole wind farm interfering with the global flow regime, and (ii) 'local scour', where the disturbed flow directly local to a pile structure leads to the formation of a conical scour pit

around the foundation [54]. Global scour due to storm surge events has been reported in the literature [100], with resulting scour depths of the order of $1D$. The typical magnitude for local scour depth, D_s, considered in design is $1.3D$. It is noteworthy that in the marine environment, scour occurs due to the combination of tides, currents and waves, which can make the estimation of scour depths very difficult [56, 101]. Since monopiles have slenderness ratios (pile penetration normalised by pile diameter, L/D) of < 6, scour can have a major impact on the stiffness and capacity of these systems. Some previous works that have investigated the effect of scour on the lateral resistance characteristics of piles are discussed herein.

Bennett et al. [52] examined the effect of scour and pile head boundary conditions on the lateral deflections of a pile group, used as the foundation for a bridge pier. The lateral behaviour was examined using the Group Equivalent Pile (GEP) method. Results showed that scour reduces the lateral capacity, which is especially significant when the scour depth exceeded the depth of the pile cap. Moreover, scour altered the influence depths of deflection, bending moment and shear, by lowering the point where the maximum value of these parameters occurred. Lin et al. [53] investigated the influence of the change in stress history of the soil due to scour on the lateral behaviour of piles. By comparing calculated results from the modified sand p-y curves against a referenced field test, they concluded that the change in the over-consolidation ratio due to scour had the most significant influence on the sand lateral resistance properties, and leads to higher resistance in the remaining sand. Ignoring this additional effect is conservative. A subsequent study by the same authors in Lin et al. [102] presents a simplified method for the analysis of laterally loaded piles in soft clay using modified p-y curves to account for scour hole dimensions (scour depth, scour width, scour-hole slope angle). By comparing the results of their model with a 3D finite difference model (developed using FLAC3D), it was observed that ignoring the scour hole dimensions could result in 10-19% larger lateral displacement at the pile head with bending moments being 6-8% larger, as compared to the case where these are explicitly considered. Zhang et al. [60] also recognised that soil stress history changes are typically ignored along with whole scour-hole geometry. They examined the behaviour of laterally loaded long-slender piles ($L/D \approx 40$) in soft clay under scoured conditions by using modified p-y curves to reflect the effects of three-dimensional scour-hole geometry (depth, width, and slope angle) as well as the stress history of the soil. The results indicated that neglecting the effect of soil stress history can be unconservative for pile foundations in soft clay affected by scour. Furthermore, neglecting the scour-hole geometry is over-conservative for design of laterally loaded piles under scour. For the purpose of design, the scour effect on the

74

5 Centrifuge modelling of the impact of local and global scour erosion
on the monotonic lateral response of a monopile in sand

pile lateral behaviour may be characterised in terms of scour depth and the stress history of the soil. Further work by the same authors extended this approach to investigate the influence of vertical loads on the lateral responses of scoured piles, taking soil stress history and scour hole geometry into consideration [61]. Mostafa [54] investigated the influence of scour type (local and global) on the lateral response of piles in cohesive and cohesionless soils using numerical modelling. The study concluded that scour had a more deleterious effect on piles installed in sand than in clay. In sand, scour depths ranging between $1D$ and $3D$ resulted in lateral pile head displacement increases of 37% to 155%, as compared to the no scour condition. Moreover, global scour caused large increases in bending moments with the result that scour had a more significant impact for piles subjected to large lateral loads due to nonlinear pile-soil interaction effects. Qi et al. [88] investigated the effect of scour type (local and global) on load-displacement p-y curves of piles for OWTs in sand using centrifuge testing. They found that, under global scour, the p-y curves in the remaining over-consolidated soil showed no obvious difference to those in the original normally consolidated soil. This finding is contradictory to the hypothesis in Lin et al. [53]. Furthermore, under local scour, they found that the remaining overburden provided a beneficial response in that the lateral soil stiffness at a given depth below the scour-hole base was greater than at the same relative depth below the original mudline. The tests were performed using relatively flexible pile with a slenderness ratio between 9.5 and 12.5.

To date, there has been considerable research undertaken on the effect of scour on the lateral response characteristics of piles using numerical modelling or scaled laboratory testing. Limited research has been undertaken, however, on the effect of scour depth and type on laterally loaded piles considering combined vertical, lateral and moment loading at the seabed level using centrifuge testing, particularly for the piles with low slenderness ratios typically used for offshore wind developments. Moreover, the influence of local scour hole size has not received significant attention in physical modelling. This paper presents the development of a centrifuge-based model specially designed to study the effect of scour on laterally loaded monopiles with low slenderness ratios. The challenge lies with the application of lateral loads and moments in a centrifuge while minimizing the constraint on the pile head fixity (i.e. the pile head should be free to rotate as per an offshore monopile). Moreover, the presence of vertical dead loading representing the self-weight of an OWT should be considered. This paper details the development of the testing arrangement in the Geo-Engineering laboratory at Delft University of Technology (TU Delft) and investigates lateral load-displacement responses and derived bending moment distributions of an instrumented pile under global scour, and two types of local

scour. The two types of local scour, termed narrow and wide in this paper, refer to the bottom width of the scour hole, where $W_b = 0$ for narrow scour, and $W_b = D$ for wide scour (see Figure 5.1).

5.2 Centrifuge modelling

5.2.1 Centrifuge facility

The TU Delft centrifuge, see Figure 5.2, is a 2 m diameter beam-type apparatus [62]. Centrifuge tests are performed on models that are geometrically A-times smaller than a prototype. The geo-centrifuge provides a unique environment of enhanced gravitational acceleration, where the expected behaviour of a full-scale geotechnical structure can be observed, with high precision, using small scale models. The centrifuge at TU Delft enables models with dimensions up to 500 mm × 240 mm × 380 mm be tested up to a maximum of 300 times the gravitational acceleration (300g). While this is possible, for practical reasons related to the operation of the data logging equipment, samples are typically tested at a limiting gravitation acceleration of 100g.
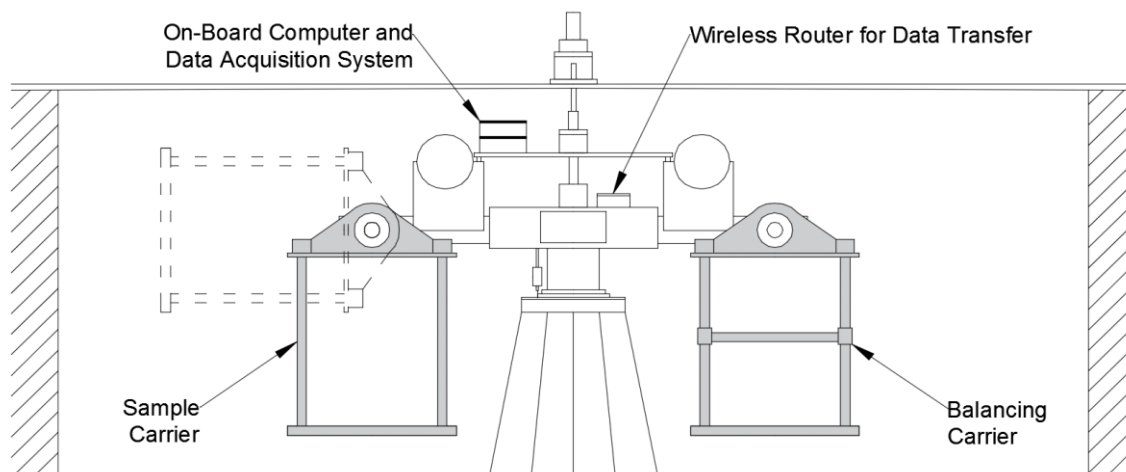

Figure 5.2 Schematic layout of the geo-centrifuge (modified after Alderlieste [6])

For simulating geotechnical structures using a centrifuge, scaling laws must be considered. Table 5.1 provides a summary of typical scaling laws for modelling of pile-type structures. In this table, A refers to the gravitational acceleration field adopted in a given test.

76

5 Centrifuge modelling of the impact of local and global scour erosion
on the monotonic lateral response of a monopile in sand

Table 5.2 Basic scaling laws for centrifuge modelling of monopiles

Term	Prototype	Model
Length	1	$1/A$
Second moment of area	1	$1/A^4$
Flexural stiffness	1	$1/A^4$
Mass	1	$1/A^3$
Force	1	$1/A^2$
Stress	1	1
Strain	1	1

5.2.2 Loading system

The tests in this study were performed at $100g$ to model a rigid monopile with a diameter of 1.8 m (at prototype scale) and L/D of 5. A two-dimensional servo actuator applies loading to the pile head, as shown in Figure 5.3. Figure 5.3 is previously shown in Chapter 2, it is reproduced herein for convenience. The loading system is capable of applying lateral loads under either load or displacement controlled conditions. The vertical dead load (V) at the pile head can be imposed by means of attaching steel blocks with different masses, to model the presence of a superstructure (details of the dead load are described in section 5.2.3). The lateral load (H) is applied at the pile head by lateral movement of the actuator, and is monitored by strain gauges located on the loading arm. The lateral displacements of the pile at the loading position (pile head) can be monitored by the lateral motor encoders, the accuracy of which are of the order of approximately 3×10^{-5} mm. For all tests performed in this study, lateral loads are applied at a height of 15 m above the seabed at prototype scale.

(a)   (b)
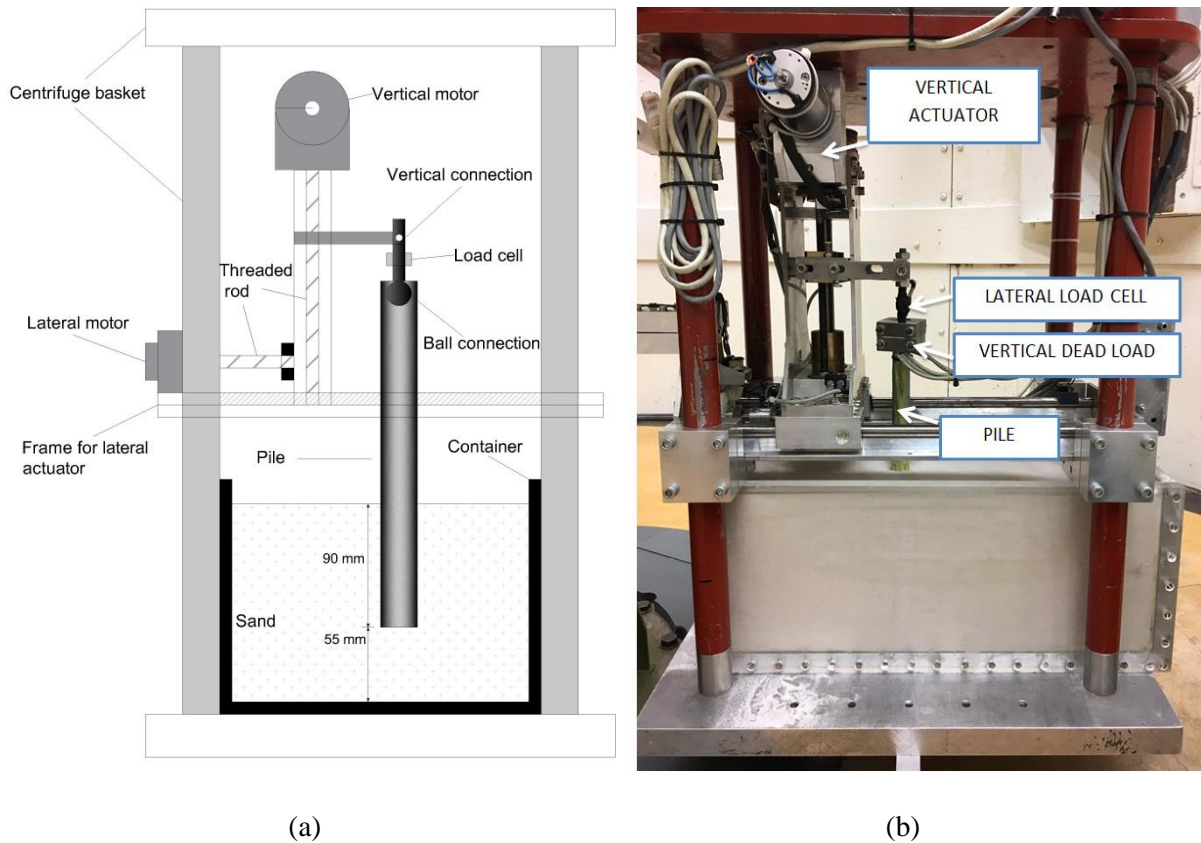
Figure 5.3 The two-dimensional loading actuator and monopile arrangement in centrifuge tests: (a) Schematic diagram; (b) Picture of pile testing arrangement

(a) BC-1   (b) BC-2   (c) BC-3   (d) BC-4
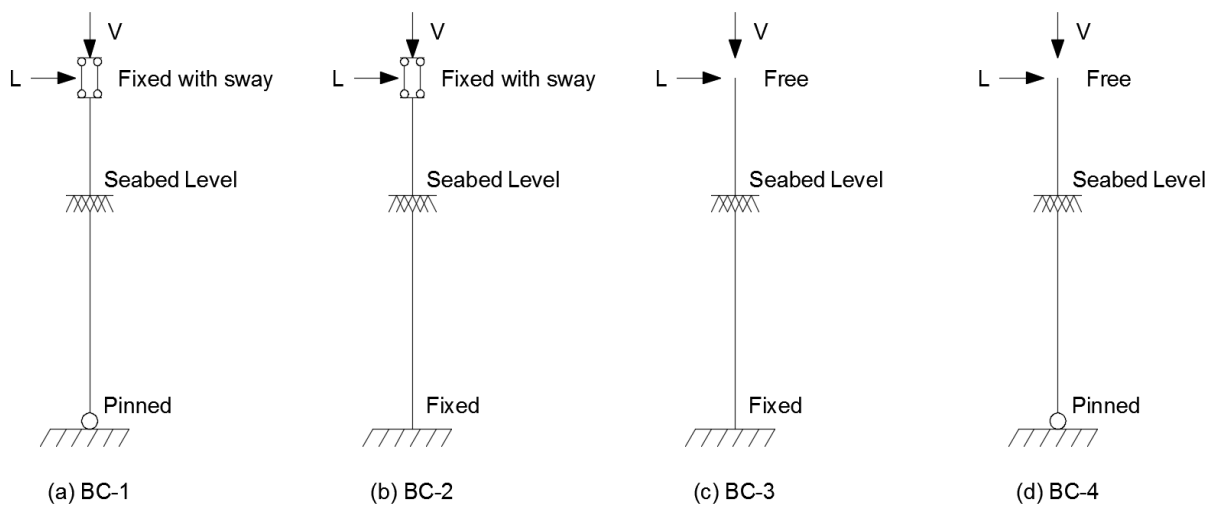
Figure 5.4 Different boundary conditions for laterally loaded piles (after Han and Frost [103]): (a) Head fixed against rotation with pile tip seated on hard soil; (b) Head fixed against rotation with pile tip embedded in hard soil; (c) Head free and pile tip embedded in hard soil; (d) Head free with pile tip seated on hard soil

78

5 Centrifuge modelling of the impact of local and global scour erosion
on the monotonic lateral response of a monopile in sand

Han and Frost [103] recognized that the load-deflection response of a laterally loaded pile is highly dependent on the boundary conditions of the pile in the ground. Various boundary conditions for piles are encountered in practice, and four typical scenarios are shown in Figure 5.4. Monopiles for offshore wind turbines will typically behave similarly to BC-4 (with some additional pile tip sway). Achieving the free head boundary condition in centrifuge tests is difficult, therefore most previous research tends to only consider lateral movement of the pile head (by implementing roller-type connection) while ignoring any pile head rotation (BC-1 and BC-2). To enable the application of a lateral load without inducing any rotational fixity associated with the loading arm, a specially-designed friction-reducing ball connection (shown in Figure 5.5) was constructed to transfer the lateral load produced by the linear actuator to the pile head. The ball is placed vertically into the open-end of the pile head, where it rests in contact with the internal shaft of the pile. A Teflon sleeve is used to minimize the interface friction between the ball and the pile internal surface. Figure 5.5(a) shows a photograph of the ball connection used in this study and Figure 5.5(b) shows the instrumented model pile with Teflon interior at the top, and the shielded strain gauges along the shaft.
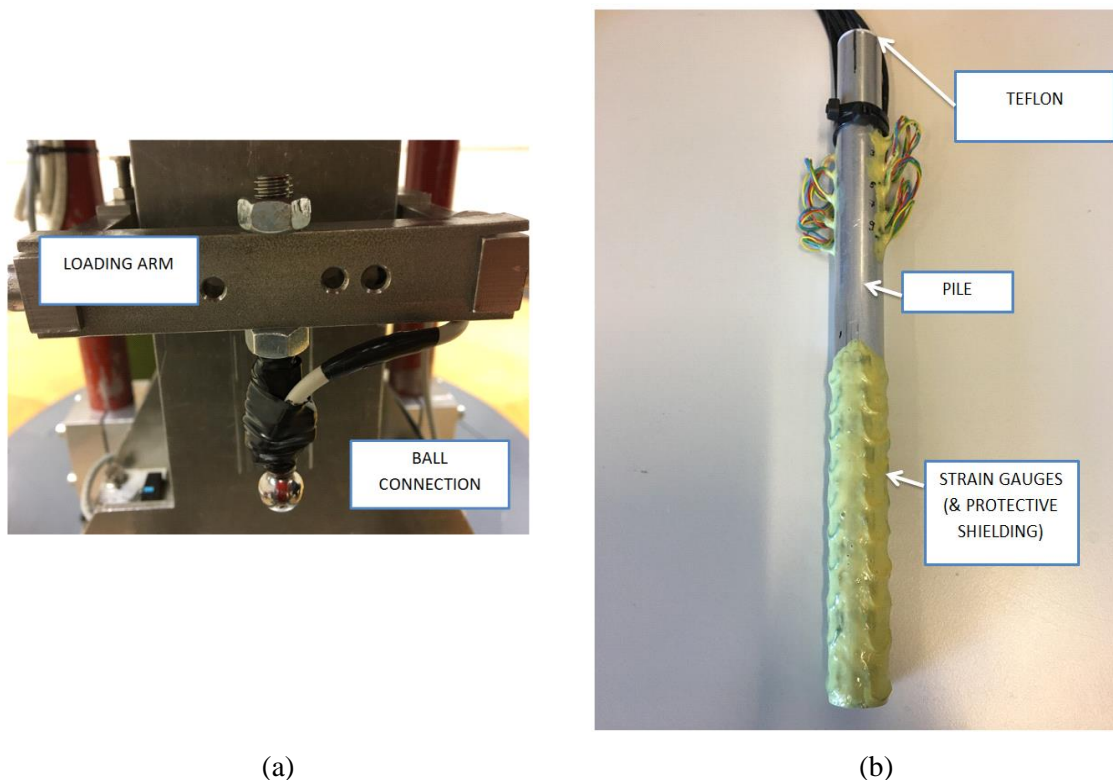

(a)   (b)

Figure 5.5 (a) Ball connection for reduced friction application of lateral load; (b) Pile with inner Teflon material for reduced friction

5.2.3 Model pile

The model pile is an open-ended cylindrical aluminium tube with an outer diameter (D) of 18 mm (see Figure 5.6). The pile diameter is selected so as to minimise boundary effects associated with the strong box, which houses the pile, and also to satisfy constraints associated with the mean grain particle size (see section 5.2.4). The strong box is fabricated from bolted plexiglas with dimensions 410 (length) × 150 (width) × 180 (height) mm^3, see Figure 5.3(b). The pile has a total length of 240 mm and is embedded 90 mm into the sand. The embedded depth is chosen so as to model a pile with slenderness ratios (L/D) between 4-6 [10, 41, 55], within the typical range for offshore monopiles. A pile with embedded length of 90 mm equates to the slenderness ratio of 5. The wall thickness of the model pile is derived based on the calculation for minimum wall thickness for monopiles [12, 18]. Using the similitude between the flexural rigidity (EI) of the prototype and the model (Table 5.1), the wall thickness is calculated to be 1 mm. Byrne et al. [25] has produced a database of piles, and present the results of the pile diameters normalised by pile wall thickness. For monopiles with $L/D = 5$, the value of D/t varied from 39 to 80. In the present analysis, the D/t value for the steel prototype pile is 60.

The pile was installed for each test by jacking in place at $1g$ prior to initiating the centrifuge. It should be noted that installing the model pile at $1g$ equates to an idealised 'wished-in-place' treatment, and does not consider the potential residual base stresses that might be developed if driven while the centrifuge is in flight. This residual stress may lead to additional base moments on the piles [104], which may alter the response characteristics. Driving the pile in-flight would require stopping of the centrifuge to adjust the loading rig for the subsequent lateral load application, which would add uncertainty surrounding the influence of the sample stress history on the results obtained. The present paper ignores the influence of installation effects.

All tests were performed at $100g$, therefore, the model pile properties correspond to a 1.8 m diameter rigid structure, with a wall thickness of 100 mm, an embedment of 9 m and a total length of 24 m at the prototype scale. The primary dimensions and material properties of the pile are provided in Table 5.2.

Ten strain-gauge pairs are installed along the pile shaft to enable the distribution of bending moments due to the applied loading be derived. The strain gauges used are FLA-3-11 fabricated by Tokyo Sokki Kenkyujo [105]. The load from the superstructure is incorporated by way of adding steel blocks with equivalent (prototype) weight of 3 MN, to the pile top. The masses

were fabricated from quadrate steel with an outer length of dimension 50 mm and a thickness of 12 mm. In the centre of each mass is a circular hole with a diameter of 18 mm to allow the masses be fixed on the pile body (see Figure 5.6).

Table 5.3 Model and corresponding prototype pile dimensions and properties

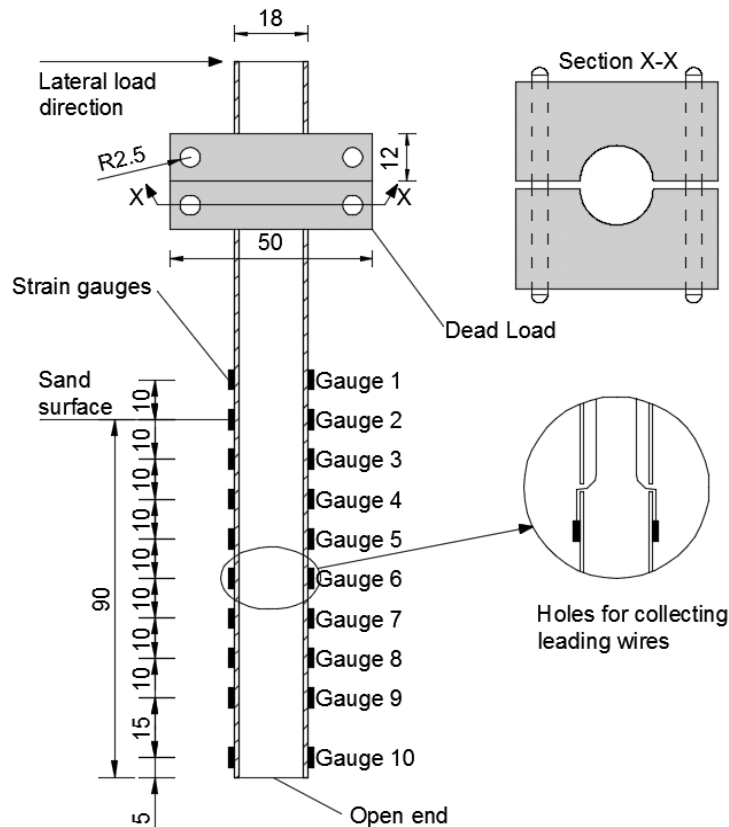| Property	Model pile	Unit
Length (embedded + additional)	90 + 150	mm
Diameter, internal	16	mm
Diameter, outside	18	mm
Wall thickness	1	mm
Young's modulus (E)	70	GPa
Moment of inertia (I)	1936	mm^4
Flexural stiffness (EI)	13.6×10^7	Nmm^2

Figure 5.6 Model pile schematic diagram with strain gauge layout (dimensions in mm)

5.2.4 Soil preparation and characterisation

Fine, uniform Geba sand [63] was used in this study. It is mainly comprised of silica (99% SiO_2) and 84.2% of the grains have a diameter between 0.1 mm and 0.2 mm. The ratio of pile diameter

to average grain size of the sands (D/D_{50}) for the tests is approximately 164, which is larger than the value of 20 and 60 suggested by Gui et al. [65] and Remaud [66], where grain size effects become negligible for laterally loaded piles [81]. A relative density (D_r) of 53% was adopted for the prepared sand used in the experiments conducted in this paper. The main properties are summarised in Table 5.3.

Table 5.4 Basic soil properties of Geba sand [69, 70]

Property	Sand
Median Particle Size, D_{50} (mm)	0.11
Curvature Coefficient, C_C	1.24
Uniformity Coefficient, C_U	1.55
Specific Gravity, G_S	2.67
Maximum Void Ratio, e_{max}	1.07
Minimum Void Ratio, e_{min}	0.64

5.2.5 Scour hole excavation

In order to study the effect of shape and type of scour erosion, it is necessary to develop a method to model scour-hole geometries in the centrifuge. To cover the main range of expected scour hole geometries, three different scour hole shapes (one for global scour and two for local scour) were considered, see Figure 5.1. Figure 5.1 shows a schematic of simplified global and local scour. In the models, D denotes pile diameter, W_t denotes top width of scour hole, W_b denotes bottom width of scour hole, D_s denotes scour depth and ω denotes slope angle of the scour hole. A range of scour depths of $1D$, $1.5D$ and $2D$ were implemented in this study to cover the ranges normally considered [19, 51, 106, 107]. Global scour was modelled through the complete removal of a given soil layer, see Figure 5.1, and typically occurs due to natural seabed migration. Local scour represents the case of a scour hole forming in the direct vicinity of a pile. To model local scour, a scour hole was created in the shape of an inverted frustum. To investigate the influence of scour-hole shape, the scour-hole base extends around the pile at a distance (W_b) varying between 0 and D. A scour hole with a base width $W_b = 0$ is termed local narrow scour while a scour hole with a base width $W_b = D$ is termed local wide scour in subsequent analyses. A scour hole side slope of 30° was adopted for all cases, which is in line with previous experiments [97, 108]. Note, the scour side slope angle is the least important factor among the three scour hole dimensions (scour depth, scour width, scour-hole slope angle) influencing the responses of laterally loaded piles [60, 109]. For this reason, it is kept constant in the present study.

82

5 Centrifuge modelling of the impact of local and global scour erosion
on the monotonic lateral response of a monopile in sand

To excavate sand to form the scour-hole shapes described, rigid moulds were fabricated, as shown schematically in Figure 5.7. These moulds, with varying depths and base widths were used to ensure the shape of the scour holes adhered to the required dimensions for each test. Each scour hole was created immediately prior to jacking the model pile at 1g and just before spinning the centrifuge up to 100g.
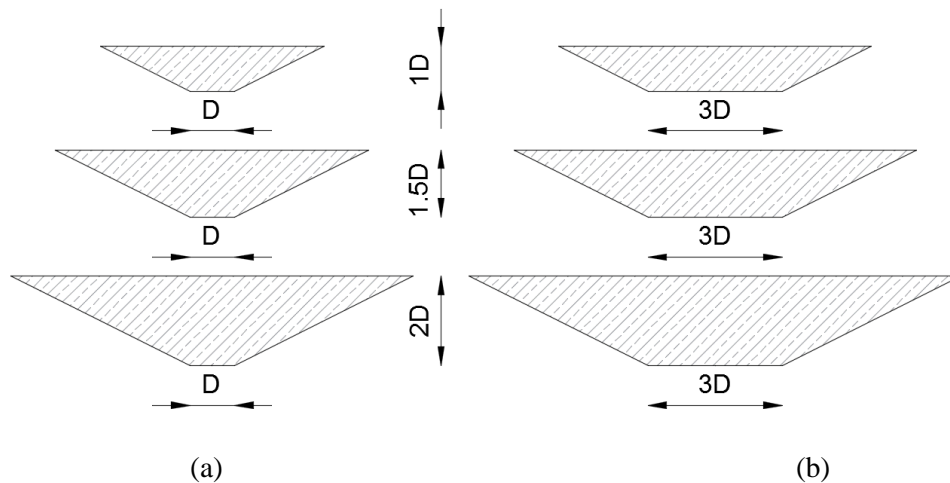
Figure 5.7 Schematics of: (a) Scour-hole moulds of local narrow scour; (b) Scour hole moulds of local wide scour

5.2.6 Testing program

Displacement controlled lateral loading is applied to the pile head by the lateral movement of the actuator at a constant displacement rate of 0.01 mm/s. Each test continues until the loading arm reaches the target displacement. The testing program comprised investigating the effect of scour depth and scour type on the lateral behaviour of the pile (capacity and bending moment). No scour, and three scour depths equating to 1D, 1.5D and 2D were studied. Moreover, three scour types, namely local narrow scour, local wide scour and global scour were also investigated to ascertain the influence of scour-hole shape (overburden dependency) on the pile lateral behaviour. Each test was undertaken twice to ensure repeatability. A constant vertical load of 3 MN was applied to represent the weight of a superstructure. The testing program is summarised in Table 5.4.

Table 5.5 Programme of centrifuge test

Test number	Scour type	Scour depth	Vertical dead load at prototype scale (MN)	Description
1	No scour	-	0, 1.5 and 3	Zero scour lateral load test
2	Global scour	$1D$	3	Scour test
3	Global scour	$1.5D$	3	Scour test
4	Global scour	$2D$	3	Scour test
5	Local wide scour	$1D$	3	Scour test
6	Local wide scour	$1.5D$	3	Scour test
7	Local wide scour	$2D$	3	Scour test
8	Local narrow scour	$1D$	3	Scour test
9	Local narrow scour	$1.5D$	3	Scour test
10	Local narrow scour	$2D$	3	Scour test

5.3 Results and discussion

The load-displacement response and bending moment profiles over the entire displacement range of the piles are reported in this section.

5.3.1 Lateral load-displacement and bending moments under zero scour condition

The pile head load-displacement response measured for the no-scour base-case condition is shown in Figure 5.8 (Test number 1). The ultimate resistance, H_u, of a pile is usually defined at a displacement equal to 10% of the pile diameter at the seabed (mudline) level. In the present study, the pile head displacement (as opposed to the seabed displacement), which is 15 m above the seabed level (at the prototype scale), is the measured parameter. For the purpose of comparison of the cases considered in this paper, H_u is defined as a pile head displacement of one pile diameter, in this case 1.8 m. In Figure 5.8, the pile is loaded up to and beyond the specified ultimate resistance, and it can be seen that the lateral resistance continues to increase to a value of 970 kN at a lateral pile-head displacement of 3 m (Figure 5.8a). The presence of a vertical load (superstructure weight) had a minimal effect on the lateral response for this pile geometry with the H_u capacity changing by approximately 1% as the vertical applied load increased from 0 to 3 MN. As a result, all remaining tests were performed with a 3 MN vertical load to represent the superstructure weight.

Figure 5.8(b) shows the bending moments derived from the strain gauge readings using 7 of the 10 strain gauge pairs for the applied loading in Figure 5.8(a). Note, because of limitations with

5 Centrifuge modelling of the impact of local and global scour erosion
on the monotonic lateral response of a monopile in sand

84

the data logger, only seven strain gauge pairs could be analysed at any one time. Bending moments are derived from bending strain measurements using Equation (5.1).

$$M(z) = EI\rho(z) \tag{5.1}$$

where EI is the flexural rigidity of the pile and $\rho(z)$ is the curvature at a given applied load, obtained as the ratio between the difference in measured compressive and tensile strains to the gauge lever arm (pile diameter) at a given depth z. Figure 5.8(c) shows the evolution in bending moment profiles along the pile as the lateral pile head displacement increased from 0.5 m to 3 m.
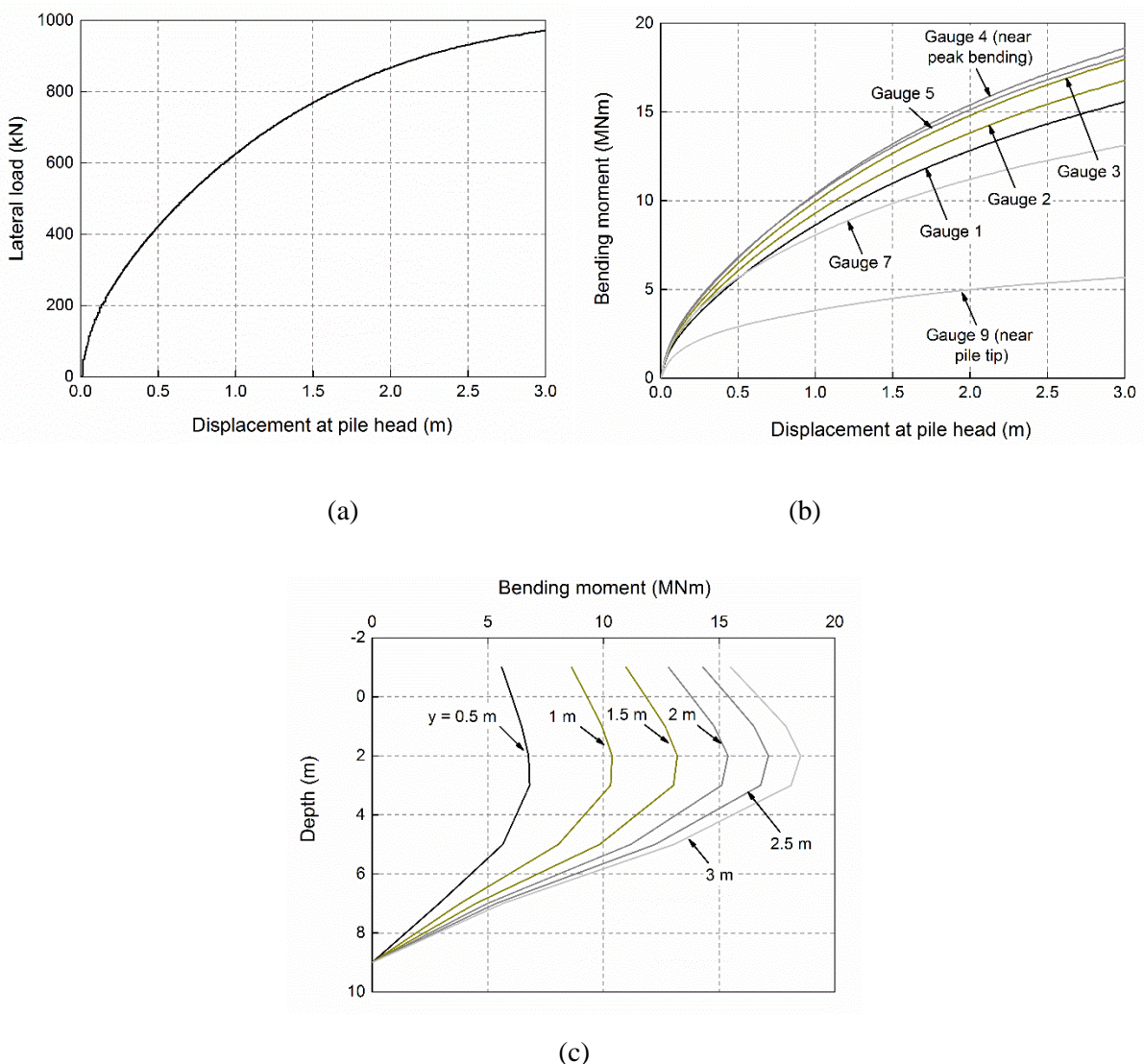

(a)

(b)

(c)

Figure 5.8 Zero scour response features from centrifuge testing at prototype scale: (a) Pile head lateral load-displacement response; (b) Bending moment measurements along the pile; (c) Bending moment profiles for different levels of pile head displacement (y)

5.3.2 Effect of scour depth on the lateral pile response

The impact of four different local scour depths are investigated in this section, namely zero scour, and scour with depths $1D$, $1.5D$ and $2D$. Only the results for a single scour shape, namely local wide scour, is considered. For this scour-hole shape, sand is removed up to a distance of $1D$ from around the pile. The influence of scour shape is investigated in a subsequent section.

The impact of increasing scour depth on the lateral load-displacement responses is shown in Figure 5.9(a). For the cases considered, the H_u value reduces from 831 kN to 234 kN as the scour depth increases to $2D$, a reduction of almost 72%.

The bending moment distributions under 0, $1D$, $1.5D$ and $2D$ scour are reported in Figure 5.9(b). As the scour depth increases, the peak bending moment M_{max} increases from 1.527 MNm to 1.86 MNm. Furthermore, the location of the maximum bending moment also moves progressively down the pile as scour depth increases. These findings are in line with previous research [52], where the influence depth is observed to increase.

(a)   (b)
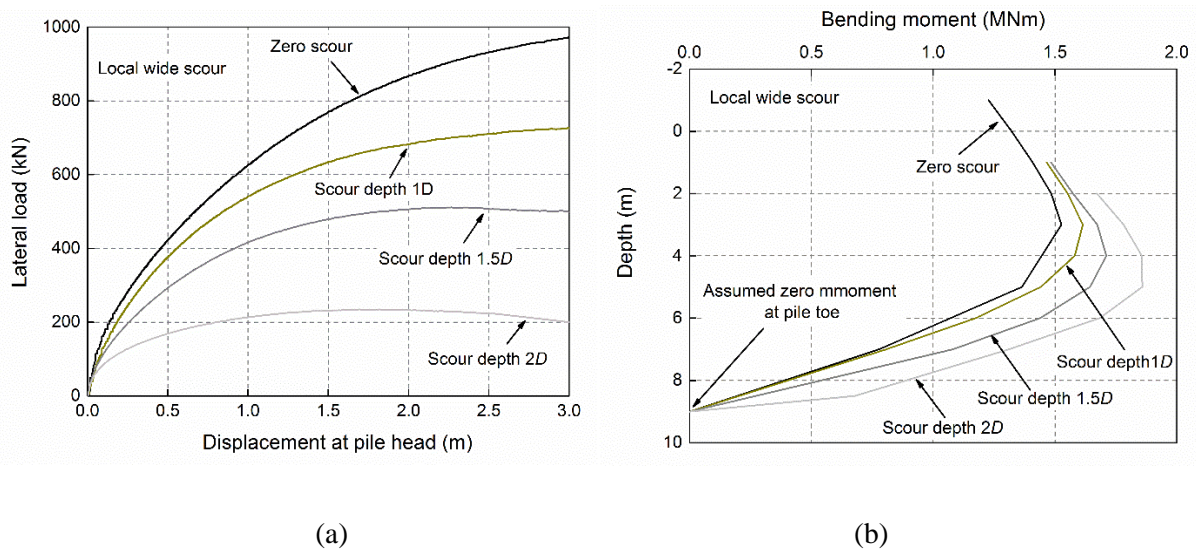
Figure 5.9 Effect of scour depth on pile response characteristics at prototype scale: (a) Lateral load-displacement response under increasing local wide scour; (b) Bending moment derived from strains for increasing scour

5.3.3 Effect of scour type on the lateral pile response

In this section, the effect of scour type on the bending moment distribution along the pile under scour is investigated. Local narrow, local wide and global scour types are compared with a view

86

5 Centrifuge modelling of the impact of local and global scour erosion
on the monotonic lateral response of a monopile in sand

to ascertaining if the scour hole shape and associated overburden influence has an effect on the resulting bending moment distribution. Figure 5.10(a) shows the bending moment distribution measured along the pile under a scour depth of $1D$, for the three scour types, due to an applied lateral load of 100 kN. Similar to previously, the bending moment increases between zero scour and $1D$ scour. Evidently, there is a difference between the local scour and global scour, in that the global scour results in a larger bending moment under the applied load than the local scour. For the scour depth of $1D$, both local narrow and local wide scour exhibit similar bending moment profiles, suggesting that for this scour depth, there is negligible difference due to the variation in overburden pressure between both local scour types. The maximum bending moment M_{max} increases 5.7% from the no scour case to the local scour case, and 10.7% from the no scour case to the global scour case. The location of the point of maximum moment increases from 3 m to 4 m below seabed level.
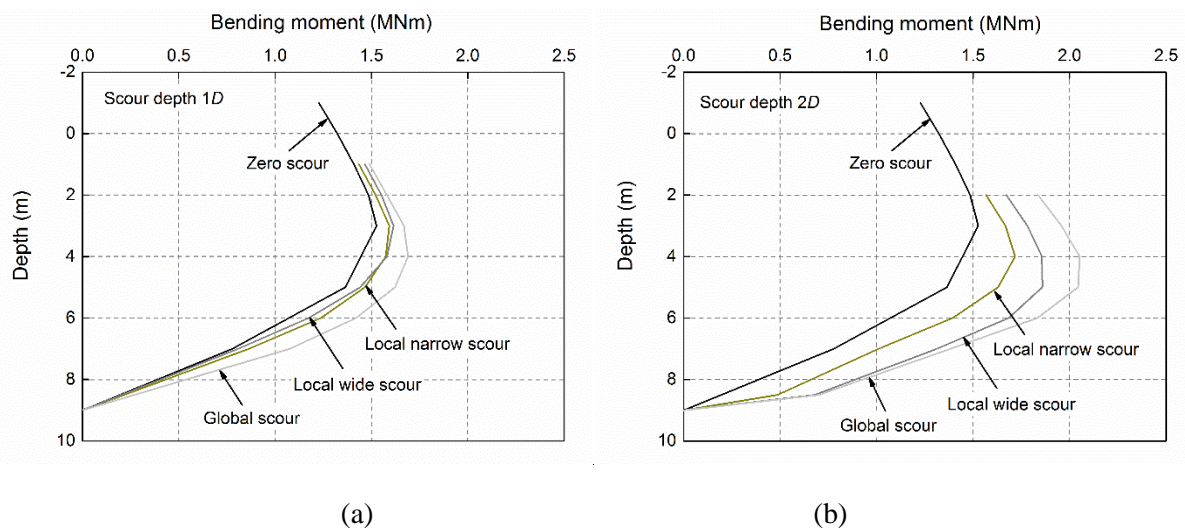

Figure 5.10 Effect of scour type on bending moments measured along pile for applied lateral load = 100 kN: (a) Bending moments for local narrow, local wide and global scour to depth $1D$; (b) Bending moments for local narrow, local wide and global scour to depth $2D$

Figure 5.10(b) shows the same information as Figure 5.10(a), but for a scour depth of $2D$. In this case, there is a clear increase in the bending moment measured between no scour and the three scour types. This suggests that soil close to the pile in the local narrow scour case provides enhanced effective confining stiffness, due to the presence of the remaining overburden. Moreover, the sand slope in the local narrow scour case provides extra lateral resistance compared with that of local wide scour case lacking sand slope effect. M_{max} increases 12.5% from the no scour to local narrow scour case, 21.7% to the local wide scour case, and 34.4% to

the global scour case. The location of the point of maximum moment increases from 3 m to 5 m below seabed level. The influence of scour hole shape is a significant finding as many previous researchers completely ignored this effect, and simplify scour as the increase in free length of a structural element, without due attention to the properties of the remaining soil [57, 110]. The physical modelling results in this article highlight that this influence should not be discounted

5.4 Conclusions

This paper presents the development of a specially designed pile lateral loading system for centrifuge model tests that minimises the pile-head rotational constraint associated with tests of this nature. A modelling scheme to evaluate lateral pile behaviour under combined lateral and moment loading at the seabed level, under various scour conditions, is undertaken using this ball-type loading system. The study has several conclusions:

1. The friction-reducing ball connection with Teflon interface is adept at providing a lateral monotonic load, with significantly reduced pile-head rotational fixity. This is useful for research on offshore monopile models, which have a free head condition. Other types of loading rigs, which use pin-type connections, have a tendency to apply a component of vertical loading to pile models as lateral displacements become large. The ball-type connection adopted in this study mitigates this issue.

2. Scour reduces the lateral capacity and stiffness of pile foundations and leads to increased bending moments along the pile under similar lateral loads applied at the pile head. Moreover, the location of the maximum bending moment occurs lower along the pile for increased scour, which may have implications for the design of monopiles with variable wall thickness. Increased pile wall thickness may be adopted in the region near surface soils to increase bending resistance locally, therefore changes in the response regime due to scour has potential design ramifications, and should be considered.

3. In addition to scour reducing lateral capacity, the shape of the scour hole has a noticeable effect on the measured bending moments. For a scour depth of $1D$, there is a distinct increase in the bending moments for the case of global scour compared to local scour. However, little difference is observed between local narrow and local wide scour at this scour depth. For the case of scour up to a depth of $2D$, however, there is a significant

88

5 Centrifuge modelling of the impact of local and global scour erosion
on the monotonic lateral response of a monopile in sand

difference between the bending moments measured for each scour type, with the bending moment consistently increasing from the no scour case to local narrow scour, to local wide scour and on to global scour. This finding suggests that designers should explicitly consider scour hole geometry in design (at least in a preliminary capacity), as it is conservative to assume the entire soil layer is removed during scour. For local scour, the overburden and sand slope close to the pile provides additional resistance to the remaining soil, reducing the bending moments relative to global scour.

This paper presented the background to the centrifuge-based analysis regime for a pile under various scour conditions. It should be noted that installation effects were not considered since the model piles were jacked into the soil at $1g$ prior to testing. If the piles were driven while in-flight, this would lead to the generation of residual base stresses, and potential moments at the pile base. While the analysis in this paper does not consider the presence of these additional base moments, the behavioural trends identified in this paper should be not affected. Further studies will expand the investigation to the influence of scour on p-y reaction curves.

6 The impact of scour on the lateral response of wind turbine monopiles: an experimental study

The majority of offshore wind structures are supported on large-diameter, rigid monopile foundations. These piles may be subjected to scour due to the waves and currents that cause a loss of soil support and consequently decrease the pile capacity and system stiffness. The results of numerical models suggest that the shape of the scour-hole affects the loss of pile capacity, however, there is a dearth of experimental test data that measure the effect. This paper presents a series of centrifuge model tests on an instrumented model pile that investigates the effects of scour-hole geometry on the response of a laterally loaded pile embedded in sand. The pile instrumentation allowed load-displacement and p-y (soil reaction-displacement) curves to be derived. Three scour geometries (global, local wide and local narrow) and three scour depths (1D, 1.5D and 2D; D, pile diameter) were modelled. Global scour was identified as the most damaging scour type, followed by local wide scour, and local narrow scour. For all the three scour types, pile moment bearing decreased almost linearly with an increase of scour depth. Simple empirical relations were proposed to evaluate the detrimental influence of scour on the pile moment capacity. A new method has been developed to allow designers to quantify the effect of scour-hole shape and severity of scour on the pile response.

6.1 Introduction

Monopiles are the most economical foundation system for Offshore Wind Turbines (OWTs) installed in shallow coastal waters [90]. The typical slenderness ratio (L/D: L, pile embedded length; D, pile diameter) for OWT monopiles is between 3 and 6 [3, 10]. Cylindrical structures such as OWT monopiles are prone to loss of soil support due to sand erosion, i.e. scour. As a consequence, the pile lateral load capacity and stiffness could be decreased, potentially resulting in large lateral displacement and rotation. Such effects can put the superstructure at risk through the generation of excessive fatigue loading as well as operational issues [111]. The shapes of various types of scour holes are illustrated in Figure 6.1. Typically, scour holes are formed in a shape approximating an inverted frustum. The slope angle (ω) is roughly equal to the angle of repose of sand, generally in the range 30 to 44° [112] and the top scour width (W_t) is often assumed to be twice the scour depth [58, 112]. Based on several experimental studies, it has been shown that the scour depth (D_s) depended on the diameter of the pile (D), Froude number of the water flow, shear stress applied to the sand surface due to the flow and soil strength [55, 113]. DNV [114] suggested the adoption of an extreme scour depth of $2D$ in offshore structure design. However, Sørensen and Ibsen [55] illustrated that this assumption ($D_s = 2D$) might be too conservative for wave induced scour holes.
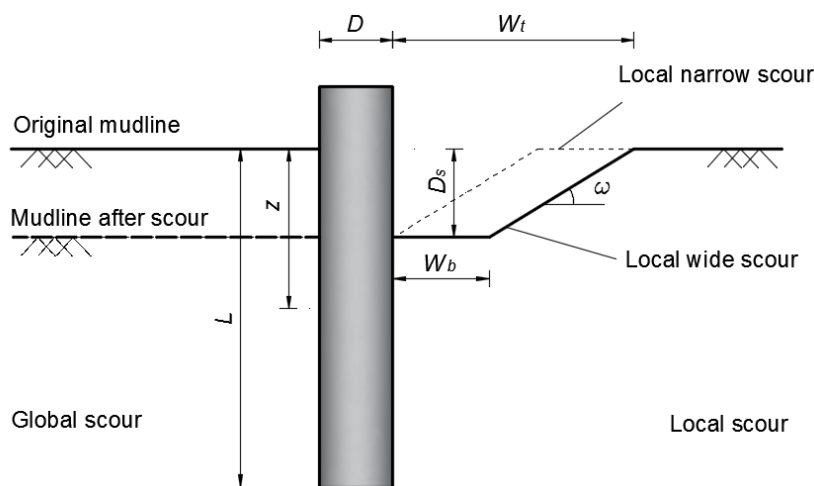

Figure 6.1 Symbols and definitions of scour-hole (modified after Li et al. [71])

One approach, and perhaps the simplest one, to model the effect of scour on the lateral monopile behaviour is to remove the affected soil layer completely. This approach simulates a so-called global scour condition (schematised on the left-hand side of Figure 6.1). The other approach is to consider three-dimensional shape of scour holes. Based on various numerical analyses, Li et

al. [109], Lin et al. [53], Mostafa [54], Qi et al. [59] and Zhang et al. [60] suggested that the assumption of a global scour can be highly conservative. Similarly, centrifuge tests on piles with L/D = 12.7 conducted by Qi et al. [59] indicated that removing the entire soil layer to the scour depth can result in a 49-68% increase in lateral displacement of the pile at a fixed load, when compared to a model that three dimensional scour-hole dimensions were incorporated. In an attempt to follow the second modelling approach, Lin et al. [13] developed simplified stiffness models for soil reaction based on Winkler model (p-y curves) assuming a wedge failure mechanism for a slender laterally loaded pile (L/D = 35) subjected to scour. Their model was verified with a three dimensional finite element model. The pile response accounted both the scour-hole geometry and the over-consolidation effect of the removed soil on the remaining soil. It was found that for global scour, the p-y curves at given depths were essentially identical when compared between those below the post-scour surface and those at the same depths without scour. In contrast, for local scour, the p-y response at a given depth was found to be much stiffer below the scour-hole base than at the same depth below the original soil surface. The authors concluded that the difference in the effects of global and local scour is attributed to the beneficial influence of the remaining overburden soil surrounding the pile in the latter case.

To address the dearth in experimental data concerning the impact of scour-hole geometry on the response of rigid monopiles, this paper presents the results of a series of centrifuge model tests conducted considering different parameters, such as scour depth and scour hole dimension as well as the magnitude of applied lateral and moment loading. Based on the measured bending moment distributions, p-y curves were derived and analysed to evaluate the impact of scour type on the tested piles. Based on the analysis of experimental data, a new design method has been developed to take the three-dimensional shape of the scour hole into account. An example of the design method is presented in the last section of the paper.

6.2 Experimental set-up

6.2.1 Model pile and soil characterisation

The model pile was open-ended and fabricated from a hollow, circular, aluminium tube with an outer diameter (D) of 18 mm and a wall thickness (t) of 1 mm. The primary dimensions and material properties of the pile can be found in Table 6.1. The pile was instrumented with ten

levels of strain gauges calibrated for measuring bending moment (see Figure 6.2). Because of constraints regarding the loading mechanism, the pile was jacked into the sand sample prior to spinning up the sample (i.e. installation at 1*g*) with the result that installation effects were not fully modelled. However, the same preparation method and testing procedure was followed for all of the tests.

The experiments were conducted using dry Geba silica sand. The geotechnical characteristics of the sand are summarised in Table 6.2. The relative density (D_r) of the prepared sand specimen was 80%.

Table 6.1. Model and corresponding prototype pile dimensions and properties (centrifuge tests were performed at 100*g*)

Property	Model pile	Prototype pile*
Length (embedded + loading eccentricity)	90 + 144 mm	9 + 14.4 m
Diameter, outer	18 mm	1.8 m
Wall thickness	1 mm	30 mm
Elasticity modulus (*E*)	70 GPa	210 GPa
Moment of inertia (*I*)	1936 mm^4	0.065 m^4
Flexural stiffness (*EI*)	0.136 kPa.m^4	13.7 GPa.m^4

*Assuming prototype pile is fabricated from steel; tests were performed at 100*g*
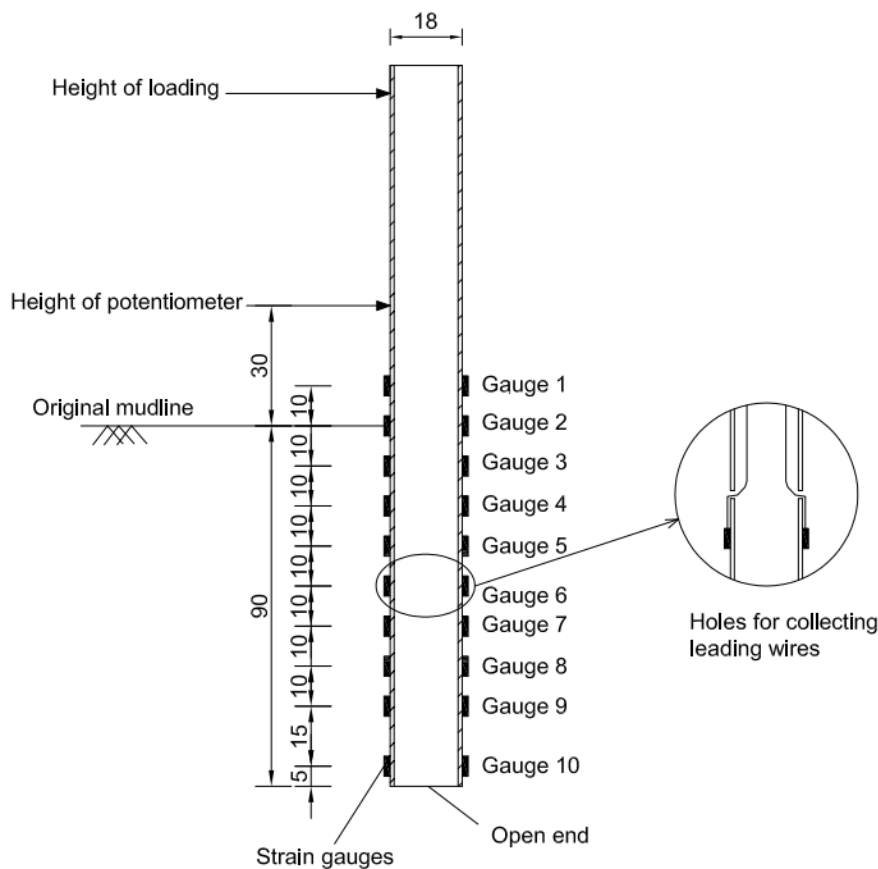

Figure 6.2 Model pile schematic diagram with strain gauge layout (dimensions in mm)

Table 6.2. Soil properties of Geba sand [69, 70]

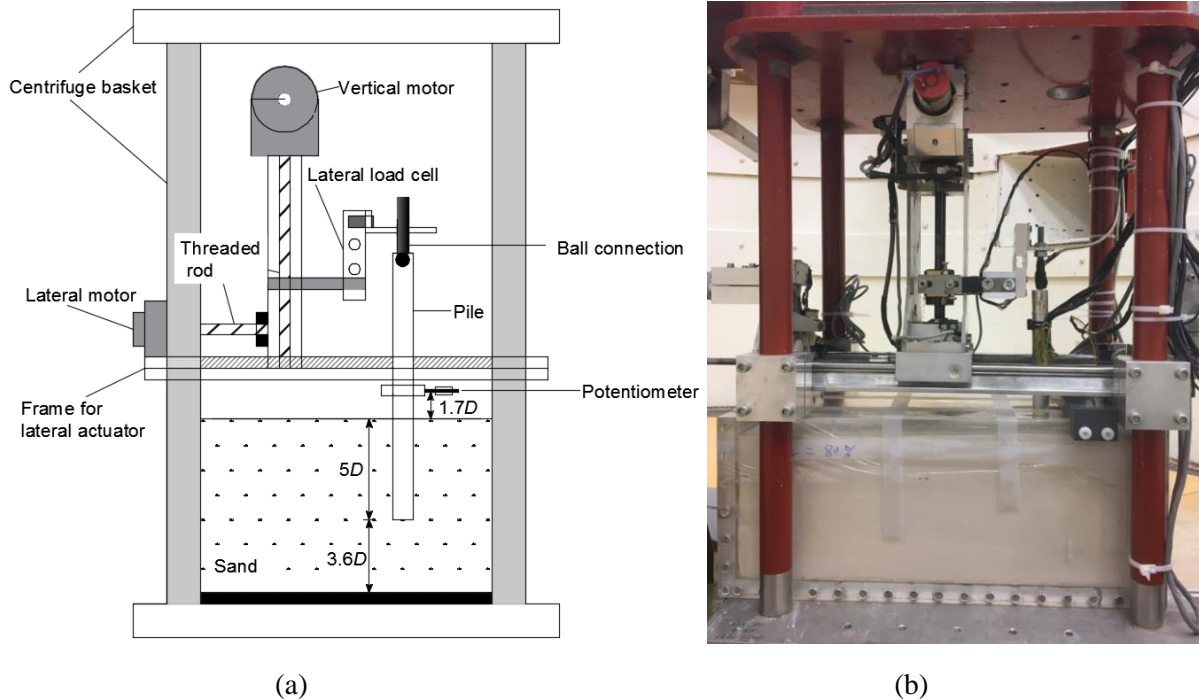| e_{min}	e_{max}	G_S	D_{50} (mm)	C_U	φ_{cr}
0.64	1.07	2.67	0.11	1.55	35°

| (a) | (b) |

Figure 6.3 Two dimensional loading actuator and pile testing setup: (a) Schematic diagram; (b) Photo

6.2.2 Centrifuge loading actuator

The experiments were performed using the beam centrifuge in the Geo-Engineering Section of TU Delft [62, 71, 80]. A two-dimensional actuator (Figure 6.3) was used to impose lateral load (*H*) at the pile head. Applied lateral load was measured by parallel beam load cell (HTC-SENSORS; TAL220; measuring range 100 N; sensitivity 0.05%). Pile lateral displacements were measured at two locations: pile top using the signal encoder of the actuator; and 1.7*D* above the sand surface using a potentiometer (ETI SYSTEMS; LCP8S-10; measuring range 0-14 mm; sensitivity 2%). These two measurements facilitate the calculation of both lateral translation and rotation of the model pile. A specially-designed friction-reducing ball connection was constructed to transfer the lateral loading with application of minimal rotational constraint at the pile top. Details of this ball connection are described by Li et al. [71] and Chortis et al. [85].

In the following, the experimental data is expressed in prototype scale. For all of the centrifuge tests performed in this study, the centrifuge acceleration level was $100g$. Lateral loading was applied at a predetermined height $e = 8D$ above the original mudline, to mimic the lateral loading and significant overturning moment resulting from combinations of wind, wave, current and other lateral load actions. The pile diameter was 1.8 m and original embedment depth was 9 m ($L/D = 5$).

6.2.3 Scour-hole formation

Three scour depths, 1.8 m ($1D$), 2.7 m ($1.5D$) and 3.6 m ($2D$), and three scour shapes, local narrow scour, local wide scour and global scour, were modelled (schematically shown in Figure 6.4). Global scour was modelled by removing the soil layer of thickness equal to different scour depths. For the tests with local scour, scour holes were created in the shape of inverted circular cones. To compare the influence of scour-hole shape, the scour-hole base extended around the pile at a distance varying between 0 and D (shown as W_b in Figure 6.1). Local narrow scour was defined when the scour-hole base has a dimension $W_b = 0$. When the scour-hole base has a dimension $W_b = D$, this was named local wide scour. The scour-hole slope angle was kept constant at 30º, which is in line with experimental investigation of Roulund et al. [108] and recommendation of Hoffmans and Verheij [98]. The scour-holes were formed after sand specimen preparation using a grab bucket and each hole was checked using specifically fabricated aluminium moulds.

6.2.4 Testing programme

Following creation of a scour-hole (when relevant), each pile was pushed into the given soil location at $1g$ using the vertical actuator operating at a rate of 0.1 mm/s to the target depth of $L = 5D$. Subsequently, the model was subjected to an enhanced acceleration field of $100g$. The lateral load was applied to the pile head by the lateral movement of actuator at a constant rate of 0.02 mm/s.

The testing programme comprises 10 tests: one monotonic load test with no scour (reference test) and nine monotonic load tests with three scour types and three scour depths, see Table 6.3. The effects of global scour, local narrow scour and local wide scour were assessed at scour depths of $1D$, $1.5D$ and $2D$.
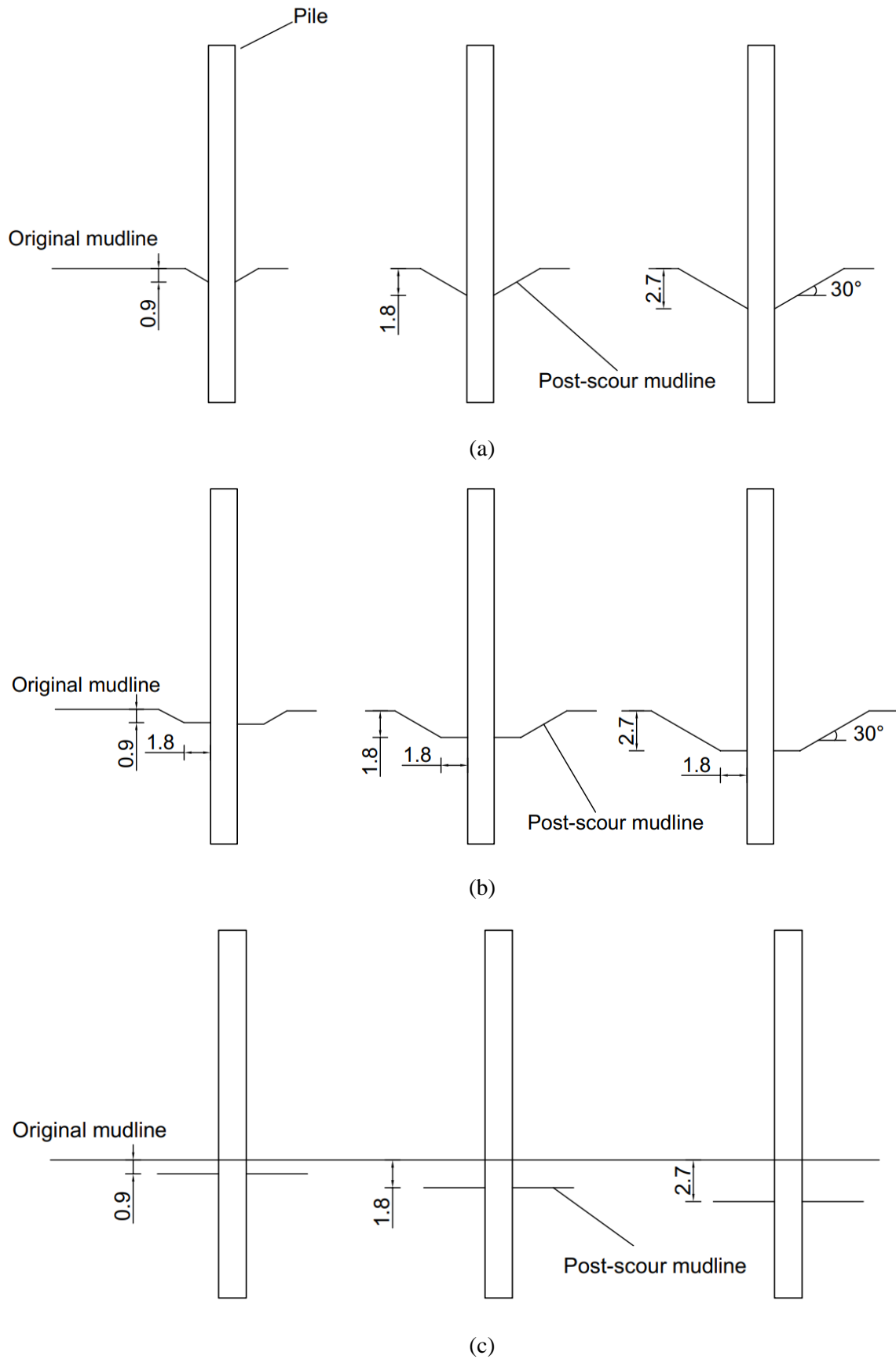
Figure 6.4 Schematic illustration of: (a) Local narrow scour; (b) Local wide scour; (c) Global scour (dimensions in m)

Table 6.3. Programme of centrifuge test

Test name	Dr (%)	Scour type	Scour depth
S-NS	80	No Scour (NS)	-
S-LN-1D	80	Local Narrow (LN)	$1D$
S-LN-1.5D	80	Local Narrow (LN)	$1.5D$
S-LN-2D	80	Local Narrow (LN)	$2D$
S-LW-1D	80	Local Wide (LW)	$1D$
S-LW-1.5D	80	Local Wide (LW)	$1.5D$
S-LW-2D	80	Local Wide (LW)	$2D$
S-GL-1D	80	Global (GL)	$1D$
S-GL-1.5D	80	Global (GL)	$1.5D$
S-GL-2D	80	Global (GL)	$2D$

6.3 Centrifuge test results

The results of the laboratory tests were investigated by plotting the angular rotation of the pile θ in response to the applied bending moment M, all measured at sand surface. Normalising these parameters enables comparison of results across scales. In this study, M and θ were normalized according to the equations suggested by LeBlanc et al. [41]:

$$\widetilde{M} = \frac{M}{L^3 D \gamma} \tag{6.1}$$

$$\tilde{\theta} = \theta \sqrt{\frac{p_a}{L\gamma}} \tag{6.2}$$

The method for data extraction is outlined in Figure 6.5 based on the test data of no scour case (S-NS). The results indicate that the pile rotation increases continuously as the applied moment increases, thus there is no distinct point which can be used to define failure. Following the recommendation of LeBlanc et al. [41], failure is defined by $\tilde{\theta} = 4^\circ = 0.0698$ rad. The moment capacity (M_R) for the pile under no scour case is 0.84.
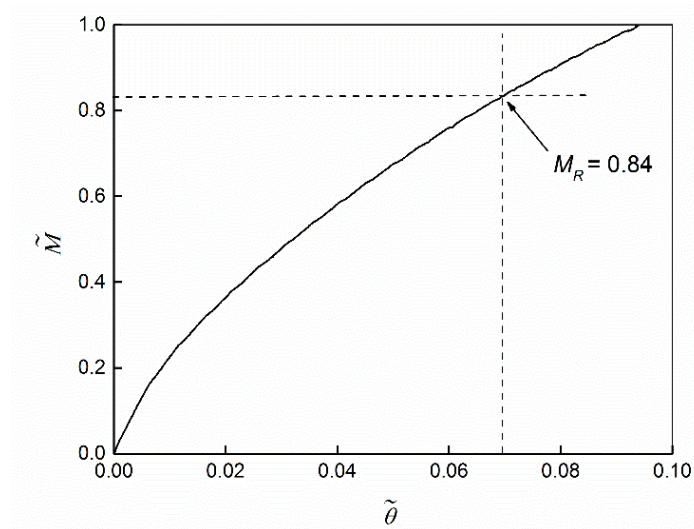
Figure 6.5 Determine of moment capacity (test S-NS)

6.3.1 *p-y* reaction curve construction

Using the strain gauge data, the measured distribution of bending moment *M(z)*, with depth z, was used to derive the soil reaction *p(z)*, by double differentiation, and the displacement profile *y(z)*, by double integration, according to the following equations:

$$p(z) = \frac{d^2 M(z)}{dz^2} \tag{6.3}$$

$$y(z) = \iint \frac{M(z)}{EI} dz dz \tag{6.4}$$

where *M(z)* is the bending moment at soil depth *z*, *EI* denotes the pile bending stiffness.

Fifth-order polynomial curve-fitting method was adopted to fit the moment data points. It was then differentiated twice and the soil response *p(z)* was evaluated at the central data point.

When determining displacement at any depth, *y(z)*, two integration constants C_1 and C_2 were determined from: 1) the measured displacement at the loading position and 2) an assumed zero deflection condition at the point with zero lateral soil resistance [74].

The measured bending moment (*M*) distributions, corresponding deduced distributions of soil resistance (*p*) and lateral pile displacement (*y*) for test S-NS are shown in Figure 6.6. It can be seen that, with the increase of lateral load, the bending moment, soil resistance and pile lateral

displacement all increase. The results generally suggest rigid pile behaviour, with significant displacement of the pile tip developed opposite to the loading direction.

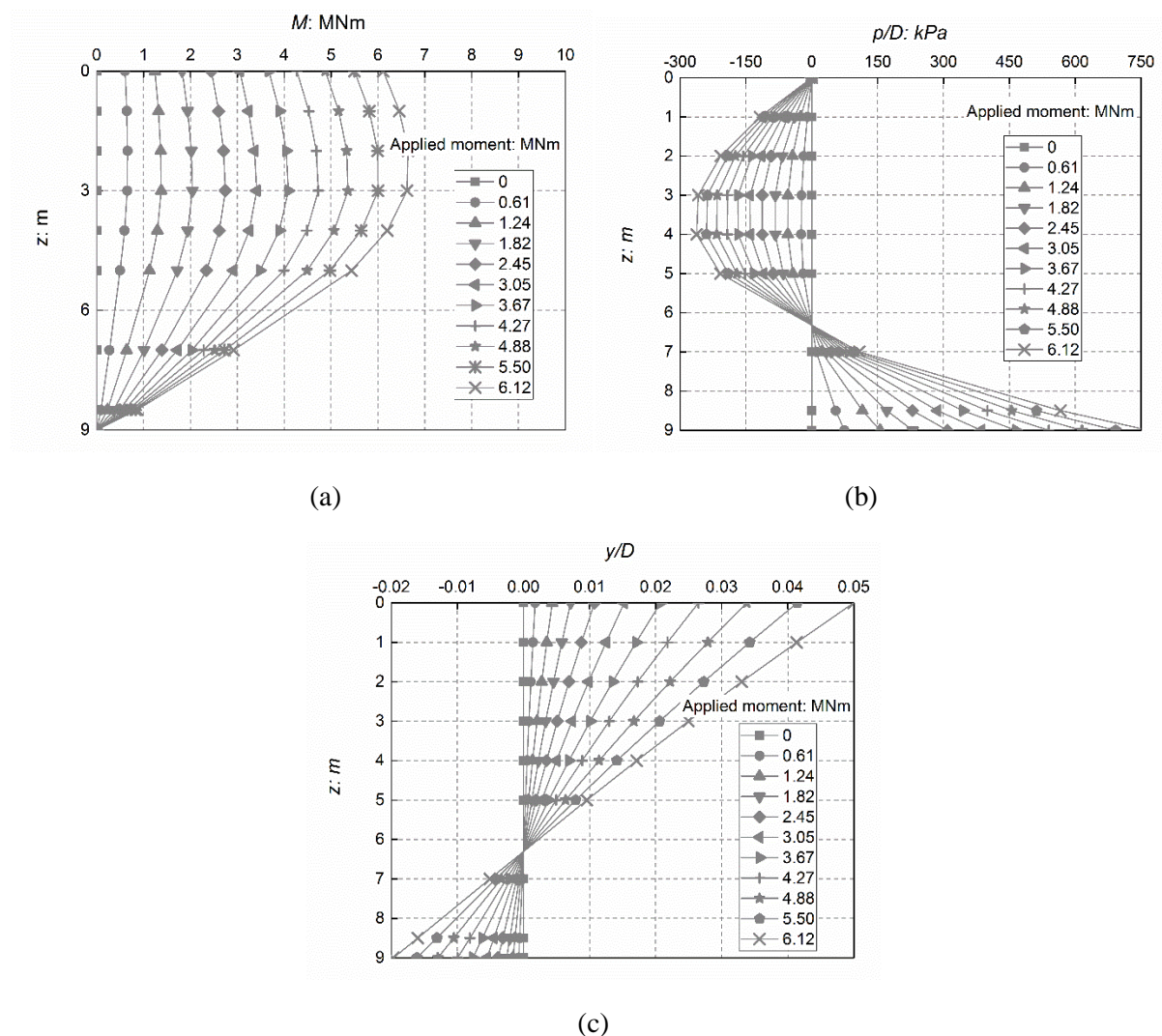(a)   (b)

(c)

Figure 6.6 Distributions of: (a) Measured bending moment; (b) Lateral soil resistance; (c) Lateral pile deflection under different values of applied bending moment (test S-NS)

The *p-y* curves were obtained by combining the soil resistance (*p*) and lateral displacement (*y*) at discrete intervals to produce curves at each depth, as shown in Figure 6.7. Absolute values are plotted, noting that the curves at depths of 7, 8.5 and 9 m correspond to passive soil pressures (negative values of displacement). The stiffness of the *p-y* curves increases rapidly with soil depths for $z \leq 4$ m, whereas the difference between the *p-y* curves on the passive displacement side also appears quite significant ($z \geq 7$ m).
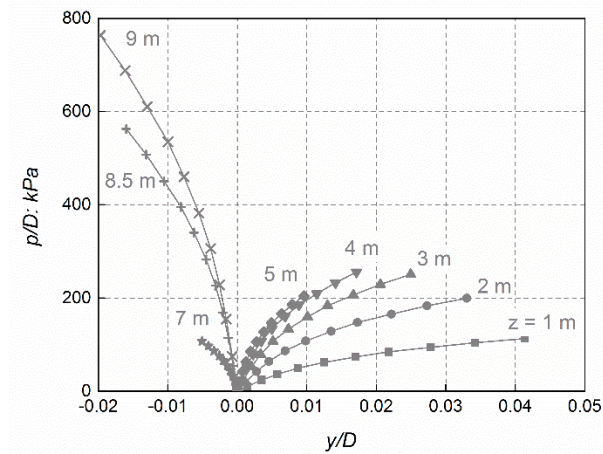
Figure 6.7 Experimental *p-y* curves at different soil depths (test S-NS)

6.3.2 Effect of scour type

The effect of the scour type, i.e. global, local wide and local narrow scour around the monopile, on the lateral behaviour of the foundation are discussed from three aspects of: (i) Moment-rotation at the sand surface, (ii) Distribution of bending moment along the pile, and (iii) Soil reaction-lateral displacement curves (*p-y* curves).

Moment-rotation relationships

Figure 6.8 shows the moment-rotation curves from centrifuge tests considering different scour types and scour depths. In all figures, the pile with no scour shows the highest initial stiffness and capacity, followed by local narrow scour, then local wide scour, and with global scour showing the lowest results. Comparing the measurements from the local narrow and local wide scour cases, results suggest that the remaining soil post scour can have considerable effect on the confining stresses and hence on the lateral stiffness of the foundation system.

As suggested by DNV [19], the typical limiting rotation is 0.5° at the soil surface, whereas a 0.25° construction tolerance should be taken into account. Therefore it gives an allowable accumulated rotation of 0.25° due to various kinds of loadings during the life time of OWTs [46], which corresponds to $\tilde{\theta}_{AAR} = 0.00375$ rad (in $\tilde{\theta}_{AAR}$, the subscript "AAR" stands for "Allowable Accumulated Rotation"). From Figure 6.8 it can be seen that, at scour depths of 1*D* and 1.5*D*, scour type has minimal effect on the initial stiffness of pile moment bearing behaviour. It suggests that when carrying out pile dynamic analysis within small strain range, scour type can be regarded as no effect especially at shallow scour depth ($D_s < 1.5D$). While at

very large scour depth ($2D$ for example), effect of scour type should certainly be taken into consideration, as the initial stiffness of pile is significantly influenced by scour type.
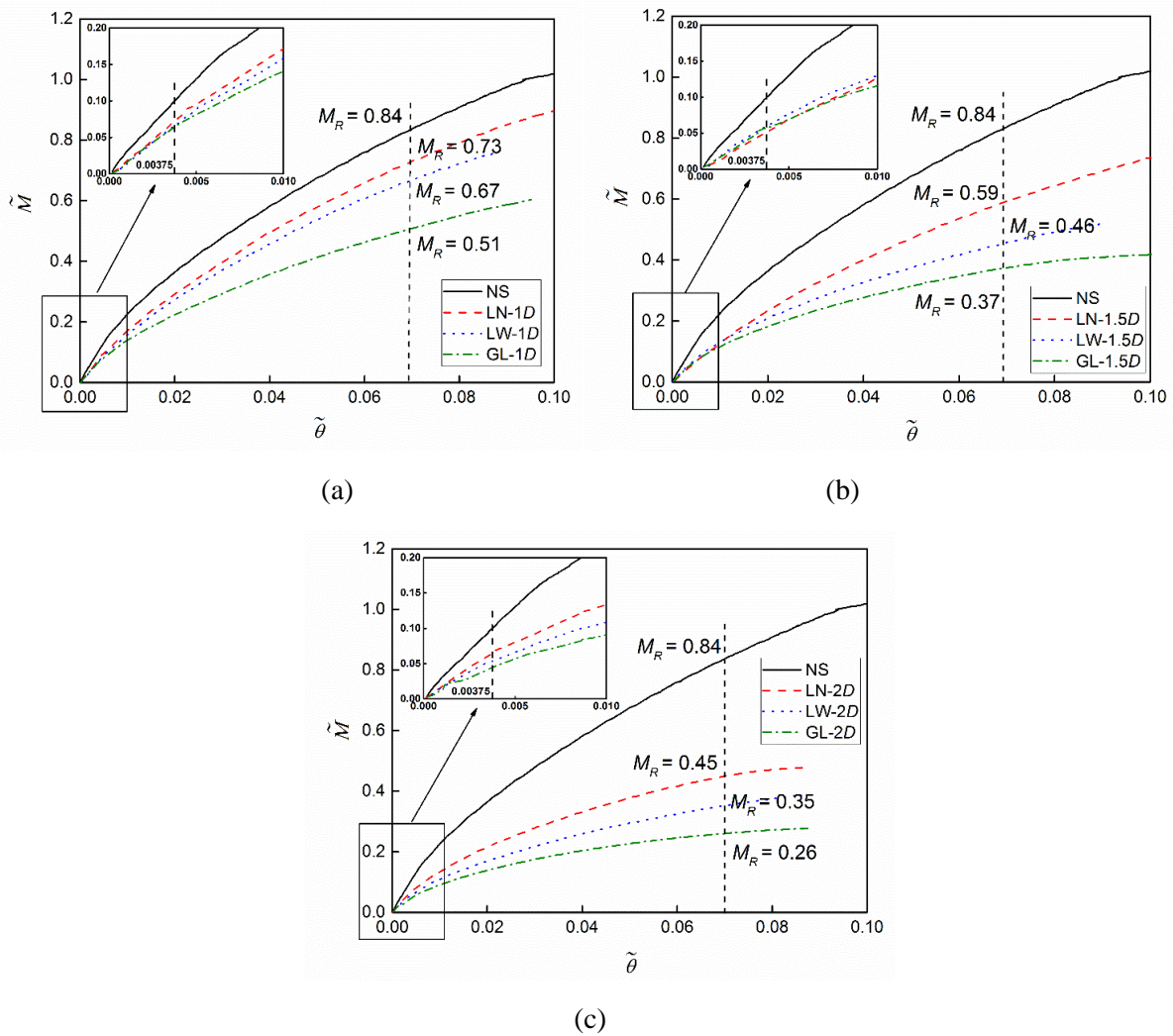

(a)

(b)

(c)

Figure 6.8 Influence of scour type on the moment-rotation response of piles: (a) Scour depth $1D$; (b) Scour depth $1.5D$; (c) Scour depth $2D$

Moment reduction factor, $M_{R,reduction}$, is used to describe the reduction of moment as a result of scour, which is defined in the following equation:

$$M_{R,reduction} = \frac{M_{R,no\ scour} - M_{R,with\ scour}}{M_{R,no\ scour}}$$
(6.5)

where $M_{R,reduction}$ denotes the reduction of M_R as a result of scour, $M_{R,no\ scour}$ is the moment capacity under no scour condition, and $M_{R,with\ scour}$ is the moment capacity under scour condition. The reduction of moment capacity compared with the reference case, increased with

scour depth, can be seen in Table 6.4, which shows reduction of 13-39% for a scour depth of 1D, increasing to 46-69% for a scour depth of 2D.

Table 6.4. Reduction of moment ($M_{R,reduction}$) as a result of scour

Scour type	$D_s = 1D$	$D_s = 1.5D$	$D_s = 2D$
Local narrow scour	0.13	0.30	0.46
Local wide scour	0.20	0.45	0.58
Global scour	0.39	0.56	0.69

Bending moment distributions

The normalised bending moment profiles of piles subjected to an external normalised bending moment of $\tilde{M}$ = 0.2 under various types and depths of scour are shown in Figure 6.9. For all scour types and depths considered, bending moment increased significantly compared to the non-scour case. This would suggest in practice that an increase of pile diameter and/or wall thickness may be required during design of a monopile installed in an area with potential of scour [12]. For scour depths of 1D and 1.5D, the moment profiles developed for the local wide scour and global scour are very similar, and those for the case of local narrow scour are slightly smaller. Therefore, it can be concluded that scour shape has a very small effect on the bending moment profile along the embedded length of pile. However, there is a clear distinction between results of different scour types as the scour depth increased to 2D.

p-y reaction curves

The *p-y* curves at a soil depth of z = 3 m are compared for different shapes of scour with depth of 1D in Figure 6.10. The results indicate that, the no-scour case shows the highest amount of soil reaction at this depth for any level of pile lateral displacement. Moreover, it can be observed that the soil elements around the piles suffering from a 1D scour condition show much lower stiffness comparing to the intact soil surface situation. The difference in the *p-y* curves between the cases of local narrow and local wide scour conditions is non-significant, compared with no scour and global scour.
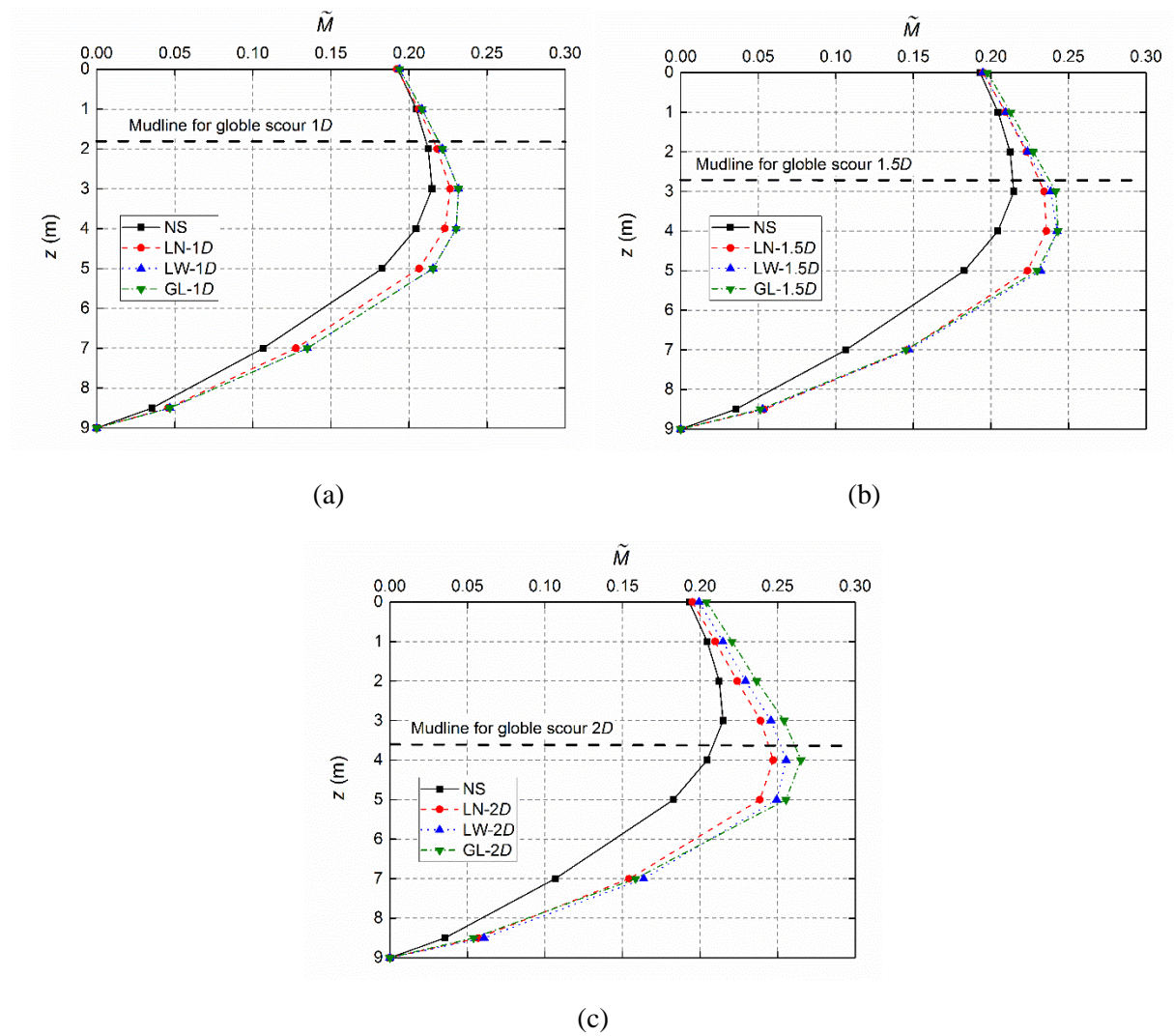
(a)   (b)

(c)

Figure 6.9 Profiles of bending moment along the pile at various scour types ($\tilde{M}$ = 0.2): (a) Scour depth 1D; (b) Scour depth 1.5D; (c) Scour depth 2D
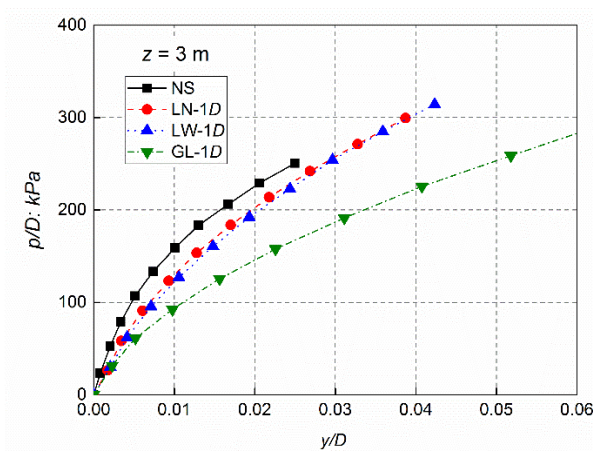

Figure 6.10 p-y curves at z = 3 m in the cases of no scour, 1D local narrow scour, 1D local wide scour and 1D global scour

The effects of scour shape and depth on the *p-y* curves are illustrated in Figure 6.11. It can be concluded that at small strains the *p-y* curves are less sensitive to the scour shape. For example, for a scour depth of 1.5*D* the initial response (*y/D* < 0.005) of *p-y* curves is not significantly affected. This observation implies that the dynamic behaviour of the pile at small strains might not be affected by the scour shape. However, at larger strains the pile under local narrow scour mobilizes the highest amount of soil resistance, followed by local wide scour, then global scour. This observation might be due to the fact that the major consequential difference between local narrow scour and local wide scour is the amount of overburden pressure and resistance provided by the sand slope near to the pile. While the difference between local wide scour and global scour lies in the overburden pressure provided by the soil above the scour base mudline.
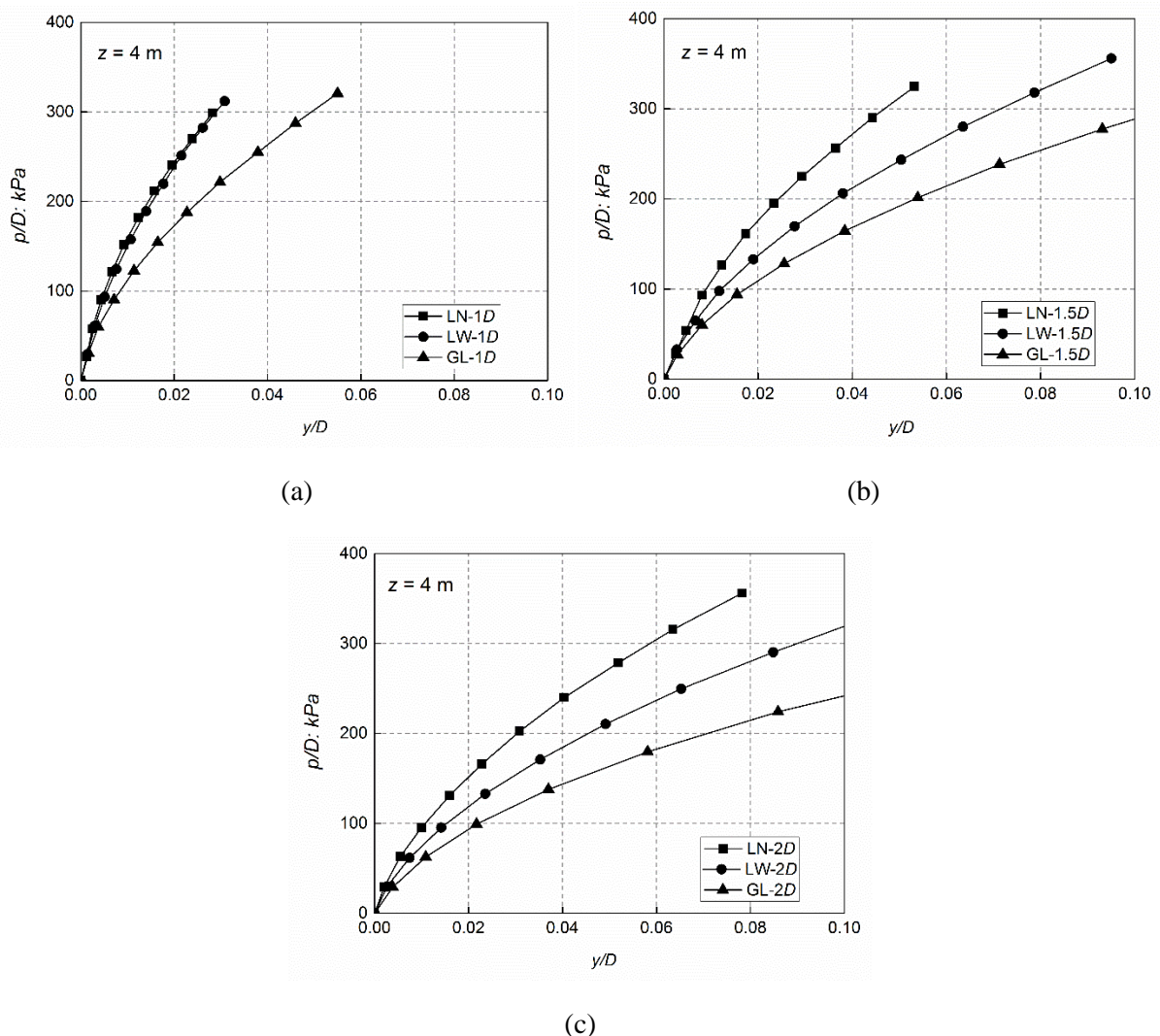

(a)   (b)

(c)

Figure 6.11 *p-y* curves for different scour types: (a) Scour depth 1*D*; (b) Scour depth 1.5*D*; (c) Scour depth 2*D*

6.3.3 Effect of scour depth

Moment-rotation relationships

Figure 6.12 shows the moment-rotation relationships at three scour types of local narrow scour (a), local wide scour (b) and global scour (c) with varying scour depths. Four different scour depths were investigated: zero scour (no scour), $1D$, $1.5D$, and $2D$. Figure 6.12 shows the same information with that shown in Figure 6.8, however, the order of the lines were rearranged, for the convenience of comparing the influence of scour depth on the pile moment-rotation behaviour. Evidently, scour has deleterious effect on both the pile moment capacity and the initial stiffness of the moment-rotation curves. With the increase of scour depth, increased reduction in moment capacity was seen. Similar trends can be found for all the three scour types in Figure 6.8(a)-(c). Reduction of moment capacity ($M_{R, reduction}$) by scour was shown previously in Table 6.4.

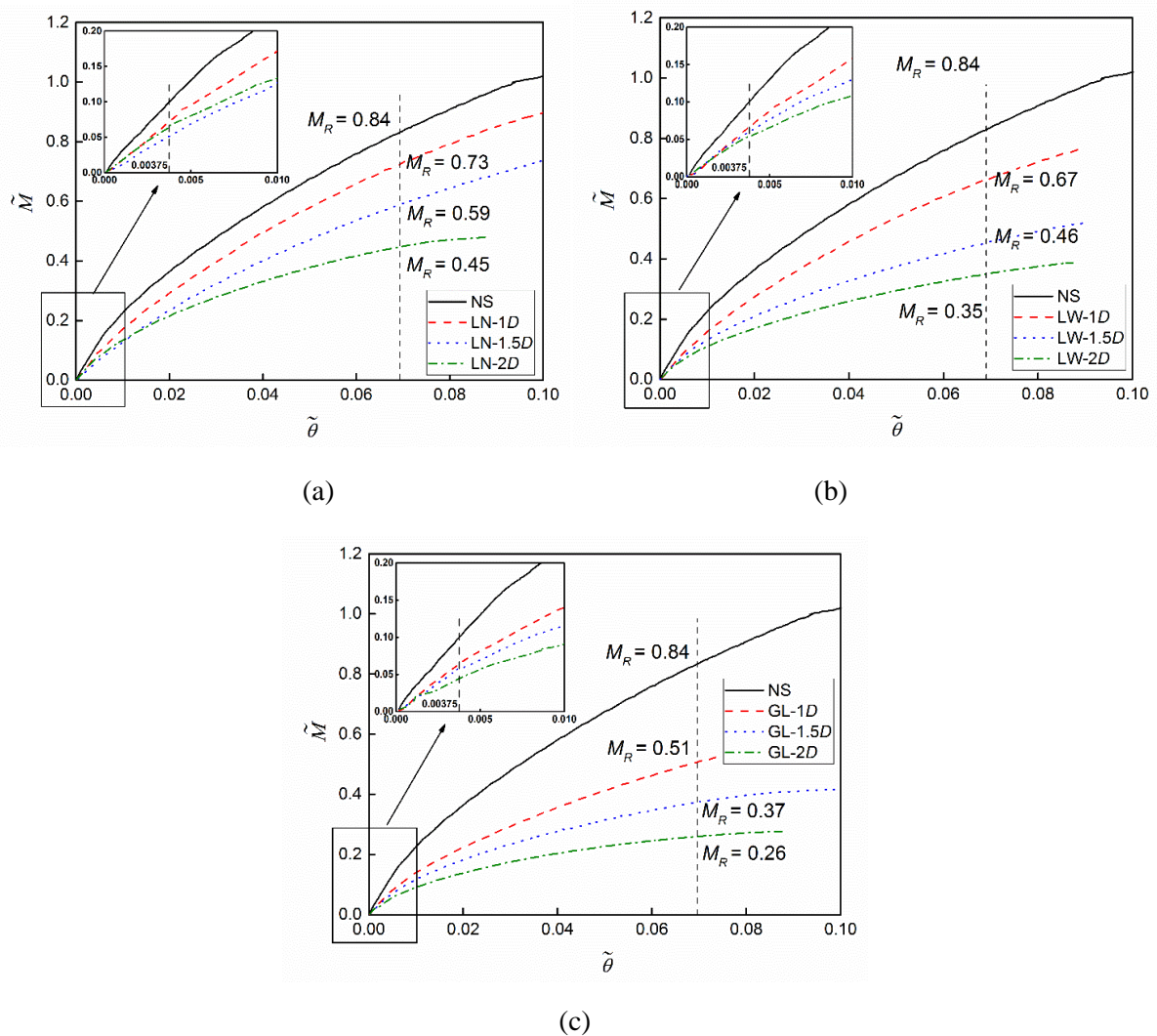(a)   (b)

(c)

Figure 6.12 Influence of scour depth on the moment-rotation response of piles: (a) Local narrow scour; (b) Local wide scour; (c) Global scour

The influence of scour depth on the rotation of laterally loaded piles subjected to a certain moment is of great interest for industry, and the results from this study are shown in Figure 6.13. The results indicate that for all three scour types, $\tilde{\theta}$ increases dramatically with the increase of scour depth (with the numbers listed in Figure 6.13). It is also shown in Figure 6.13 that the increasing influence of scour on the normalized rotation of the pile can be up to 348% (2D global scour case).
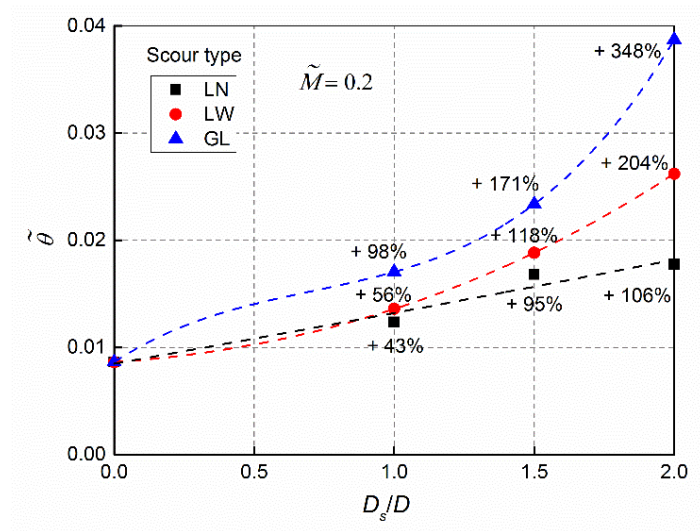

Figure 6.13 Influence of scour depth on the normalized pile rotation ($\widetilde{M}$ = 0.2)

The effects of scour depth on the moment resistance of laterally loaded piles subjected to various types of scour are shown in Figure 6.14. The results indicate that for all three scour types, $\widetilde{M}$ decreases almost linearly with the increase of scour depth. The rate of this decrease has a direct relationship with the amount of pile normalized rotation, $\tilde{\theta}$.
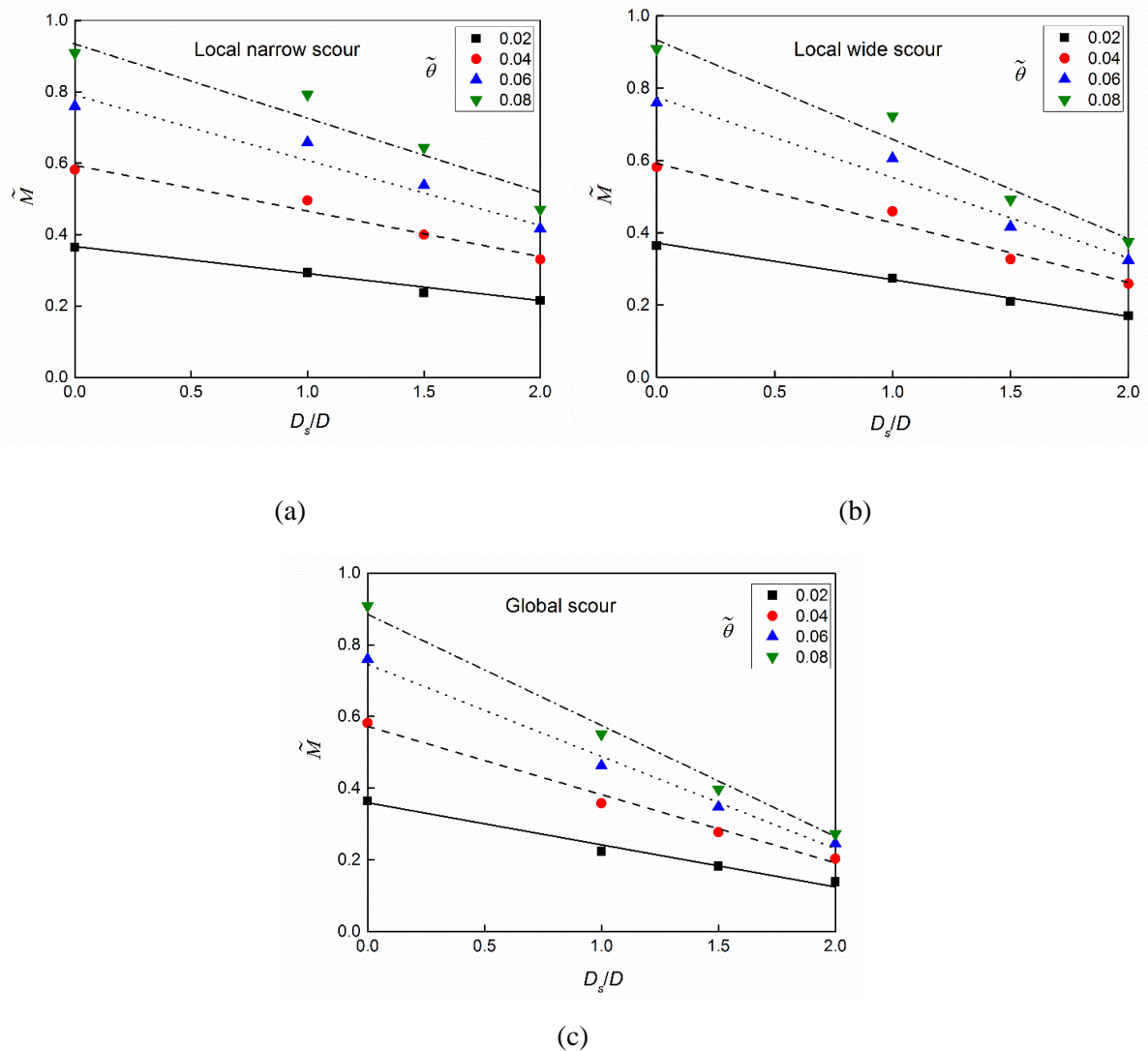
(a)   (b)

(c)

Figure 6.14 Influence of scour depth on the moment bearing resistance: (a) Local narrow scour; (b) Local wide scour; (c) Global scour

Bending moment distributions

The effects of scour depth on the bending moment profiles along the pile for various types of scour are plotted in Figure 6.15. From Figure 6.15(a), for a given applied moment, increasing scour depth causes an increase in the bending moment acting along the pile. Increasing scour depth leads to an increase in the peak bending moment, and also moves the location of the peak moment into larger soil depth. These findings are in line with previous publication of Bennett et al. [52]. As mentioned in section 6.3.2, the pile wall thickness and the pile diameter might need to be increased in order to resist the increased amount of bending moment caused by scour, according to Arany et al. [12]. Same trends can also be found in Figure 6.15(b)-(c).
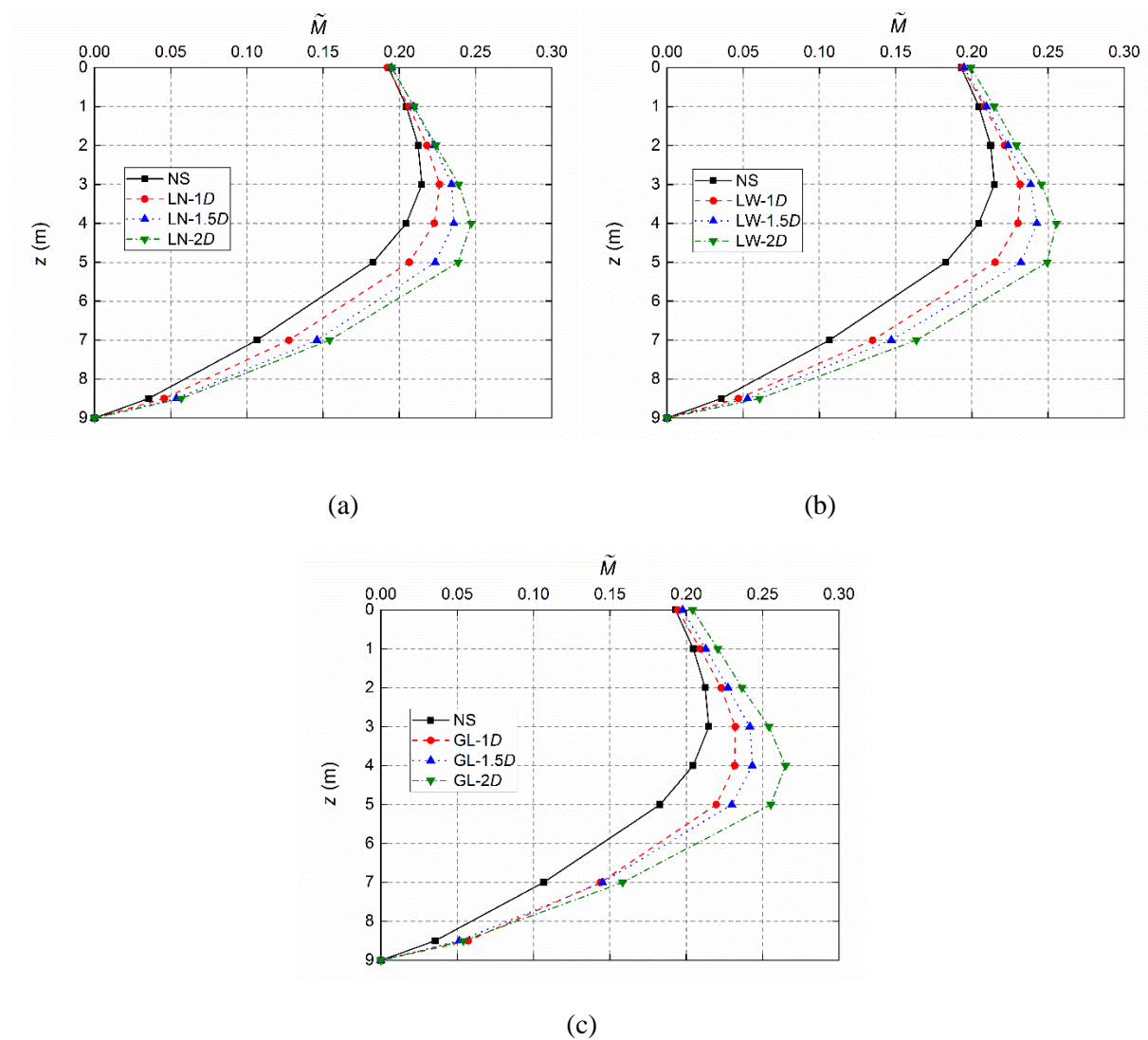
(a)

(b)

(c)

Figure 6.15 Profiles of bending moment along the pile at various scour depths ($\widetilde{M}$ = 0.2): (a) Local narrow scour; (b) Local wide scour; (c) Global scour

p-y reaction curves

Figure 6.16 shows the *p-y* curves under different scour depths, for local narrow scour (a), local wide scour (b) and global scour (c), separately. Generally, at a certain scour type and soil depth *z*, with the increase of scour depth the *p-y* curves become less and less stiff. This is because, with the increase of scour depth, the thickness of the over-lying soil layer above the evaluated point is decreased. The decreased overburden pressure would induce decrease in the soil resistance under it.

(a)   (b)

(c)
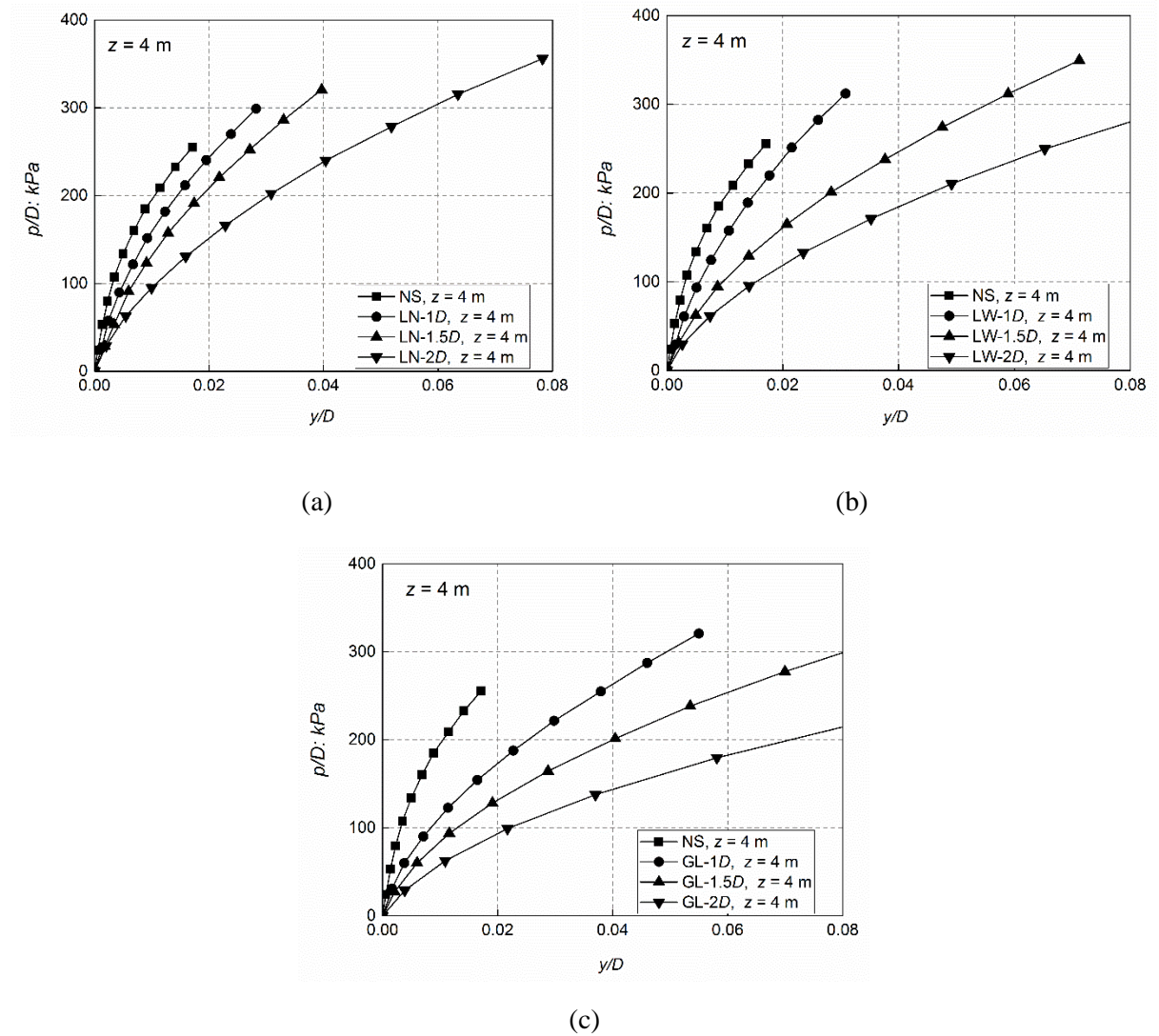
Figure 6.16 *p-y* curves at different scour depths: (a) Local narrow scour; (b) Local wide scour; (c) Global scour

6.4 New design method

Based on the centrifuge tests results a new design method is developed to consider the three-dimensional shape of the local scour holes around the monopile. The first part of this section will discuss the basics of the method by introduction of an equivalent scour depth according to the shape of the local scour. The steps of the proposed method are presented for a case study in the second part.

6.4.1 Equivalent scour depth z_{equ}

The results from the centrifuge tests indicate that the detrimental effects of scour are generally less in case of local scour compared with those of global scour. Therefore, as a practical approach to account for the effects of local scour types compared with global scour on the pile moment capacity, the term "additional soil depth (z_{add})" is introduced and is defined in Equation (6.6). In this approach, the beneficial effect of local scour types is deemed as an additional soil layer lying above assumed global scour, which leads to a larger pile embedment length (L) after local scour and a smaller loading eccentricity (e), as illustrated in Figure 6.17. In this figure, the terms $z_{add, LN}$ and $z_{add, LW}$ denote additional soil depth to account for local narrow scour (LN) and local wide scour (LW), respectively. Another term "equivalent scour depth (z_{equ})" is introduced hereafter, which signifies the effective scour depth after taking into account the compensation effect by local scour types compared with global scour, which is defined by Equation (6.7).

$$z_{add} = \delta \cdot D_s \tag{6.6}$$

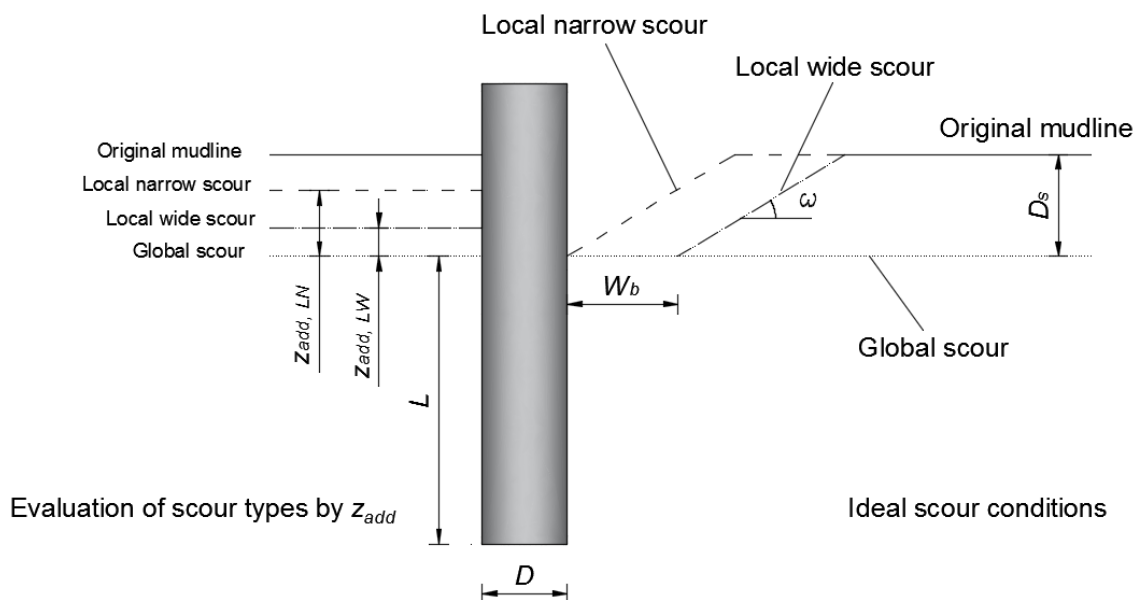$$z_{equ} = D_s - z_{add} = D_s \cdot (1 - \delta) \tag{6.7}$$

Figure 6.17 Illustration of the additional soil depth (z_{add})

Compared with global scour, the improvement in moment capacity by local scour types is quantified by "additional soil depth factor" δ. Therefore, the condition of global scour is set as

the base level for δ, i.e. no compensation effect is introduced which corresponds to $\delta = 0$. Consequently, the condition of no scour can be set as the upper boundary for δ and it can be considered as "full compensation", which corresponds to $\delta = 1$. Thus, δ for the local scour types ranges between 0 and 1.

Figure 6.18 shows influence of scour type on the moment bearing resistance at various scour depths, along with the strategy to determine the "additional soil depth factor" δ experimentally. For example, for 1D local narrow and 2D local wide scour conditions, δ would be equal to 0.66 and 0.17, respectively. This means that the equivalent scour depths for these two cases are 0.34D and 1.66D, respectively. The equivalent scour depths for various conditions are summarised in Table 6.5.
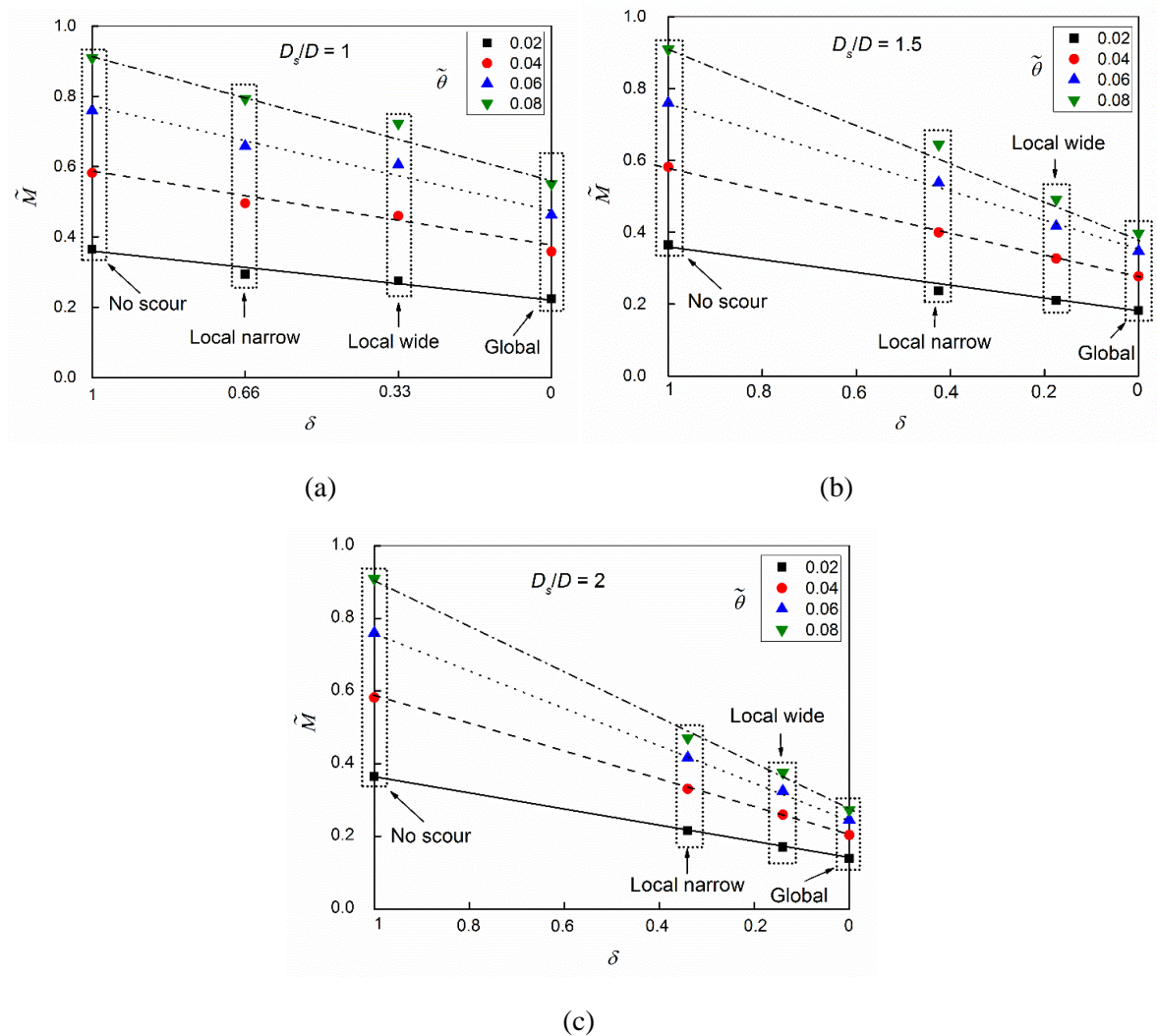

(a)

(b)

(c)

Figure 6.18 Determination of the additional soil depth factor (δ): (a) Scour depth 1D; (b) Scour depth 1.5D; (c) Scour depth 2D
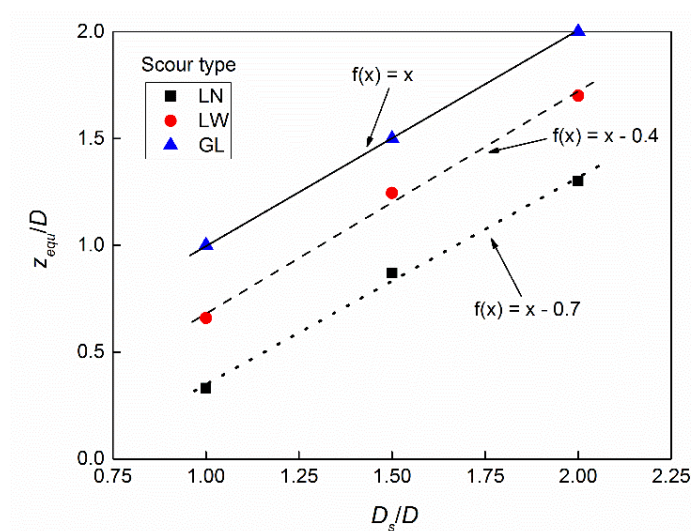
Table 6.5. Equivalent scour depth (z_{equ})

Scour type	$D_s = 1D$	$D_s = 1.5D$	$D_s = 2D$
Local narrow scour	0.33D	0.87D	1.3D
Local wide scour	0.66D	1.245D	1.7D
Global scour ($= D_s$)	1D	1.5D	2D

As a practical approach to incorporate effects of scour type on equivalent scour depth (z_{equ}), the data from Table 6.5 was used to plot the relationship between z_{equ}/D and D_s/D considering different scour types, which is shown in Figure 6.19. Linear fits between z_{equ}/D and D_s/D were found and the following empirical equation was generated:

$$\frac{z_{equ}}{D} = \frac{D_s}{D} - f \tag{6.8}$$

in this equation: $f = 0$, for global scour; $f = 0.4$, for local wide scour; $f = 0.7$, for local narrow scour.

In this way, the beneficial effect of local scour shapes can be practically considered as shallower global scours, when design pile foundation from moment capacity perspective. The derived empirical equation offers a straightforward approach to calculate the equivalent scour depth (z_{equ}).

Figure 6.19 Influence of scour type on the equivalent scour depth (z_{equ})

6.4.2 Reduction of pile moment capacity caused by scour

The data from Table 6.4 was used to plot the relationship between $M_{R,reduction}$ and scour depth (D_s) considering different scour types, which is shown in Figure 6.20. Linear equations have been used to fit the data, resulting in the following general equation:

$$M_{R,reduction} = 0.35\frac{D_s}{D} + r \tag{6.9}$$

in this equation, r is a fitting parameter and is equal to 0.05, -0.16 and -0.2 for global scour, local wide scour and local narrow scour, respectively.

Using this method, the detrimental influence of scour on the moment capacity can be directly related to the scour depth and scour type. In the practical application, depending on the formation of the scour-hole, as long as the scour type and scour depth are primarily estimated, the moment capacity reduction factor $M_{R,reduction}$ can be estimated from Figure 6.20, and then be employed by the following equation to determine the "design pile moment capacity under scour condition ($M_{R,with\ scour}$)":

$$M_{R,with\ scour} = M_{R,no\ scour} \times (1 - M_{R,reduction}) \tag{6.10}$$

in this equation, $M_{R,with\ scour}$ is the designed pile moment capacity considering the influence of scour, and $M_{R,no\ scour}$ is the design pile moment capacity when no scour erosion is considered.
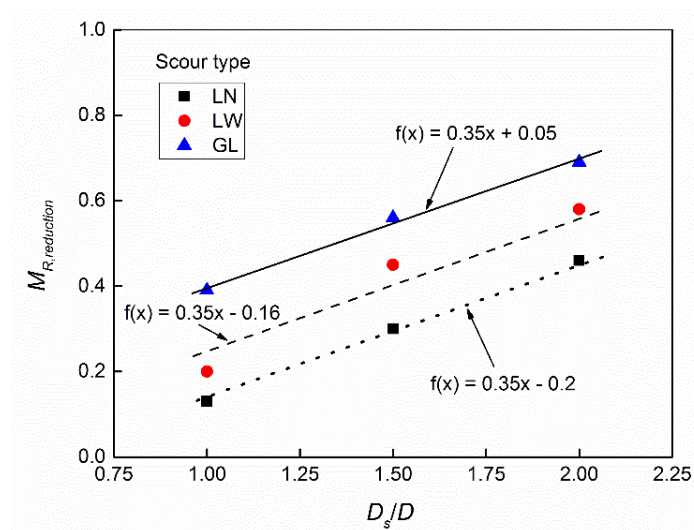

Figure 6.20 $M_{R,reduction}$ vs. D_s/D

6.4.3 Example

An example is given to demonstrate the use of the proposed equivalent scour depth method in this part. Consider a rigid monopile, with $L/D = 5$, driven into sand with a relative density of 80%. The task is to determine the equivalent scour depth (z_{equ}) and the design pile moment capacity under scour condition ($M_{R,\,with\,scour}$) from the equivalent moment capacity point of view, when a pile is subjected to local wide scour with a scour depth of 1.2D. The design pile moment capacity when there is no scour erosion is signified by $M_{R,\,no\,scour}$.

According to Figure 6.19, the non-dimensional coefficient f under local wide scour condition is 0.4. Therefore, z_{equ} can be calculated using Equation (6.8):

$$\frac{z_{equ}}{D} = \frac{D_S}{D} - f = \frac{1.2D}{D} - 0.4 = 0.8 \tag{6.11}$$

This result indicates that local wide scour with a scour depth of 1.2D equivalents to global scour with a scour depth of 0.8D.

According to Figure 6.20, the non-dimensional coefficient r under local wide scour condition is -0.16. Therefore, the moment capacity reduction factor ($M_{R,\,reduction}$) can be calculated from Equation (6.9):

$$M_{R,\,reduction} = 0.35\frac{D_S}{D} + r = 0.35 \times 1.2 - 0.16 = 0.26 \tag{6.12}$$

Accordingly, the design pile moment capacity under this specific scour condition ($M_{R,\,with\,scour}$) can be calculated according to Equation 6.10:

$$M_{R,\,with\,scour} = M_{R,\,no\,scour} \times (1 - M_{R,\,reduction}) = 0.74 M_{R,\,no\,scour} \tag{6.13}$$

In summary, the equivalent scour depth is 0.8D and the moment capacity of the pile would decrease by 26% in case of a local wide scour to a depth of 1.2D.

6.5 Conclusions

As a process of soil erosion, scour broadly occurs around offshore wind turbine monopiles, which decreases the pile capacity and might potentially lead to failure of the structure. A series of centrifuge tests was carried out at $100g$ on a model monopile installed in dense sand with embedment ratio of 5 to investigate the effect of scour on the foundation lateral response. Three scour types (local narrow scour, local wide scour and global scour) and three scour depths ($1D$, $1.5D$ and $2D$) were considered in this investigation, which represent a range of common scour shapes in real engineering applications. Empirical equations were derived to evaluate the beneficial effect of local scour types compared with the assumption of a global scour condition, and to assess the detrimental effect of increased scour depth on pile moment capacity. The following conclusions can be drawn from this study:

1. Scour type has significant influence on the pile moment-rotation behaviour. Piles under local narrow scour show the highest moment capacity, followed by local wide scour, and then by global scour condition. At scour depths of $1D$ and $1.5D$, scour type has minimal effect on the stiffness of the pile at small rotations, which signifies that in pile dynamic analysis within small strain range the effect of scour type could be ignored. However, the results indicate that in case of a global scour condition to a depth of $2D$, negative effect of scour on the stiffness of pile should certainly be taken into consideration.

   At the same soil depth (z) and lateral displacement (y), pile under local narrow scour mobilizes the highest amount of soil resistance (p), followed by local wide scour, then global scour. The major consequential difference between local narrow scour and local wide scour was speculated as the amount of overburden pressure and resistance provided by the sand slope near to the pile. While the difference between local wide scour and global scour was suspected to be due to the overburden pressure provided by the soil above the scour base. According on this hypothesis, the beneficial effect of local scour types could be regarded as additional soil layers lying above global scour. Empirical equations were derived to calculate the equivalent scour depth (z_{equ}), which can be implemented in the current monopile foundation design methodology.

2. The pile moment capacity was found to decrease almost linearly with the increase of scour depth, in all the three scour types (local narrow scour, local wide scour and global scour). The pile initial stiffness decreases with increasing scour depth as well.

Increasing scour depth leads to increase in the peak bending moment and moves the location of the peak moment into deeper soil.

When the scour depth D_s is in the range of [1D, 2D], the detrimental effect of scour on the moment capacity considering influence of scour depth and scour type was described by empirical equations for a monopile with L/D = 5 installed in dense sand. In the practical application, depending on the marine hydraulic environment, as long as the type and depth of the scour-hole are estimated, the moment capacity reduction factor $M_{R, reduction}$ could be calculated and employed to determine the "design pile moment capacity under scour condition ($M_{R, with\ scour}$)". In this way, the traditional design method which neither fully considers the effect of scour shape nor properly addresses the effect of scour depth could be improved.

7 Conclusions and recommendations

Monopile foundations used to support offshore wind turbines (OWTs) resist large lateral and moment loads from wind and waves and can be affected, by scour erosion, when the seabed is unprotected. Monopiles used for OWTs are open-ended steel tubes with low L/D (L, pile embedded length; D, pile diameter) ratios. Limited experimental studies have been conducted to investigate the lateral behaviour of rigid monopiles subjected to combined vertical and lateral loads, and inconsistent conclusions are often seen. The lateral cyclic load exerted on the monopile has sophisticated combination of different directional characteristics and amplitudes. Discrepancy is seen regarding to influence of cyclic load on the accumulation of the pile head displacement, evolution of pile secant stiffness, change of bending moment, and alternation of the p-y reaction curves.

Scour erosion can be detrimental to the pile serviceability during its whole life span, however, in the current design code the scour-hole geometry is ignored and removal of the soil to the scour depth is accepted as a general case, which is considered to lead to over-conservative design. Therefore, the main objective of this research was to clarify the influence of combined vertical and lateral loads, lateral cyclic load and scour erosion on the lateral response of monopile in sand by experimental investigation. For the purpose of achieving optimal monopile design, reducing the foundation cost for offshore wind turbines and increasing their competitiveness as an energy source.

7.1 Concluding remarks

7.1.1 Influence of vertical load on the pile lateral response

Various loading methods and pile properties were involved in the experiments in literature, which leads to inconsistent conclusions upon the effect of vertical load on pile lateral response. In centrifuge combined loading test, the most challenging part exists in applying vertical load and lateral load simultaneously on the pile, while keeping the pile top similar freedoms as in real application. The novelty of the current research lies in: (i) the specially designed ball connection along with the Teflon collar, which allows the pile top to move and rotate freely; (ii)

applying vertical load by fixing dead weight directly on the pile body, which helped successfully apply vertical load and lateral load at the same time while avoiding causing any pile-head constraint. A series of vertical, lateral, and combined loading tests were performed on both pre-installed model piles at $1g$ condition, and in-flight jacked piles with different L/D ratios. In all the combined load tests, the vertical load was applied prior to lateral load.

On the pile with L/D ratio of 5, the increase of vertical load increases both the pile initial stiffness and lateral capacity. The *p-y* curves derived in the absence of applied vertical load subsequently increased in stiffness and resistance (at corresponding displacements) when vertical load was applied, which leads to increase in the stiffness of monopile lateral load-displacement behaviour. This trend is the same for the *p-y* curves at each soil depth. Installing the piles in-flight leads to a higher retention of lateral stresses, which manifest as a larger initial stiffness and higher resistance at corresponding displacements than for piles pre-installed at $1g$. Therefore modelling the correct pile installation stress level is very important to reflect realistic pile load-displacement behaviour.

On the pile with L/D ratio of 3, the pile lateral capacity was found to increase dramatically under smaller amount of vertical load ($V < 0.44V_u$); while for higher vertical load considered, early failure in the sand might happen, therefore the beneficial effects reduced in a manner similar to the behaviour observed for shallow footings. It means when design monopiles under combined vertical and lateral loads, attention should be paid not only to pile L/D ratio, but also the applied vertical load level. Considering the complexity in the evaluation of effect of vertical load on pile lateral response, a general conclusion regardless of pile L/D ratio and applied vertical load level is not possible to be achieved.

7.1.2 Influence of lateral cyclic load on the pile lateral response

The cyclic load test results demonstrated that the force-controlled one-way and two-way lateral cyclic loading induce increasing accumulated permanent pile lateral displacement. The accumulation rates are different according to load characteristics. Compared with one-way loading, cyclic characteristic of two-way asymmetric loading is a more serious cyclic characteristic when evaluating the pile accumulated displacement. In real application if two-way asymmetric loading plays the dominate role on an offshore wind turbine which is designed base on the assumption of one-way loading, the turbine might fail after smaller number of load

cycles than designed. In the storm load test, the accumulated displacement in the normal load cycles just following the storm load cycles appeared to be in a decreasing trend, until reached constant in the last few cycles.

Within the tested sand condition (dry sand, with relative densities of 80% and 50%) and limited number of load cycles applied (maximum number of load cycles in a test is 153) in this experimental program, cyclic loading was found to always increase the pile secant stiffness, and the increase rate was found to be independent of sand relative density. When the applied load changed from one-way to two-way, an increasing rate on accumulation of pile secant stiffness was observed. An increase in the cyclic load magnitude leaded to an increase in the secant stiffness accumulation rate. The pile maximum bending moment was found to be not sensitive to the change of cycle number.

Above the pile pivot point (z/D = 0.56 to 2.78), the soil reaction p shows a very tiny decrease trend when the cycle number increases. While below the pile pivot point (z/D = 3.89 to 5), the soil reaction p is barely influenced by the cycle number. In general, the API [18] method predicts much higher initial stiffness and ultimate soil reaction for each depth.

7.1.3 Influence of scour erosion on the pile lateral response

Scour reduces the lateral capacity of pile foundations and increases bending moments along the pile (under the same lateral load). Moreover, the location of the peak bending moment occurs lower along the pile for increased scour depth, which may have ramifications for the design of monopiles unprotected against scour. In addition to scour reducing lateral capacity, the shape of the scour-hole has a noticeable effect on the bending moment measured.

Scour type has significant influence on the pile moment-rotation behavior. Pile under local narrow scour shows the highest moment capacity, followed by local wide scour, then global scour. At the same soil depth (z), pile under local narrow scour mobilizes the highest amount of soil resistance, followed by local wide scour, then global scour. The major consequential difference between local narrow scour and local wide scour was speculated as the amount of overburden pressure and resistance provided by the sand slope near to the pile. While the difference between local wide scour and global scour lies in the overburden pressure provided by the soil above the scour base line. The beneficial effect of local scour types could be regarded

as additional soil layers laying above global scour. Empirical equations were derived to calculate the equivalent scour depth, which can be coded into the current monopile foundation design methodology.

The pile moment capacity and initial stiffness were found to decrease almost linearly with the increase of scour depth, in all the three scour types (local narrow scour, local wide scour, and global scour). With the increase of scour depth, the *p-y* curves become less and less stiff, in all the three scour types. At shallow depths, the influence of scour type is more evident on the derived *p-y* curves, but becomes less significant as the depth increases. This indicates significant overburden dependency on the resistance properties of the soil, an effect which becomes lower for deeper depths. The detrimental effect of scour on the moment capacity considering influence of scour depth and scour type were described by empirical equations. The traditional design method which does not fully consider the effect of scour shape and does not properly address the effect of scour depth could be improved.

7.2 Recommendations for future research

This dissertation investigated experimentally the lateral response of monopiles under combined vertical and lateral loads, lateral cyclic load, and scour erosion. Based on the findings from this study, some recommendations for further research are suggested below:

1. The effect of pile installation method on the response of monopiles under combined loading is worthy of further investigation. In this study, pre-installed model piles and in-flight jacked piles were considered. A pile driving system may be employed with the present experimental equipment to drive model piles in-flight. Results from combined loading tests among pre-installed, jacked, and driven piles could then be compared.

2. Considering the effect of cyclic load on the pile lateral response, further research is advised to be extended to take pile installation stress level and pile installation method into consideration. The number of exerted load cycles in a single test could be increased, to more than 10 000, in order to reflect the pile long term loading behaviour.

3. For simplification, only certain kinds of scour shapes (local narrow scour, local wide scour and global scour) and scour depths (1*D*, 1.5*D* and 2*D*) were studied in this research, and the

scour slope angle was modelled as a constant value. In future work, using a wider range of scour slope angle, scour base width, and scour depth could be a future topic, better capturing the scour shapes as faced in the real conditions.

4. The same experimental work of this dissertation may be carried out for different soil conditions (i.e. clay, multi-layered soil samples prepared by alternating layers of sand with different properties) in order to simulate closer field conditions. This research could be continued by employing different model piles, i.e. piles with different shapes, *L/D* ratios, materials, or top fixity conditions. The behaviour of tripod pile or suction pile subjected to combined vertical and lateral loads, lateral cyclic load, and/or scour erosion could be investigated with the same procedure proposed in this study.

References

[1] T. Burton, N. Jenkins, D. Sharpe, and E. Bossanyi, *Wind energy handbook*, John Wiley & Sons (2011).

[2] I. IRENA, *Renewable power generation costs in 2017*. Report, International Renewable Energy Agency, Abu Dhabi (2018).

[3] X. Wu, Y. Hu, Y. Li, J. Yang, L. Duan, T. Wang, T. Adcock, Z. Jiang, Z. Gao, and Z. Lin, *Foundations of offshore wind turbines: A review*, Renewable and Sustainable Energy Reviews 104, 379-93 (2019).

[4] M. Premalatha, T. Abbasi, and S. A. Abbasi, *Wind energy: Increasing deployment, rising environmental concerns*, Renewable and Sustainable Energy Reviews 31, 270-88 (2014).

[5] R. Perveen, N. Kishor, and S. R. Mohanty, *Off-shore wind farm development: Present status and challenges*, Renewable and Sustainable Energy Reviews 29, 780-92 (2014).

[6] E. Alderlieste, *Experimental Modelling of Lateral Loads on Large Diameter Mono-pile Foundations in Sand*, MSc thesis, Delft University of Technology (2010).

[7] Malhotra, S. 2011. *Design and construction considerations for offshore wind turbine foundations in North America*. Proceedings GeoFlorida 2010: Advances in Analysis, Modeling and Design, West Palm Beach, Florida, USA, February 20–24th, 2010, ed. D. O. Fratta, A. J. Puppala, and B. Muhunthan, Vol. 2, 1533–42, GSP 199. Red Hook, NY, USA: Curran Associates, Inc

[8] Arshad, M. and B.C. O'Kelly, *Analysis and Design of Monopile Foundations for Offshore Wind-Turbine Structures*. Marine Georesources & Geotechnology, 2015.

[9] J. Velarde, *Design of monopile foundations to support the DTU 10 MW offshore wind turbine,* Master thesis, Delft University of Technology & Norwegian University of Science and Technology (2016).

[10] P. Doherty and K. Gavin, *Laterally loaded monopile design for offshore wind farms*, Proceedings of the ICE-Energy 165(1), 7-17 (2011).

[11] S. Fan, B. Bienen, and M. F. Randolph, *Centrifuge study on effect of installation method on lateral response of monopiles in sand*, International Journal of Physical Modelling in Geotechnics, 1-13 (2019).

[12] L. Arany, S. Bhattacharya, J. Macdonald, and S. Hogan, *Design of monopiles for offshore wind turbines in 10 steps*, Soil Dynamics and Earthquake Engineering 92, 126-52 (2017).

[13] C. Lin, J. Han, C. Bennett, and R. L. Parsons, *Analysis of laterally loaded piles in sand considering scour hole dimensions*, Journal of Geotechnical and Geoenvironmental Engineering 140(6), 0401-4024 (2014).

[14] Bhattacharya, S., *Challenges in Design of Foundations for Offshore Wind Turbines*. Engineering and Technology Reference, 2014.

[15] K. Lesny and J. Wiemann, *Design aspects of monopiles in German offshore wind farms*, Proceedings of the International Symposium on Frontiers in Offshore Geotechnics. AA Balkema Publishing, 383-389 (2005).

[16] C. Anagnostopoulos and M. Georgiadis, *Interaction of axial and lateral pile responses*, Journal of Geotechnical Engineering 119, 793-798 (1993).

[17] S. Karthigeyan, V. Ramakrishna, and K. Rajagopal, *Numerical investigation of the effect of vertical load on the lateral response of piles*, Journal of Geotechnical and Geoenvironmental Engineering 133(5), 512-21 (2007).

[18] R. API, *Geotechnical and foundation design considerations*, American Petroleum Institute, Washington, DC, USA (2011).

[19] G. DNV, *DNVGL-ST-0126: Support structures for wind turbines*, Oslo, Norway (2016).

[20] L. Mu, X. Kang, K. Feng, M. Huang, and J. Cao, *Influence of vertical loads on lateral behaviour of monopiles in sand*, European Journal of Environmental and Civil Engineering 22(sup1), 286-301 (2018).

[21] O. Karasev, G. Talanov, and S. Benda, *Investigation of the work of single situ-cast piles under different load combinations*, Soil Mechanics and Foundation Engineering 14(3), 173-7 (1977).

[22] W. Lu and G. Zhang, *Influence mechanism of vertical-horizontal combined loads on the response of a single pile in sand*, Soils and foundations 58(5), 1228-39 (2018).

[23] N. Jain, G. Ranjan, and G. Ramasamy, *Effect of vertical load on flexural behaviour of piles*, Geotechnical Engineering 18(2), 185–204 (1987).

[24] J. Lee, *Experimental investigation of the load response of model pilesin sand,* PhD thesis, Purdue University (2008).

[25] B. Byrne, R. McAdam, H. Burd, G. Houlsby, C. Martin, K. Gavin, P. Doherty, D. Igoe, L. Zdravković, and D. Taborda, *Field testing of large diameter piles under lateral loading for offshore wind applications* In Proceedings of the XVI ECSMGE Geotechnical Engineering for Infrastructure and Development, 1255–1260, London: Institution of Civil Engineers (2015).

[26] C. Chang and R. Whitman, *Drained permanent deformation of sand due to cyclic loading*, Journal of geotechnical engineering 114(10), 1164-1180 (1988).

[27] S. Kramer and E. Heavey, *Lateral load analysis of nonlinear piles*, Journal of geotechnical engineering 114(9), 1045-1049 (1988).

[28] O. Kusakabe, *Foundations*, Geotechnical centrifuge technology, 118-167 (1995).

[29] R.L. Little and J.L. Briaud, *Full scale cyclic lateral load tests on six single piles in sand.* Texas A&M University, College Station, TX, USA (1988).

[30] S. Mezazigh, *Etude expérimentale des pieux chargés latéralement: proximité d'un talus et effet de groupe*, Nantes (1995).

[31] C. Morrison and L. Reese, *A Lateral-Load Test of a Full-Scale Pile Group in Sand*, Texas University at Austin Geotechnical Engineering Center (1988).

[32] L. Reese, W. Cox, and F. Koop, *Analysis of laterally loaded piles in sand*. Offshore Technology in Civil Engineering Hall of Fame Papers from the Early Years, 95-105 (1974).

[33] D. Remaud, *Pieux sous charges latérales: étude expérimentale de l'effet de groupe*, PhD thesis (1999).

[34] W. R. Cox, L. C. Reese, and B. R. Grubbs, *Field testing of laterally loaded piles in sand*, Offshore Technology Conference, Houston, TX, paper no. 2080 (1974).

[35] J. Long and G. Vanneste, *Effects of cyclic lateral loads on piles in sand*, Journal of geotechnical engineering 120(1), 225-244 (1994).

[36] S. Lin and J. Liao, *Permanent strains of piles in sand due to cyclic lateral loads*, Journal of geotechnical and geoenvironmental engineering 125(9), 798-802 (1999).

[37] L. Verdure, J. Garnier, and D. Levacher, *Lateral cyclic loading of single piles in sand*, International journal of physical modelling in geotechnics 3(3), 17-28 (2003).

[38] J. Peng, B. Clarke and M. Rouainia, *A device to cyclic lateral loaded model piles*, Geotechnical Testing Journal 29(4), 341-347 (2006).

[39] T. Gerber and K. Rollins, *Cyclic P-Y curves for a pile in cohesive soil*, Geotechnical Earthquake Engineering and Soil Dynamics IV, 1-10 (2008).

[40] P. Cuéllar, M. Baeßler, and W. Rücker, *Ratcheting convective cells of sand grains around offshore piles under cyclic lateral loads*, Granular Matter 11(6), 379 (2009).

[41] C. LeBlanc, G. Houlsby, and B. Byrne, *Response of stiff piles in sand to long-term cyclic lateral loading*, Geotechnique 60(2), 79-90 (2010).

[42] Z. Li, S. Haigh, and M. Bolton, *Centrifuge modelling of mono-pile under cyclic lateral loads*, Physical Modelling in Geotechnics, 965-70 (2010).

[43] R. T Klinkvort, *Centrifuge modelling of drained lateral pile-soil response: Application for offshore wind turbine support structures*, Technical University of Denmark (DTU) (2013).

[44] W. Li, D. Igoe, and K. Gavin, *Field tests to investigate the cyclic response of monopiles in sand*, Proceedings of the Institution of Civil Engineers-Geotechnical Engineering 168(5), 407-21 (2015).

[45] G. Nicolai, L. B. Ibsen, C. O'Loughlin, and D. White, *Quantifying the increase in lateral capacity of monopiles in sand due to cyclic loading*, Geotechnique Letters 7(3), 245-52 (2017).

[46] P. Truong, B. Lehane, V. Zania, and R. T. Klinkvort, *Empirical approach based on centrifge testing for cyclic deformations of laterally loaded piles in sand*, Géotechnique 69(2), 133–145 (2018).

[47] C. N. Abadie, B. W. Byrne, and G. T. Houlsby, *Rigid pile response to cyclic lateral loading: laboratory tests*, Géotechnique, 1-14 (2018).

[48] Q. Yang, Y. Gao, D. Kong, and B. Zhu, *Centrifuge modelling of lateral loading behaviour of a "semi-rigid" Mono-pile in soft clay*, Marine Georesources & Geotechnology 37(10), 1205-16 (2019).

[49] M. Lee, K. T. Bae, I. W. Lee, and M. Yoo, *Cyclic p-y Curves of Monopiles in Dense Dry Sand Using Centrifuge Model Tests*, Applied Sciences 9(8), 1641 (2019).

[50] L. Reese, S. Wang, and J. Long, *Scour from cyclic lateral loading of piles*. In Offshore Technology Conference (1989).

[51] Y. N. Kishore, S. N. Rao, and J. Mani. *Influence of the Scour on Laterally Loaded Piles*, In the 12th International Conference of International Association for Computer Methods and Advances in Geomechanics. Red Hook, NY (2008).

[52] C. R. Bennett, C. Lin, R. Parsons, and J. Han, *Evaluation of behavior of a laterally loaded bridge pile group under scour conditions*, In Structures Congress 2009: Don't Mess with Structural Engineers: Expanding Our Role. Reston, VA: American Society of Civil Engineers. 290-9 (2009).

[53] C. Lin, C. Bennett, J. Han, and R. Parsons, *Scour effects on the response of laterally loaded piles considering stress history of sand*. Computers and Geotechnics 37(7-8), 1008-1014 (2010).

[54] Y. E. Mostafa, *Effect of local and global scour on lateral response of single piles in different soil conditions*, Engineering 4(6), 297 (2012).

[55] S. P. H. Sørensen and L. B. Ibsen, *Assessment of foundation design for offshore monopiles unprotected against scour*, Ocean Engineering 63, 17-25 (2013).

[56] L.J. Prendergast, K. Gavin, and P. Doherty. *An Investigation into the Effect of Scour on the Natural Frequency of an Offshore Wind Turbine*, Ocean Engineering 101, 1-11 (2015).

[57] L. J. Prendergast, D. Hester, and K. Gavin. *Determining the Presence of Scour around Bridge Foundations Using Vehicle-Induced Vibrations*, Journal of Bridge Engineering 21(10), 1-14 (2016).

[58] C. Lin, J. Han, C. Bennett, and R. L. Parsons, *Analysis of laterally loaded piles in sand considering scour hole dimensions*, Journal of Geotechnical and Geoenvironmental Engineering 140(6), 0401-4024 (2014).

[59] W. Qi, F. Gao, M. Randolph, and B. Lehane, *Scour effects on p–y curves for shallowly embedded piles in sand*, Géotechnique 66(8), 648-60 (2016).

[60] H. Zhang, S. Chen, and F. Liang, *Effects of scour-hole dimensions and soil stress history on the behavior of laterally loaded piles in soft clay under scour conditions*, Computers and Geotechnics 84, 198-209 (2017).

[61] F. Liang, H. Zhang, and S. Chen, *Effect of vertical load on the lateral response of offshore piles considering scour-hole geometry and stress history in marine clay*, Ocean Engineering 158, 64-77 (2018).

[62] H. Allersma, *The University of Delft geotechnical centrifuge*, Centrifuge 94, 47–52 (1994).

[63] SibelcoEurope, *Technical data: Geba sand*, Eurogrit BV (2016).

[64] D. Mašin, *Calibration of sand hypoplastic model on Geba sand data*, Internal report issued for Royal IHC, Netherlands (Charles University in Prague, 2017).

[65] M. Gui, M. Bolton, J. Garnier, J. Corte, G. Bagge, J. Laue, and R. Renzi, *Guidelines for cone penetration tests in sand*, Centrifuge 98: International Conference, 155-60 (1998).

[66] D. Remaud, *Pieux sous charges latérales: étude expérimentale de l'effet de groupe*, PhD thesis (1999).

[67] J. Garnier, C. Gaudin, S. M. Springman, P. Culligan, D. Goodings, D. Konig, B. Kutter, R. Phillips, M. Randolph, and L. Thorel, *Catalogue of scaling laws and similitude questions in geotechnical centrifuge modelling*, International Journal of Physical Modelling in Geotechnics 7(3), 1-27 (2007).

[68] K. Prakasha, H. Joer, and M. Randolph, *Establishing a model testing capability for deep water foundation systems*, 309-15 (2005).

[69] A. Maghsoudloo, A. Askarinejad, R. de Jager, F. Molenkamp, and M. Hicks, *Experimental investigation of pore pressure and acceleration development in static liquefaction induced failures in submerged slopes*, Physical Modelling in Geotechnics, Volume 2, 987-92 (2018).

[70] R. R. De Jager, A. Maghsoudloo, A. Askarinejad, and F. Molenkamp, *Preliminary results of instrumented laboratory flow slides*, Delft, The Netherlands Elsevier Ltd 212-9 (2017).

[71] Q. Li, L. Prendergast, A. Askarinejad, G. Chortis, and K. Gavin, *Centrifuge Modeling of the Impact of Local and Global Scour Erosion on the Monotonic Lateral Response of a Monopile in Sand*, Geotechnical Testing Journal 43(5) (2020).

[72] J. Xue, K. Gavin, G. Murphy, P. Doherty, and D. Igoe, *Optimization technique to determine the py curves of laterally loaded stiff piles in dense sand*, Geotechnical Testing Journal 39(5), 842-54 (2016).

[73] K. Yang and R. Liang, *Methods for deriving py curves from instrumented lateral load tests*, Geotechnical testing journal 30(1), 31-8 (2006).

[74] J. Wang and C. Qi, *P-y Curves of Piles in Saturated Degradation Sands with Residual Pore Water Pressures*, In Proceedings of the 18th international offshore and polar engineering conference, Vancouver, Canada, 690-697. Cupertino, CA, USA: International Society of Offshore and Polar Engineers (ISOPE) (2008).

[75] WindEurope, *Offshore Wind in Europe: Key trends and statistics 2017* (2018).

[76] A. Askarinejad, G.Chortis, Q. Li, L. J. Prendergast, R. Brinkgreve, and K. Gavin, *Physical and numerical modelling of the effect of scouring on the lateral behaviour of monopiles*, Proceedings of the XVII   ECSMGE, Reykjavik, Iceland (2011).

[77] R. Nova and L. Montrasio, *Settlements of shallow foundations on sand*, Géotechnique 41(2), 243-56 (1991).

[78] R. Butterfield and G. Gottardi, *A complete three-dimensional failure envelope for shallow footings on sand*, Géotechnique 44(1), 181-4 (1994).

[79] M. Bransby and M. Randolph, *The effect of skirted foundation shape on response to combined V-M-H loadings*, International Society of Offshore and Polar Engineers 9(3), 214-218 (1998).

[80] W. Zhang and A. Askarinejad, *Centrifuge modelling of submarine landslides due to static liquefaction*, Landslides 16(10), 1921-38 (2019).

[81] J. Garnier, C. Gaudin, S. M. Springman, P. Culligan, D. Goodings, D. Konig, B. Kutter, R. Phillips, M. Randolph, and L. Thorel, *Catalogue of scaling laws and similitude questions in geotechnical centrifuge modelling*, International Journal of Physical Modelling in Geotechnics 7(3), 1-27 (2007).

[82] I. Nunez, P. Hoadley, M. Randolph, and J. Hulett, *Driving and tension loading of piles in sand on a centrifuge*, 353-62 Rotterdam, the Netherlands: A. A. Balkema (1988).

[83] W. Zhang and A. Askarinejad, *Behaviour of buried pipes in unstable sandy slopes*, Landslides 16(2), 283-93 (2019).

[84] S. Karthigeyan, V. Ramakrishna, and K. Rajagopal, *Numerical investigation of the effect of vertical load on the lateral response of piles*, Journal of Geotechnical and Geoenvironmental Engineering 133(5), 512-21 (2007).

[85] G. Chortis, A. Askarinejad, L. Prendergast, Q. Li, and K. Gavin, *Influence of scour depth and type on p–y curves for monopiles in sand under monotonic lateral loading in a geotechnical centrifuge*, Ocean Engineering, 106838 (2020).

[86] M. Achmus, *Design of axially and laterally loaded piles for the support of offshore wind energy converters*, Proceedings of the Indian Geotechnical Conference GEOtrendz, Mumbai, India, 92-102 (2010).

[87] Y. W. Choo and D. Kim, *Experimental Development of the p-y Relationship for Large-Diameter Offshore Monopiles in Sands: Centrifuge Tests*, Journal of Geotechnical and Geoenvironmental Engineering 142(1), 04015058 (2015).

[88] W. Qi, F. Gao, M. Randolph, and B. Lehane, *Scour effects on p–y curves for shallowly embedded piles in sand*, Géotechnique 66(8), 648-60 (2016).

[89] R. A. McAdam, B. W. Byrne, G. T. Houlsby, W. J. Beuckelaers, H. J. Burd, K. G. Gavin, D. J. Igoe, R. J. Jardine, C. M. Martin, and A. Muir Wood, *Monotonic laterally loaded pile testing in a dense marine sand at Dunkirk*, Géotechnique, 1-13 (2019).

[90] B. W. Byrne, H. J. Burd, L. Zdravković, R. A. McAdam, D. M. Taborda, G. T. Houlsby, R. J. Jardine, C. M. Martin, D. M. Potts, and K. G. Gavin, *PISA: new design methods for offshore wind turbine monopiles*, Revue Française de Géotechnique 158), 3 (2019).

[91] R. T. Klinkvort, O. Hededal, and M. Svensson, *Laterally cyclic loading of monopile in dense sand*, Proceedings of the 15th European Conference on Soil Mechanics and Geotechnical Engineering (2011).

[92] R. T. Klinkvort and O. Hededal, *Lateral response of monopile supporting an offshore wind turbine*, Proceedings of the ICE-Geotechnical Engineering 166(2), 147-58 (2013).

[93] A. Askarinejad, A. Philia Boru Sitanggang, and F. Schenkeveld, *Effect of pore fluid on the behavior of laterally loaded offshore piles modelled in centrifuge*, Seoul, 897-900 (2017).

[94] H. Qin and W. D. Guo, *Response of static and cyclic laterally loaded rigid piles in sand*, Marine Georesources & Geotechnology 34(2), 138-53 (2016).

[95] R.L. Little and J.L. Briaud, *Full scale cyclic lateral load tests on six single piles in sand*. Texas A&M University, College Station, TX, USA (1988).

[96] L. J. Prendergast, C. Reale, and K. Gavin. *Probabilistic Examination of the Change in Eigenfrequencies of an Offshore Wind Turbine under Progressive Scour Incorporating Soil Spatial Variability*, Marine Structures 57, 87-104 (2018).

[97] C. Wang, X. Yu, and F. Liang, *A Review of Bridge Scour: Mechanism, Estimation, Monitoring and Countermeasures*, Natural Hazards 87 (3), 1881-1906 (2017).

[98] G. J. Hoffmans and H. J. Verheij, *Scour manual*, CRC press (1997).

[99] B. M. Sumer and J. Fredsøe. *The Mechanics of Scour in the Marine Environment*, Hackensack, NJ, World Scientific (2002).

[100] I. N. Robertson, H. R. Riggs, S. C. S. Yim, and Y. L. Young. *Lessons from Hurricane Katrina Storm Surge on Bridges and Buildings*, Journal of Waterway, Port, Coastal, and Ocean Engineering 133(6), 463-483 (2007).

[101] V. Negro, J.-S. Lopez-Gutiérrez, M. D. Esteban, and C. Matutano. *Uncertainties in the Design of Support Structures and Foundations for Offshore Wind Turbines*, Renewable Energy 63, 125-132 (2014).

[102] C. Lin, C. Bennett, and R. L. Parsons, *Analysis of Laterally Loaded Piles in Soft Clay Considering Scour-Hole Dimensions,* Ocean Engineering 111, 461-70 (2016).

[103] J. Han and J. D. Frost. *Load-Deflection Response of Transversely Isotropic Piles under Lateral Loads*." International Journal for Numerical and Analytical Methods in Geomechanics 24(5), 509-529 (2000).

[104] G. Murphy, D. Igoe, P. Doherty, and K. Gavin. *3D FEM Approach for Laterally Loaded Monopile Design*, Computers and Geotechnics 100, 76-83 (2018).

[105] Tokyo Sokki Kenkyujo, *Strain Gauge Product Information* (2018).

[106] B. Sumer, M., J. Fredsøe, and N. Christiansen. *Scour around Vertical Pile in Waves*, Journal of Waterway, Port, Coastal and Ocean Engineering 118(1), 15-31 (1992).

[107] B. Sumer, M., F. Hatipoglu, and J. Fredsøe. *Wave Scour around a Pile in Sand, Medium Dense, and Dense Silt*, Journal of Waterway, Port, Coastal, and Ocean Engineering 133(1), 14-27 (2007).

[108] A. Roulund, B. M. Sumer, J. Fredsøe, and J. Michelsen, *Numerical and experimental investigation of flow and scour around a circular pile*, Journal of Fluid Mechanics 534, 351-401 (2005).

[109] F. Li, J. Han, and C. Lin, *Effect of Scour on the Behavior of Laterally Loaded Single Piles in Marine Clay*, Marine Georesources & Geotechnology 31 (3), 271-89 (2013).

[110] S. Li, S. He, H. Li, and Y. Jin, *Scour Depth Determination of Bridge Piers Based on Time-Varying Modal Parameters: Application to Hangzhou Bay Bridge*, Journal of Bridge Engineering 22(12), 1-13 (2017).

[111] Q. Li, L. Prendergast, A. Askarinejad, and K. Gavin, *Effect of scour on the behavior of a combined loaded monopile in sand*, 9th European Conference on Numerical Methods in Geotechnical Engineering, Porto, Portugal (2018).

[112] E. Richardson and S. Davis, *Evaluating scour at bridges (HEC-18)*, US Department of Transportation, Federal Highway Administration, Colorado, 4th edn FHWA NHI, 01-001 (2001).

[113] J. S. Jones, R. T. Kilgore, and M. P. Mistichelli, *Effects of footing location on bridge pier scour*, Journal of Hydraulic Engineering 118(2), 280-90 (1992).

[114] G. DNV, *Design of Offshore Wind Turbine Structures (DNV-OS-J101)*, Det Norske Veritas AS, Oslo (2014).

Notations

Latin Symbols

A	centrifuge acceleration rate
A_N	peak point of cyclic p-y curve
C_1, C_2	integration constants for deriving pile displacement
C_C	curvature coefficient of sand
C_U	uniformity coefficient of sand
D	pile outer diameter
D_{50}	average grain size of sand
D_r	relative density of sand
D_s	scour depth
e	load eccentricity
e_{min}	minimum void ratio of sand
e_{max}	maximum void ratio of sand
E	elasticity modulus

f	non-dimensional fitting parameters for evaluating scour effect
g	gravitational acceleration
G_S	specific gravity of sand
H	lateral load
H_{max}	maximum load in a cycle
H_{min}	minimum load in a cycle
H_u	pile lateral capacity
$H_{u,V=0}$	pile lateral capacity under pure lateral load
$H_{u,V>0}$	pile lateral capacity under combined vertical and lateral load
I	moment of inertia
k_i	initial stiffness of soil reaction-displacement curve
k_{ini}	initial stiffness of load-displacement curve
K	secant stiffness
K_1	secant stiffness in the first cycle
K_c	non-dimensional functions for the prediction of initial secant stiffness under cyclic loading
K_s	non-dimensional functions for the prediction of initial secant stiffness under cyclic loading
K_S	secant stiffness in monotonic loading
K_N	secant stiffness in the Nth cycle
L	pile embedded length
L_T	total length of pile
M	bending moment
M_{max}	maximum bending moment along the pile
M_R	moment capacity
$M_{R,no\ scour}$	moment capacity under no scour condition
$M_{R,reduction}$	moment reduction factor
$M_{R,\ with\ scour}$	moment capacity under scour condition
$\widetilde{M}$	normalized moment

N	cycle number
p	lateral soil reaction
p_0	lateral soil reaction when the applied vertical load is zero
p_a	atmospheric pressure
p_u	ultimate soil reaction
p_V	lateral soil reaction when the applied vertical load is a non-zero value
$P1$	pile 1
$P2$	pile 2
$P3$	pile 3
r	non-dimensional fitting parameters for evaluating scour effect
R_0	distance from pile pivot point to pile toe
R_b	non-dimensional functions for the prediction of secant stiffness under cyclic loading
R_c	non-dimensional functions for the prediction of secant stiffness under cyclic loading
t	pile wall thickness
T_b	non-dimensional functions for the prediction of pile displacement under cyclic loading
T_c	non-dimensional functions for the prediction of pile displacement under cyclic loading
W_b	scour base width
W_t	top scour width
V	vertical load
V_u	pile vertical capacity
V_{u_pre}	pile vertical capacity on pre-installed pile
y	lateral displacement
$y_{max,1}$	maximum pile lateral displacement in the 1st cycle
$y_{max,N}$	maximum pile lateral displacement in the Nth cycle
z	depth under mudline
z_{add}	additional soil depth

$z_{add, LN}$	additional soil depth to account for local narrow scour
$z_{add, LW}$	additional soil depth to account for local wide scour
z_{equ}	equivalent scour depth

Greek Symbols

α	displacement accumulation rate
β	stiffness accumulation rate
γ	unit weight of sand
θ	pile rotation
θ_N	pile rotation in the Nth
$\tilde{\theta}$	normalized pile rotation
$\tilde{\theta}_{AAR}$	normalized allowable accumulated rotation
φ_{cr}	critical friction angle of sand
ζ_c	cyclic characteristics ratio
ζ_b	cyclic amplitude ratio
ϑ	normalized pile lateral capacity
ρ	pile curvature
χ	improvement in soil resistance
ω	scour slope angle
δ	additional soil depth factor

Acknowledgements

Curriculum Vitae

Qiang Li

14-01-1991   Born in Weifang, China

Education

2008–2012	Undergraduate in Civil Engineering
	Shandong Construction University, P.R. China
2012–2015	Postgraduate in Engineering Mechanics
	Hohai University, P.R. China
2015–2020	Ph.D. Candidate in Geotechnical Engineering
	Technische Universiteit Delft, the Netherlands

List of Publications

Journal Publications

6. **Q. Li**, A. Askarinejad, and K. Gavin, *p-y curves of rigid monopiles under one-way lateral cyclic loading: centrifuge modelling*, ready to submit.

5. **Q. Li**, A. Askarinejad, and K. Gavin, *Lateral response of rigid monopiles subjected to cyclic loading: centrifuge modelling*, ICE - Geotechnical Engineering (accepted).

4. **Q. Li**, A. Askarinejad, and K. Gavin, *The impact of scour on the lateral response of wind turbine monopiles: an experimental study*, Canadian Geotechnical Journal (under review).

3. **Q. Li**, A. Askarinejad, L.J. Prendergast, and K. Gavin, *Experimental investigation of the effect of vertical loading on the lateral behaviour of monopiles in sand*, Ocean Engineering (under review).

2. **Q. Li**, L.J. Prendergast, A. Askarinejad, G. Chortis, and K. Gavin, *Centrifuge modelling of the impact of scour erosion on the monotonic lateral response of a monopile in sand*, Geotechnical Testing Journal 43, 5 (2020).

1. G. Chortis, A. Askarinejad, L.J. Prendergast, **Q. Li**, and K. Gavin, *Influence of scour depth and type on p-y curves for monopiles in sand under monotonic lateral loading in a geotechnical centrifuge*, Ocean Engineering, 106838 (2019).

Conference Publications

2. A. Askarinejad, G. Chortis, **Q. Li**, L.J. Prendergast, R. Brinkgreve, and K. Gavin, *Physical and numerical modelling of the effect of scouring on the lateral behaviour of monopiles*, Proceedings of the XVII ECSMGE-2019, Iceland (2019).

1. **Q. Li**, L.J. Prendergast, A. Askarinejad, and K. Gavin, *Effect of scour on the behavior of a combined loaded monopile*, 9th European Conference on Numerical Methods in Geotechnical Engineering, Portugal (2018).